Dissertation

Put forward by

Robert Lilow, M. Sc.

born in Frankfurt (Oder), Germany

Oral examination: 02.07.2018

STRUCTURE FORMATION IN
DARK AND BARYONIC MATTER WITHIN
RESUMMED KINETIC FIELD THEORY

Referees:

Prof. Dr. Matthias Bartelmann

Prof. Dr. Jan Martin Pawlowski

Abstract

We combine a novel approach to cosmic structure formation called Kinetic Field Theory (KFT) [1] with resummation methods to investigate the small-scale structure formation in dark and baryonic matter. For pure dark matter, we compute the first nonlinear corrections to the density contrast power spectrum and compare these to the results obtained in standard Eulerian perturbation theory (SPT). We find that we can precisely reproduce the SPT 1-loop result if we adopt the same expansion scheme as SPT. However, we also show that the natural expansion scheme of resummed KFT is actually fundamentally different and might thus be able to overcome the problems of SPT when trying to describe nonlinear structure formation. To describe the effect of baryons, we demonstrate how isothermal and adiabatic gas dynamics can be implemented consistently into resummed KFT and how a system of gravitationally coupled dark and baryonic matter can generally be treated in this framework. In the isothermal case, we further investigate the linear evolution of this coupled system in a cosmological setting. Our results show a suppression of the baryonic power spectrum on scales below approximately $1\,\mathrm{Mpc}/h$ which is qualitatively comparable to simulation results but underpredicts the effect by nearly an order of magnitude. Furthermore, simulations show an enhancement of the dark matter power spectrum absent in our results. We expect these deviations to decrease once adiabatic gas dynamics and nonlinear corrections are taken into account.

Zusammenfassung

Wir kombinieren einen neuen Ansatz zur Beschreibung kosmischer Strukturbildung, Kinetische Feldtheorie (KFT) [1] genannt, mit Resummierungsmethoden, um die kleinskalige Strukturbildung in dunkler und baryonischer Materie zu untersuchen. Für reine dunkle Materie berechnen wir die ersten nichtlinearen Korrekturen zum Leistungsspektrum des Dichtekontrasts und vergleichen diese mit den Ergebnissen der Eulerschen Standard-Störungstheorie (SPT). Es stellt sich heraus, dass wir die 1-Schleifen-Resultate aus SPT exakt reproduzieren, wenn wir das gleiche Expansionsschema wie SPT verwenden. Allerdings zeigen wir auch, dass sich das natürliche Expansionsschema der resummierten KFT davon grundlegend unterscheidet und deshalb möglicherweise dazu in der Lage ist, die Probleme zu überwinden, die SPT bei der Beschreibung nichtlinearer Strukturbildung hat. Zur Beschreibung baryonischer Effekte demonstrieren wir, wie isotherme und adiabatische Gasdynamik konsistent in resummierte KFT implementiert werden können und wie man ein System gravitativ gekoppelter dunkler und baryonischer Materie in diesem Formalismus allgemein behandelt. Im isothermen Fall untersuchen wir außerdem die lineare Entwicklung dieses gekoppelten Systems in einem kosmologischen Kontext. Unsere Ergebnisse zeigen eine Unterdrückung des baryonischen Leistungsspektrums auf Skalen unterhalb ungefähr $1\,\mathrm{Mpc}/h$, die mit Simulationsergebnissen zwar qualitativ vergleichbar sind, die Stärke des Effekts jedoch um fast eine Größenordnung unterschätzen. Des Weiteren zeigen die Simulationen eine Erhöhung des Leistungsspektrums dunkler Materie, die sich in unseren Resultaten nicht beobachten lässt. Wir erwarten, dass sich diese Abweichungen verringern werden, sobald die adiabatische Gasdynamik sowie nichtlineare Korrekturen berücksichtigt werden.

Contents

1. Introduction

Studying the evolution of cosmic structures allows us to extend our current knowledge on the nature of gravity as well as the matter content of our universe. With upcoming astronomical surveys like Euclid and LSST this endeavour will reach an entirely new level, as they will probe the matter distribution down to scales of less than 1 Mpc/h with percent-level precision.

Contrasting these observations with theoretical predictions will be challenging: While conventional Eulerian and Lagrangian analytic descriptions of structure formation provide accurate predictions on linear and mildly nonlinear scales larger than approximately 20 Mpc/h, it has been notoriously difficult for them to reach further into the nonlinear regime. This is largely due to the fact that they assume matter to move along a unique velocity field. With collisionless dark matter dominating cosmic structures, however, particle trajectories can cross and form multiple streams, at which point this uniqueness assumption breaks down.

Numerical N-body simulations, on the other hand, are able to describe the nonlinear small-scale dynamics, as they follow the phase-space trajectories of individual tracer particles. But they offer only little insight into the underlying principles of structure formation and are computationally very expensive, especially when trying to cover large cosmological parameter spaces or to extract 3-point or higher-order statistics. These non-Gaussian statistics, though, are crucial for constraining the cosmological model, as they contain most of the information on nonlinear structure growth and are also required to estimate covariance matrices.

An analytic framework of cosmic structure formation capable of describing the evolution of the 2-point as well as higher-order statistics of the matter distribution down to the scales probed by upcoming surveys would hence be a highly desirable tool for future cosmological research. A novel approach developed by Bartelmann et al. in [1], dubbed Kinetic Field Theory (KFT), aims at providing exactly this. Unlike conventional analytic approaches, KFT is built on the full Hamiltonian dynamics of classical particles in phase-space and can thus be seen as an analytic analogue to an N-body simulation. First results obtained within this framework are very promising [1, 2].

In [3] we presented a reformulation of KFT that allows to partially resum the interactions between particles and showed how this yields the linear large-scale growth of structures purely from Hamiltonian particle dynamics. In this thesis, we develop this resummed KFT further, aiming at providing an accurate description of the formation of small-scale structures as well.

This development proceeds along two lines: On the one hand, reaching our goal requires a well-controlled and precise computation of the nonlinear evolution of the matter distribution under the influence of gravity. We will investigate the feasibility of achieving this within resummed KFT by computing the first nonlinear corrections to the evolution of the dark matter 2-point statistics and comparing these with the results obtained from an Eulerian approach.

But even the most precise treatment of nonlinear structure growth in dark matter will not be able to predict the full small-scale matter distribution accurately, as there are also baryonic effects

becoming relevant at these scales. These include the influence of the collisional baryonic gas dynamics, radiative cooling as well as astrophysical feedback processes, for example from star formation, supernovae or active galactic nuclei. Our second line of development is thus concerned with the incorporation of these baryonic effects into resummed KFT. As a first step, we show in this thesis how isothermal and adiabatic gas dynamics can be included, and investigate the linear structure formation in a gravitationally coupled system of dark and baryonic matter.

This thesis is structured as follows: We begin with a short review of the foundations of cosmology in general and cosmic structure formation in particular in chapter 2. After that, we introduce the framework of KFT in chapter 3 – including a summary of the basic formalism and a derivation of its resummed form. In this chapter, we further demonstrate the general properties of the resummed KFT approach by applying it to a simple non-cosmological test system. In chapter 4, we then use this framework to describe linear as well as nonlinear structure formation in pure dark matter and compare our findings to the Eulerian results. Afterwards, we demonstrate in chapter 5 how the gas dynamics of baryonic matter can be incorporated into resummed KFT, and investigate the linear evolution of a system of gravitationally coupled dark and baryonic matter. In the end, we will summarise our results and conclusions in chapter 6.

2. Cosmology

In this chapter we present a brief summary of the basics of cosmology and conventional approaches to cosmic structure formation, focussing on those aspects relevant for the considerations in this thesis. For a more detailed introduction into these matters, we refer the reader to [4] and [5], respectively.

2.1. Cosmological standard model

2.1.1. Space-time dynamics

The aim of cosmology is to describe and understand the structure and evolution of our universe at large. It is thus concerned with length scales so large that most of the four fundamental interactions become irrelevant. The strong and the weak interactions are inherently confined to the scales of subatomic particles, and even electromagnetism, despite its infinite interaction length, plays essentially no role for cosmology since the cosmic matter content is electrically neutral on average.[1] Hence, the only interaction relevant on cosmic scales is gravity.

As gravity is described by Einstein's General Relativity [6], this is also the natural language of cosmology. The geometry of space-time, characterised by its metric $g_{\mu\nu}$, is thus described by Einstein's field equations,

$$G_{\mu\nu} = \frac{8\pi G}{c^4}\, T_{\mu\nu} + \Lambda\, g_{\mu\nu}\,, \tag{2.1}$$

where $G_{\mu\nu}$ is the Einstein field tensor constructed from first and second derivatives of the metric, $T_{\mu\nu}$ is the energy-momentum tensor of the cosmic matter and radiation content, and Λ is the cosmological constant. Furthermore, G denotes the gravitational constant and c is the speed of light. To solve this set of highly nonlinear differential equations, cosmology makes two crucial assumptions:

1. The universe is spatially isotropic, i.e. independent of direction, about our position if averaged over sufficiently large scales.

2. Our position in the universe is by no means preferred to any other. This is known as the cosmological principle.

The combination of these two assumptions implies that on large enough scales our universe has to be spatially isotropic around all of its points, and thus it must also be spatially homogeneous.

---

[1] There are magnetic fields with surprisingly large coherence lengths, but their energy density is very low.

The most general form of the metric under the symmetry constraints of spatial isotropy and homogeneity is characterised by the line element

$$ds^2 = g_{\mu\nu}\,dx^\mu dx^\nu = -c^2 dt^2 + a^2(t)\left[\frac{dr^2}{1-\kappa r^2} + r^2\Big(d\theta^2 + \sin^2(\theta)\,d\varphi^2\Big)\right], \tag{2.2}$$

where (r, θ, φ) are spherical polar coordinates, κ is a constant parametrising the curvature of spatial hypersurfaces and $a(t)$ is the scale factor which describes how these hypersurfaces expand or shrink with time. Isotropy and homogeneity further imply $T_{\mu\nu}$ to take the form of the stress-energy tensor of a perfect fluid, described only by the cosmic fluid's mean pressure $\bar{P}$ and its mean energy density $\bar{\rho}c^2$. Using this ansatz for the momentum-energy tensor and the metric (2.2) reduces Einstein's field equations to two differential equations for the scale factor,

$$\left(\frac{\dot{a}}{a}\right)^2 = \frac{8\pi G}{3}\bar{\rho} - \frac{\kappa c^2}{a^2} + \frac{\Lambda c^2}{3}\,, \tag{2.3}$$

$$\frac{\ddot{a}}{a} = -\frac{4\pi G}{3}\left(\bar{\rho} + \frac{3\bar{P}}{c^2}\right) + \frac{\Lambda c^2}{3}\,, \tag{2.4}$$

known as Friedmann's equations. The metric (2.2) is called Friedmann-Lemaître-Robertson-Walker (FLRW) metric if the scale factor a satisfies the Friedmann equations.

Combining these two equations yields the adiabatic equation

$$\frac{d}{dt}\big(a^3 \bar{\rho}\,c^2\big) + \bar{P}\,\frac{d}{dt}\big(a^3\big) = 0\,, \tag{2.5}$$

which describes the conservation of energy. Together with an equation of state that couples the pressure P and density ρ,

$$P = w\,\rho c^2\,, \tag{2.6}$$

it allows us to characterise the evolution of the mean densities of different forms of matter. Here, w denotes the equation of state parameter. For non-relativistic matter, pressure can be neglected on large scales, i.e. $w_m \approx 0$, while one finds $w_r = 1/3$ for radiation and relativistic matter. Inserting these equations of state into the adiabatic equation yields

$$\bar{\rho}_m = \bar{\rho}_{m,0}\,a^{-3}\,, \qquad \bar{\rho}_r = \bar{\rho}_{r,0}\,a^{-4} \tag{2.7}$$

for the mean densities of non-relativistic matter and radiation, respectively. Here, $\bar{\rho}_{m,0}$ and $\bar{\rho}_{r,0}$ denote the values of these mean densities at today's time t_0, corresponding to the normalisation $a(t_0) = 1$ of the scale factor. Given this normalisation, we further define the cosmological redshift $z := 1/a - 1$ which describes the wavelength shift of photons caused by the expansion of space.

Conventionally, the first Friedmann equation (2.3) is re-expressed in terms of the Hubble function $H := \dot{a}/a$ and the dimensionless density parameters

$$\Omega_r := \frac{8\pi G}{3H^2}\,\bar{\rho}_r\,, \qquad \Omega_m := \frac{8\pi G}{3H^2}\,\bar{\rho}_m\,, \qquad \Omega_\kappa := -\frac{\kappa c^2}{a^2 H^2}\,, \qquad \Omega_\Lambda := \frac{\Lambda c^2}{3H^2}\,. \tag{2.8}$$

It then reads

$$H^2 = H_0^2\left[\Omega_{r,0}\,a^{-4} + \Omega_{m,0}\,a^{-3} + \Omega_{\kappa,0}\,a^{-2} + \Omega_{\Lambda,0}\right], \tag{2.9}$$

where the values of the dimensionless density parameters today, $\Omega_{j,0} := \Omega_j(t_0)$, satisfy

$$1 = \Omega_{\mathrm{r},0} + \Omega_{\mathrm{m},0} + \Omega_{\kappa,0} + \Omega_{\Lambda,0}\,. \tag{2.10}$$

The current standard model of cosmology, the ΛCDM model, describes a FLRW cosmology that is spatially flat, $\Omega_{\kappa,0} = 0$, and whose matter content is dominated by a form of matter called cold dark matter. In contrast to ordinary matter, in cosmology usually referred to as baryonic matter, dark matter does not interact electromagnetically. From the perspective of cosmology, its dynamics are thus only subject to gravity and can be considered collisionless. Furthermore, "cold" means that it consists of non-relativistic particles. While the precise nature of these particles is still an open question, the existence of dark matter currently presents the simplest model able to explain the observed structures in the universe.

To account for the two types of matter, we introduce separate dimensionless density parameters $\Omega_{\mathrm{m}}^{\mathrm{d}}$ and $\Omega_{\mathrm{m}}^{\mathrm{b}}$ for the dark and baryonic matter, respectively,

$$\Omega_{\mathrm{m}} = \Omega_{\mathrm{m}}^{\mathrm{d}} + \Omega_{\mathrm{m}}^{\mathrm{b}}\,. \tag{2.11}$$

For all calculations in this thesis, we will further use the following parameter values,

$$H_0 = 70\,\frac{\mathrm{km/s}}{\mathrm{Mpc}}\,, \quad \Omega_{\mathrm{r},0} = 0\,, \quad \Omega_{\mathrm{m},0}^{\mathrm{d}} = 0.26\,, \quad \Omega_{\mathrm{m},0}^{\mathrm{b}} = 0.04\,, \quad \Omega_{\Lambda,0} = 0.7\,. \tag{2.12}$$

Note that, in reality, $\Omega_{\mathrm{r},0}$ is not actually vanishing. But its value is small enough that we can safely neglect it during the matter- and Λ-dominated epochs that we will be concerned with [7].

2.1.2. Cosmic expansion history

According to the ΛCDM model, the history of our universe started approximately 13.8 billion years ago in a hot big bang, corresponding to a scale factor of $a = 0$, and continuously expanded ever since. The details of its evolution in the first fractions of a second are still debated, but it is widely believed that it underwent a period of rapid, accelerated expansion known as cosmic inflation, which could explain the flatness and isotropy of the universe observed today. Crucially for us, inflationary models also predict the emergence of the primordial seeds of cosmic structure formation from quantum fluctuations.

The expansion history following inflation is conventionally divided into different epochs corresponding to the dominant form of matter or energy at the time, according to (2.9). It started with the radiation-dominated epoch, during which the Hubble function scaled like $H \propto a^{-2}$, i. e. the expansion of the universe began to decelerate. In this epoch, protons and neutrons formed the first nuclei, but photon temperatures where still too high for electrons to bind to these nuclei. Therefore, photons, nuclei and electrons formed a strongly coupled plasma.

At a redshift of $z \approx 3600$, the energy density of radiation dropped below that of matter and the matter-dominated epoch started. During this era, the cosmic expansion decelerated even further, $H \propto a^{-3/2}$. At a redshift of $z \approx 1090$, the photon temperature had decreased to a value of $T^{\mathrm{p}} \approx 3000K$ and thus became low enough to allow protons and electrons to combine into neutral hydrogen atoms, resulting in the decoupling of matter and radiation. After that, the temperature of the decoupled photons continued to drop, reaching a value of $T_0^{\mathrm{p}} = 2.726\,\mathrm{K}$ today. Measurements

of this cosmic microwave background (CMB) radiation provide strong observational evidence for the large-scale isotropy of the universe and yield tight constraints on the parameters of our cosmological model. After the decoupling of the CMB, the hierarchical formation of ever larger cosmic structures under the influence of gravity sets in. The first stars formed around a redshift of $z \approx 20$, leading to the reionisation of matter, and at $z \approx 6$ galaxies started to form.

From a cosmological perspective, the Λ-dominated epoch began only very recently at a redshift of $z \approx 0.4$. It is characterised by an accelerated expansion of space with an approximately constant Hubble function, and presents the latest expansion epoch within a ΛCDM cosmology.

2.2. Structure formation

2.2.1. Statistics of fluctuations

So far, we only considered the evolution of our universe on the largest scales where it can be considered homogeneous. On smaller scales, though, this idealised assumption has to be relaxed to allow the existence of structures – including our very selves. To describe these structures, we have to consider fluctuations of the cosmic density field ρ around its mean value $\bar{\rho}$.

For this purpose, we introduce the density contrast δ,

$$\delta := \frac{\rho - \bar{\rho}}{\bar{\rho}}, \tag{2.13}$$

describing the relative density fluctuations. To satisfy the fundamental cosmological symmetry assumptions, it has to be a statistically homogeneous and isotropic random field. Thus, we are interested in its statistical properties rather than its actual value. But as its mean must vanish by construction, the simplest non-trivial statistical property we can investigate is its variance, described by the density contrast correlation function between two points $\vec{r}$ and $\vec{r}'$,

$$\xi(|\vec{r} - \vec{r}'|) := \left\langle \delta(\vec{r})\, \delta(\vec{r}') \right\rangle. \tag{2.14}$$

Due to homogeneity and isotropy, it can only depend on the distance between both points.

Conventionally, the central quantity used to characterise cosmic structures is its Fourier transform, the density contrast power spectrum P_δ which is defined as the variance of δ in Fourier space,

$$\left\langle \delta(\vec{k}, t)\, \delta(\vec{k}', t) \right\rangle =: (2\pi)^3\, \delta_\mathrm{D}(\vec{k} + \vec{k}')\, P_\delta(k, t). \tag{2.15}$$

The appearance of the Dirac delta distribution and the fact that the power spectrum only depends on the modulus of $\vec{k}$ are the consequences of statistical homogeneity and isotropy, respectively.

Before we can describe the evolution of structures, we of course have to know their statistics at some initial point in time first. As mentioned in subsection 2.1.2, cosmic inflation predicts the emergence of primordial macroscopic density perturbations from quantum fluctuations. The resulting power spectrum usually takes the form of a power law,

$$P_\delta^{(\mathrm{prim})}(k) \propto k^{n_\mathrm{s}}, \tag{2.16}$$

where the so-called spectral index n_s is predicted to be close to unity [8, 9]. Observations confirm this and find an explicit value of $n_\mathrm{s} = 0.967$ [7]. Simple inflationary models further predict

these fluctuations to be Gaussian and thus fully characterised by this power spectrum alone [10]. While more sophisticated models also allow primordial non-Gaussianities, there is currently no observational evidence for their existence [11]. In this thesis, we will hence consider Gaussian initial conditions.

2.2.2. Linear evolution

The conventional Eulerian approach to investigate the growth of the primordial density fluctuations assumes that the cosmic matter and radiation content on the scales of these fluctuations is still well described by a fluid. This fluid should then obey the continuity, Euler and Poisson equations,

$$\frac{\partial \rho}{\partial t} + \vec{\nabla}_r \cdot (\rho \, \vec{v}) = 0 \,, \tag{2.17}$$

$$\frac{\partial \vec{v}}{\partial t} + \left(\vec{v} \cdot \vec{\nabla}_r \right) \vec{v} = -\frac{\vec{\nabla}_r P}{\rho} + \vec{\nabla}_r V_G \,, \tag{2.18}$$

$$\nabla_r^2 V_G = 4\pi G \left(\rho - \bar{\rho} \right), \tag{2.19}$$

where $\vec{v}$ and V_G are the velocity field and the gravitational potential of the cosmic fluid, respectively.

It is then convenient to introduce coordinates that are comoving with the background expansion, $\vec{q} := \vec{r}/a$, which allow to decompose the velocity $\vec{v}$ into the background Hubble velocity $\vec{v}_H$ and the peculiar comoving velocity $\vec{u}$,

$$\vec{v} = \dot{\vec{r}} = \dot{a}\vec{q} + a\dot{\vec{q}} = H\vec{r} + a\vec{u} = \vec{v}_H + a\vec{u} \,. \tag{2.20}$$

Expressing the equations (2.17) to (2.19) in terms of comoving coordinates and linearising them in δ and $\vec{u}$ yields

$$\dot{\delta} + \vec{\nabla}_q \cdot \vec{u} = 0 \,, \tag{2.21}$$

$$\dot{\vec{u}} + 2H\vec{u} = -\frac{w\vec{\nabla}_q \delta}{a^2} - \frac{\vec{\nabla}_q V_G}{a^2} \,, \tag{2.22}$$

$$\nabla_q^2 V_G = 4\pi G \bar{\rho} a^2 \delta \,. \tag{2.23}$$

Inserting the divergence of the second equation into the first one then leaves us with a single equation for the density contrast,

$$\ddot{\delta} + 2H\dot{\delta} = \frac{w\nabla_q^2 \delta}{a^2} + 4\pi G \bar{\rho}\delta \,. \tag{2.24}$$

This linear evolution equation will describe the evolution of the density fluctuations as long as they are small, $\delta \ll 1$.

While this is the case during the radiation-dominated epoch, it turns out that one additionally has to take general-relativistic effects on scales larger than the Hubble radius $r_H := c/H$ into account to capture the correct evolution in this era. The Hubble radius sets the maximal scale of perturbations which can be in causal contact. Therefore, fluctuations with a wavelength

larger than r_H are not suppressed by radiation pressure. Solving (2.24) under this constraint shows that the resulting matter density contrast power spectrum at some time t_i early in the matter-dominated era scales like

$$P_\delta^{(\mathrm{i})}(k) := P_\delta(k, t_\mathrm{i}) \propto \begin{cases} k^{n_s} & \text{if } k \ll k_\mathrm{eq}, \\ k^{n_s - 4} & \text{if } k \gg k_\mathrm{eq}. \end{cases} \tag{2.25}$$

Here, k_eq denotes the wavenumber corresponding to the size of the Hubble radius at the time of matter-radiation equality. The precise behaviour around $k \approx k_\mathrm{eq}$ has to be determined by a more careful analysis of the full coupled Einstein-Boltzmann equations. In this thesis, we will use the fitting formula found by Bardeen, Bond, Kaiser and Szalay (BBKS) [12]. As we are interested in structure formation during the matter-dominated epoch, we will consider $P_\delta^{(\mathrm{i})}$ as the initial power spectrum in our analysis.

To describe the subsequent linear evolution of the density contrast of pressureless matter, we define the linear growth factor D_+ via[2]

$$\delta(t) =: \delta(t_\mathrm{i}) \frac{D_+(t)}{D_+(t_\mathrm{i})} \tag{2.26}$$

and insert this ansatz into (2.24) evaluated at $w = 0$. The resulting linear differential equation for D_+ reads

$$\ddot{D}_+ + 2H\dot{D}_+ = 4\pi G \bar{\rho}_\mathrm{m} D_+ = \frac{3}{2} \Omega_m H^2 D_+ \,, \tag{2.27}$$

where we used (2.8) in the second step. For a ΛCDM cosmology, its solution is well-described by the fitting formula

$$D_+ = \frac{5a}{2} \Omega_\mathrm{m} \left[\Omega_\mathrm{m}^{4/7} - \Omega_\Lambda + \left(1 + \frac{1}{2}\Omega_\mathrm{m}\right)\left(1 + \frac{1}{70}\Omega_\Lambda\right) \right]^{-1} \tag{2.28}$$

given in [13]. The power spectrum of the linearly evolving density contrast is then given by

$$P_\delta^{(\mathrm{lin})}(k, t) := P_\delta^{(\mathrm{i})}(k) \frac{D_+^2(t)}{D_+^2(t_\mathrm{i})} \,. \tag{2.29}$$

The only thing left is to fix the overall amplitude of the power spectrum, which is typically characterised in terms of the variance on some given scale R,

$$\sigma_R^2 := \int \frac{\mathrm{d}^3 k}{(2\pi)^3} P_\delta(k) \, W_R^2(k) \,, \tag{2.30}$$

where $W_R(k)$ is the Fourier transform of a window function of width R. Conventionally, the value of today's variance on a scale of $8\,\mathrm{Mpc}/h$, σ_8, is specified. In this thesis, we will use a value of $\sigma_8 = 0.8$.

---

[2]Note that inserting the ansatz (2.26) into (2.21) implies the initial comoving velocity field $\vec{u}(t_\mathrm{i})$ to be a Gaussian random field that is correlated with $\delta(t_\mathrm{i})$.

2.2.3. Nonlinear evolution

The linear Eulerian description of the evolution of the density contrast presented in the previous subsection breaks down once δ approaches unity. Describing the subsequent growth of structures thus requires a nonlinear treatment instead. One possibility is to expand the fluid equations (2.17) and (2.18) to higher orders in the density contrast and the peculiar velocity. This approach is known as Eulerian perturbation theory and will be discussed in more detail in subsection 4.3.3.

Another conventional analytic approach to cosmic structure formation is Lagrangian perturbation theory which follows the spatial trajectories of particles, rather than considering the dynamics of the density and velocity fields. Its central object of interest is the displacement field $\vec{\Psi}$ that describes the mapping between the initial and final particle positions,

$$\vec{q}(t) =: \vec{q}^{(i)} + \vec{\Psi}(\vec{q}^{(i)}, t) \ . \tag{2.31}$$

Starting from the equations of motion for the particle positions, one can derive an evolution equation for $\vec{\Psi}$ which is then solved perturbatively. For more details on this we refer the reader to [5]. Its linear solution is found to be given by

$$\vec{\nabla}_{q^{(i)}} \vec{\Psi}^{(1)}(\vec{q}^{(i)}, t) = -\delta(\vec{q}^{(i)}) D_+(t) \tag{2.32}$$

and describes particles moving on straight lines with a constant peculiar comoving velocity $\vec{u}$, as can be seen by using (2.26) and comparing with (2.21). In the Zel'dovich approximation, these trajectories are extrapolated beyond the validity range of the linear Eulerian description [14], which captures the onset of nonlinear structure formation, but generally underpredicts the growth of power [5].

For both of these approaches, Eulerian and Lagrangian perturbation theory, it is however notoriously difficult to describe cosmic structure formation in the strongly nonlinear regime [15–36]. The reason for this lies in the fact that most of the cosmic matter content consists of collisionless dark matter particles whose trajectories can cross and form multiple streams during the gravitational collapse of cosmic structures. At this point, both the Eulerian and Lagrangian descriptions break down. In the Eulerian approach this is due to the fact that it assumes a smooth and single-valued velocity field, and can thus only describe a single stream of matter. The Lagrangian approach, on the other hand, assumes a unique mapping between initial and final particle positions, which is violated when two particles meet at the same position. In this case, the inverse Jacobian determinant of the mapping, needed to compute the density field, diverges.

To describe the full nonlinear evolution of cosmic structures, one thus has to resort to N-body simulations. These sample the cosmic matter distribution inside a given volume at some initial point in time by a finite number of particles and then evolve the positions and velocities of all individual particles according to their Hamiltonian equations of motion. At the desired final time, correlation functions or power spectra of the cosmic density and velocity fields can be computed from the particle positions and velocities.

While N-body simulations currently provide the most accurate description of structure formation in the nonlinear regime, they are at the same time computationally very expensive – even though a large number of sophisticated numerical schemes have been developed to compute the gravitational forces acting between the particles as efficiently as possible. This becomes

particularly problematic when one needs to investigate large cosmological parameter spaces or wants to extract higher-order correlators of the matter distribution. An analytic approach that is capable of describing the formation of cosmic structures far within the nonlinear regime would thus be a highly desirable tool. In chapter 4 we will investigate if the framework of Kinetic Field Theory might be a promising candidate for this.

2.2.4. Baryonic effects

So far, we treated the complete non-relativistic matter content of the universe as being pressureless and thus only subject to gravity during structure formation. However, this is not true for baryonic matter which also interacts electromagnetically. Due to the fact that baryons only make up a small portion of the total matter content, neglecting their influence might be a good first approximation, but there are at least two regimes in cosmic structure formation where baryonic effects become relevant.

The first of these concerns the evolution of density fluctuations prior to recombination. During that time, we have to take into account that baryons, unlike dark matter, were strongly coupled to photons via Compton scattering. The dynamics of such a coupled photon-baryon plasma is then characterised by repulsive pressure forces and attractive gravitational forces counteracting each other. This creates oscillations in their density field with a characteristic wavelength set by the effective speed of sound in the plasma, first described in [37].

Once photons and baryons decouple, these baryon acoustic oscillations (BAO) leave their imprint in both individual components. In the case of the photons this can be observed in the spectrum of CMB temperature fluctuations. For baryons, on the other hand, it leads to a peak in the density contrast correlation function whose position is set by the oscillation wavelength at the time of the decoupling. The respective baryon power spectrum then shows oscillatory features with a frequency corresponding to this peak position. Crucially, since baryons and dark matter couple gravitationally this also affects the dark matter spectrum, though to a lesser extent. Solving the coupled Boltzmann equations for photons, baryons and dark matter numerically allows to describe the formation of BAOs very accurately, and the resulting power spectrum is well-described by a fitting formula found by Eisenstein & Hu [38].

The second regime where baryonic effects are important is the formation of cosmic structures on very small scales below the Jeans length of the baryonic gas [39]. On these scales, its pressure is not negligible compared to the gravitational interactions any more and prevents the gravitational collapse of baryonic structures. Consequently, this results in a partial suppression of the growth of structures in the total matter content compared to a system of pure dark matter. Furthermore, in contrast to dark matter, baryonic matter is able to lose energy via radiative processes. This heat loss leads to a contraction of baryonic gas clouds crucial for the formation of galaxies [40, 41]. Beyond that, baryons are also affected by many different astrophysical processes like star formation, supernovae or active galactic nuclei.

To describe the small-scale structure formation in the combined dark and baryonic matter correctly, it is thus insufficient to consider their gravitational dynamics alone. One also has to take all of the baryonic effects just mentioned into account, which renders this task even harder than it already was. The state-of-the-art technique for this are hydrodynamical simulations that additionally include models for the different astrophysical feedback processes [42].

Incorporating all of this into an analytic framework for galaxy formation is most likely infeasible. But it might well be possible that including only some of these effects turns out to be sufficient to describe the *statistics* of small-scale structures. In chapter 5 we take a very first step into this direction by investigating the incorporation of baryonic gas dynamics into KFT.

3. Kinetic Field Theory

In the previous chapter we have discussed how conventional approaches to cosmic structure formation are inherently limited by their inability to describe crossing streams of particles. In this chapter, we will thus introduce the framework of KFT which allows to overcome these limitations by taking the full phase-space dynamics of microscopic particles into account.

At its very core, KFT is based on the Martin-Siggia-Rose formalism to describe classical systems in terms of a path integral approach similar to quantum field theory [43]. This was first applied to Hamiltonian dynamics by Gozzi et al. in [44, 45] and further developed into a full field theoretic description of kinetic theory by Mazenko and Das in [46, 47]. Building on these pioneering works, we extended the KFT framework to describe the dynamics of an initially correlated ensemble of particles and applied this to cosmic structure formation in [1].

We start by summarising the general framework of KFT, following the derivation in [1], and show how correlation functions of the density and other collective fields can be computed in a perturbative expansion in orders of the particle interactions. Afterwards, we present a reformulation of this framework that results in a partial resummation of this perturbation series. This will be the approach used in all following chapters.

3.1. General framework of KFT

3.1.1. Path integral for classical N-particle system

Consider a classical N-particle system described by the phase-space trajectories $\vec{x}_j(t)$ of its individual particles, $j = 1, \ldots, N$. To condense the notation, we will combine these single-particle vectors into N-particle tensors $\boldsymbol{x}(t)$, adopting the conventions introduced in [1] and [48],

$$\boldsymbol{a}(t) := \sum_{j=1}^{N} \vec{a}_j(t) \otimes \vec{e}_j \, , \tag{3.1}$$

$$\boldsymbol{a} \cdot \boldsymbol{b} := \sum_{j=1}^{N} \int_{t_{\mathrm{i}}}^{\infty} \mathrm{d}t \; \vec{a}_j(t) \cdot \vec{b}_j(t) \, . \tag{3.2}$$

where $\vec{e}_j$ is the N-dimensional Cartesian base vector with entries $\left(\vec{e}_j \right)_i = \delta_{ij}$ and t_{i} denotes the initial time.

The initial phase-space configuration $\boldsymbol{x}^{(\mathrm{i})} := \boldsymbol{x}(t_{\mathrm{i}})$ of such an N-particle system is assumed to be characterised by a probability distribution $\mathcal{P}_{\mathrm{i}}\big(\boldsymbol{x}^{(\mathrm{i})}\big)$ and its dynamics at times $t \geq t_{\mathrm{i}}$ shall be governed by some equations of motion $E[\boldsymbol{x}(t)] = 0$. A central idea of KFT is to encapsulate both

of these in the partition function

$$Z = \int d\boldsymbol{x}^{(\mathrm{i})}\, \mathcal{P}_{\mathrm{i}}\big(\boldsymbol{x}^{(\mathrm{i})}\big) \int\limits_{\boldsymbol{x}^{(\mathrm{i})}} \mathcal{D}\boldsymbol{x}\; \delta_{\mathrm{D}}\big[\boldsymbol{x}(t) - \boldsymbol{x}^{(\mathrm{cl})}\big(\boldsymbol{x}^{(\mathrm{i})}, t\big)\big]\,. \tag{3.3}$$

Here, the dynamics is incorporated by functionally integrating over all possible phase-space trajectories $\boldsymbol{x}(t)$ starting from an initial configuration $\boldsymbol{x}^{(\mathrm{i})}$, where a functional Dirac delta distribution ensures that only the classical N-particle trajectory $\boldsymbol{x}_{\mathrm{cl}}\big(\boldsymbol{x}^{(\mathrm{i})}, t\big)$, which solves the equations of motion, contributes. The stochastic initial conditions are then taken into account by averaging over the initial probability distribution $\mathcal{P}_{\mathrm{i}}\big[\boldsymbol{x}^{(\mathrm{i})}\big]$.

Since the full solution of the equations of motion is generally not known, we have to re-express the delta distribution in (3.3) in terms of the equations of motion themselves,

$$\delta_{\mathrm{D}}\big[\boldsymbol{x}(t) - \boldsymbol{x}^{(\mathrm{cl})}\big(\boldsymbol{x}^{(\mathrm{i})}, t\big)\big] = \delta_{\mathrm{D}}\big[E[\boldsymbol{x}(t)]\big]\; \det\left[\frac{\delta E[\boldsymbol{x}(t)]}{\delta \boldsymbol{x}(t')}\right]\bigg|_{\boldsymbol{x}(t) = \boldsymbol{x}^{(\mathrm{cl})}(\boldsymbol{x}^{(\mathrm{i})}, t)}\,. \tag{3.4}$$

In this work, we will only consider dynamics for which the functional Jacobian determinant on the right-hand-side is just a constant that can be absorbed into the normalisation of the path integral measure.[1] The partition function can then be brought into the more convenient form

$$Z = \int d\Gamma_{\mathrm{i}} \int\limits_{\boldsymbol{x}^{(\mathrm{i})}} \mathcal{D}\boldsymbol{x} \int \mathcal{D}\boldsymbol{\chi}\; \mathrm{e}^{\mathrm{i}\boldsymbol{\chi}\cdot E[\boldsymbol{x}]} \tag{3.5}$$

by expressing the delta distribution in terms of a functional Fourier integral with respect to an auxiliary field $\boldsymbol{\chi}$ with components $\vec{\chi}_j$ conjugate to $\vec{x}_j$ and defining the short-hand notation

$$\int d\Gamma_{\mathrm{i}} := \int d\boldsymbol{x}^{(\mathrm{i})}\, \mathcal{P}_{\mathrm{i}}\big(\boldsymbol{x}^{(\mathrm{i})}\big) \tag{3.6}$$

for the initial phase-space average.

If we further introduce the combined microscopic field $\psi := (\boldsymbol{x}, \boldsymbol{\chi})$ and define the microscopic action

$$S_{\psi}[\psi] := \boldsymbol{\chi} \cdot E[\boldsymbol{x}]\,, \tag{3.7}$$

then the partition function takes a form resembling the path integral in conventional nonequilibrium quantum and statistical field theories very closely,

$$Z = \int d\Gamma_{\mathrm{i}} \int\limits_{\boldsymbol{x}^{(\mathrm{i})}} \mathcal{D}\psi\; \mathrm{e}^{\mathrm{i}S_{\psi}[\psi]}\,. \tag{3.8}$$

Note that the equations of motion are recovered if we require the variation of the action S_{ψ} with respect to the auxiliary field $\boldsymbol{\chi}$ to vanish,

$$0 \stackrel{!}{=} \frac{\delta S_{\psi}[\psi]}{\delta \boldsymbol{\chi}} = E[\boldsymbol{x}]\,. \tag{3.9}$$

---

[1]See [46] for an example of how to treat dynamics with non-constant Jacobian determinant.

The equations of motion of the systems we are interested in are first-order differential equations and can hence be written as

$$E[\boldsymbol{x}] = \dot{\boldsymbol{x}} + E_0[\boldsymbol{x}] + E_I[\boldsymbol{x}] \,, \tag{3.10}$$

where E_0 gathers all contributions linear in $\boldsymbol{x}$, considered to describe the free evolution of the system, and E_I collects all contributions nonlinear in $\boldsymbol{x}$, which we interpret as interactions.[2] In that case the microscopic action also splits into a free and an interacting part,

$$S_\psi[\psi] = S_{\psi,0}[\psi] + S_{\psi,I}[\psi] \tag{3.11}$$

where

$$S_{\psi,0}[\psi] := \boldsymbol{\chi} \cdot \left(\dot{\boldsymbol{x}} + E_0[\boldsymbol{x}] \right) \,, \tag{3.12}$$

$$S_{\psi,I}[\psi] := \boldsymbol{\chi} \cdot E_I[\boldsymbol{x}] \,. \tag{3.13}$$

For this class of equations of motion, it has been shown in [45] that the Jacobian determinant appearing in (3.4) can be written as

$$\det\left[\frac{\delta E[\boldsymbol{x}(t)]}{\delta \boldsymbol{x}(t')} \right] = \exp\left\{ -\frac{1}{2} \int\limits_0^\infty \mathrm{d}t \int\limits_0^\infty \mathrm{d}t' \, \mathrm{tr}\, \frac{\delta\left(E_0[\boldsymbol{x}(t)] + E_I[\boldsymbol{x}(t)] \right)}{\delta \boldsymbol{x}(t')} \right\} \,, \tag{3.14}$$

where the trace runs over all components of $\boldsymbol{x}$. Using this relation, we can explicitly check our assumption of the Jacobian determinant being constant for all types of dynamics considered in this thesis.

A fact that we will make regular use of is that the non-interacting equations of motion, due to their linearity, can always be solved in terms of a retarded Green's function $\boldsymbol{G}$,

$$\boldsymbol{x}^{(0)}\left(\boldsymbol{x}^{(i)}, t\right) := \boldsymbol{x}^{(cl)}\left(\boldsymbol{x}^{(i)}, t\right)\Big|_{E_I=0} = \boldsymbol{G}(t, t_i)\,\boldsymbol{x}^{(i)} \,, \tag{3.15}$$

with

$$\boldsymbol{G}(t, t') := G(t, t') \otimes \mathcal{I}_N \propto \theta(t - t') \,, \tag{3.16}$$

where $\mathcal{I}_N$ denotes the N-dimensional identity matrix. The free evolution of any system is thus always fully characterised by specifying the initial phase-space probability distribution $\mathcal{P}_i$, describing the initial conditions, and the single-particle Green's function G, describing the free dynamics.

In this thesis we will mostly consider Hamiltonian systems, whose phase-space is spanned by the particles' positions and momenta, $\vec{x}_j(t) = \left(\vec{q}_j(t), \vec{p}_j(t) \right)$. Accordingly, the conjugate auxiliary fields take the form $\vec{\chi}_j = (\vec{\chi}_{q_j}, \vec{\chi}_{p_j})$, and it is useful to gather the individual position and momentum components $\vec{q}_j, \vec{p}_j, \vec{\chi}_{q_j}$ and $\vec{\chi}_{p_j}$ into their own N-particle tensors $\boldsymbol{q}, \boldsymbol{p}, \boldsymbol{\chi}_q$ and $\boldsymbol{\chi}_p$, respectively.

The dynamics of such a system is governed by Hamilton's equations,

$$0 = E[\boldsymbol{x}] = \dot{\boldsymbol{x}} - \mathcal{J} \boldsymbol{\nabla}_{\boldsymbol{x}} \mathcal{H}[\boldsymbol{x}], \qquad \mathcal{J} := \begin{pmatrix} 0 & \mathcal{I}_3 \\ -\mathcal{I}_3 & 0 \end{pmatrix} \otimes \mathcal{I}_N \,, \tag{3.17}$$

---

[2]We should point out that the distinction between free and interacting terms simply by their linearity or nonlinearity is not always applicable. Interactions via an harmonic potential, for example, would correspond to linear terms in the Hamiltonian. For all systems considered in this thesis, though, there is no such ambiguity.

whose Jacobian determinant (3.14) is always equal to unity, as the trace over the symplectic matrix $\mathcal{J}$ vanishes identically. Note that this statement is equivalent to Liouville's theorem [49]. The Hamiltonian shall take the form $\mathcal{H} = \mathcal{H}_0 + \mathcal{H}_I$, with $\mathcal{H}_0$ being at most quadratic in $\boldsymbol{x}$, describing the free evolution, and $\mathcal{H}_I$ containing all interaction terms. In addition, we restrict ourselves to systems without external forces and assume that $\mathcal{H}_I$ is the total potential energy generated by a superposition of single-particle potentials $v(q, t)$ acting between all individual particles,

$$\mathcal{H}_I[\boldsymbol{x}(t)] = \mathcal{H}_I[\boldsymbol{q}(t)] := \frac{1}{2} \sum_{\substack{j,k=1 \\ j \neq k}}^{N} v\left(|\vec{q}_j - \vec{q}_k|, t\right) . \tag{3.18}$$

Then, the free and interacting parts of the action become

$$S_{\psi,0}[\psi] = \boldsymbol{\chi} \cdot \left(\dot{\boldsymbol{x}} - \mathcal{J} \boldsymbol{\nabla}_{\boldsymbol{x}} \mathcal{H}_0[\boldsymbol{x}]\right) , \tag{3.19}$$

$$S_{\psi,I}[\psi] = \boldsymbol{\chi}_{\boldsymbol{p}} \cdot \boldsymbol{\nabla}_{\boldsymbol{q}} \mathcal{H}_I[\boldsymbol{q}], \tag{3.20}$$

where we explicitly used that $\mathcal{H}_I$ only depends on the particle positions. If we further define the different components of the single-particle Green's function as

$$\mathcal{G}(t, t') := \begin{pmatrix} g_{qq}(t, t')\, \mathcal{I}_3 & g_{qp}(t, t')\, \mathcal{I}_3 \\ g_{pq}(t, t')\, \mathcal{I}_3 & g_{pp}(t, t')\, \mathcal{I}_3 \end{pmatrix} , \tag{3.21}$$

the complete dynamics of such a system is fully characterised by the five functions g_{qq}, g_{qp}, g_{pq}, g_{pp} and v.

3.1.2. Collective fields

Usually, one is not interested in the microscopic state of the system but rather in its macroscopic properties. For this purpose, it is useful to introduce some collective fields $\Phi[\psi]$ whose cumulants, i. e. connected correlation functions, will contain the desired macroscopic information. Following [48], we choose $\Phi := \left(\Phi_f, \Phi_B\right)$ with Φ_f being the Klimontovich phase-space density and Φ_B the phase-space response field,

$$\Phi_f\left(\vec{x}, t\right) := \sum_{j=1}^{N} \delta_D\left(\vec{q} - \vec{q}_j(t)\right)\, \delta_D\left(\vec{p} - \vec{p}_j(t)\right) , \tag{3.22}$$

$$\Phi_B\left(\vec{x}, t\right) := \sum_{j=1}^{N} \vec{\chi}_{p_j}(t) \cdot \vec{\nabla}_q\, \delta_D\left(\vec{q} - \vec{q}_j(t)\right)\, \delta_D\left(\vec{p} - \vec{p}_j(t)\right) . \tag{3.23}$$

The latter encodes how the particle momenta are changed by a given interaction potential. For our purposes it will be more convenient to work in the Fourier space conjugate to phase-space, with $\vec{s} := (\vec{k}, \vec{l}\,)$ denoting the Fourier vector conjugate to $\vec{x} = (\vec{q}, \vec{p})$. The corresponding Fourier

transforms of the two collective fields are given by

$$\Phi_f(\vec{s}, t) = \sum_{j=1}^{N} e^{-i\vec{k}\cdot\vec{q}_j(t) - i\vec{l}\cdot\vec{p}_j(t)}, \tag{3.24}$$

$$\Phi_B(\vec{s}, t) = \sum_{j=1}^{N} \vec{\chi}_{p_j}(t) \cdot i\vec{k} \, e^{-i\vec{k}\cdot\vec{q}_j(t) - i\vec{l}\cdot\vec{p}_j(t)}. \tag{3.25}$$

The collective fields Φ_f and Φ_B allow us to express the interacting part of the action defined in (3.20) as

$$S_{\psi,\mathrm{I}}[\psi] = \int\mathrm{d}1 \int\mathrm{d}2 \, \Phi_f(-1)\,\sigma_{fB}(1, -2)\,\Phi_B(2), \tag{3.26}$$

where we used the conventional abbreviations $(\pm r) := (\pm\vec{s}_r, t_r)$ as well as

$$\int\mathrm{d}r := \int\frac{\mathrm{d}^6 s_r}{(2\pi)^6} \int_{t_\mathrm{i}}^{\infty}\mathrm{d}t_r, \tag{3.27}$$

and defined the interaction matrix element

$$\sigma_{fB}(1, 2) = \sigma_{Bf}(2, 1) := -v(k_1, t_1)\,(2\pi)^3\,\delta_\mathrm{D}(\vec{k}_1 + \vec{k}_2)\,(2\pi)^3\,\delta_\mathrm{D}(\vec{l}_1)\,(2\pi)^3\,\delta_\mathrm{D}(\vec{l}_2)\,\delta_\mathrm{D}(t_1 - t_2). \tag{3.28}$$

The delta functions of $\vec{l}_1$ and $\vec{l}_2$ appearing in (3.28) are a consequence of the interaction potential being independent of the particle momenta.

As we will frequently encounter integrals over 1- and 2-point functions similar to those in (3.26), introducing a short-hand notation for these will greatly improve the clarity of the calculations. For general 1-point functions $A_1(1)$, $B_1(1)$ and 2-point functions $A_2(1, 2)$, $B_2(1, 2)$ we thus define their dot products as

$$A_1 \cdot B_1 := \int\mathrm{d}\bar{1} \, A_1(-\bar{1})\,B_1(\bar{1}), \tag{3.29}$$

$$(A_2 \cdot B_1)(1) := \int\mathrm{d}\bar{1} \, A_2(1, -\bar{1})\,B_1(\bar{1}), \tag{3.30}$$

$$(A_1 \cdot B_2)(1) := \int\mathrm{d}\bar{1} \, A_1(-\bar{1})\,B_2(\bar{1}, 1), \tag{3.31}$$

$$(A_2 \cdot B_2)(1, 2) := \int\mathrm{d}\bar{1} \, A_2(1, -\bar{1})\,B_2(\bar{1}, 2). \tag{3.32}$$

Using this notation, the interacting part of the action condenses to

$$S_{\psi,\mathrm{I}}[\psi] = \Phi_f \cdot \sigma_{fB} \cdot \Phi_B. \tag{3.33}$$

We can now construct the generating functional of collective-field correlators by introducing the source field $H := (H_f, H_B)$ conjugate to the combined collective field Φ into the partition function (3.8),

$$Z_\Phi[H] := \int\mathrm{d}\Gamma_\mathrm{i} \int_{x^{(\mathrm{i})}} \mathcal{D}\psi \, e^{iS_{\psi,0}[\psi] + i\Phi_f[\psi]\cdot\sigma_{fB}\cdot\Phi_B[\psi] + iH\cdot\Phi[\psi]}. \tag{3.34}$$

Functional derivatives of its logarithm $W_\Phi[H] := \ln Z_\Phi[H]$ with respect to the source field H, evaluated at $H = 0$, yield the collective-field cumulants, i.e. the connected collective-field correlation functions,

$$G_{f\cdots fB\cdots B}(1,\ldots,n_f,1',\cdots,n'_B) := \left\langle \Phi_f(1)\cdots\Phi_f(n_f)\,\Phi_B(1')\cdots\Phi_B(n'_B)\right\rangle_{\mathrm{c}} \tag{3.35}$$

$$= \frac{\delta}{\mathrm{i}\delta H_f(1)}\cdots\frac{\delta}{\mathrm{i}\delta H_f(n_f)}\frac{\delta}{\mathrm{i}\delta H_B(1')}\cdots\frac{\delta}{\mathrm{i}\delta H_B(n'_B)}\,W_\Phi[H]\bigg|_{H=0}. \tag{3.36}$$

Any macroscopic physical observable of the system can then be derived from the pure phase-space density cumulants $G_{f\cdots f}$. Of particular interest are their momentum moments. In real space, these can be computed by multiplying an n_f-point phase-space density cumulant with an appropriate function of the momenta, $F_p(\vec{p}_1,\ldots,\vec{p}_{n_f})$, before integrating over these arguments. In Fourier space, this translates to applying the derivative operator

$$\hat{F}_p := F_p\left(\mathrm{i}\frac{\partial}{\partial\vec{l}_1},\ldots,\mathrm{i}\frac{\partial}{\partial\vec{l}_{n_f}}\right)\Bigg|_{\vec{l}_1=\cdots=\vec{l}_{n_f}=0}. \tag{3.37}$$

In the simplest case $F_p = 1$ this reduces a phase-space density cumulant to a cumulant of the spatial number density field Φ_ρ,

$$G_{\rho\cdots\rho}(\vec{k}_1,t_1,\ldots,\vec{k}_{n_f},t_{n_f}) = G_{f\cdots f}(1,\ldots,n_f)\Big|_{\vec{l}_1=\cdots=\vec{l}_{n_f}=0}. \tag{3.38}$$

For interacting particles, the collective cumulants can generally only be computed perturbatively. This assumes that the non-interacting theory, described by the free generating functional

$$Z_{\Phi,0}[H] := \int \mathrm{d}\Gamma_\mathrm{i}\int_{x^{(\mathrm{i})}}\mathcal{D}\psi\;\mathrm{e}^{\mathrm{i}S_{\psi,0}[\psi]+\mathrm{i}H\cdot\Phi[\psi]}, \tag{3.39}$$

is exactly solvable in the sense that the free collective-field cumulants

$$G^{(0)}_{f\cdots fB\cdots B}(1,\ldots,n_f,1',\cdots,n'_B) = \frac{\delta}{\mathrm{i}\delta H_f(1)}\cdots\frac{\delta}{\mathrm{i}\delta H_f(n_f)}\frac{\delta}{\mathrm{i}\delta H_B(1')}\cdots\frac{\delta}{\mathrm{i}\delta H_B(n'_B)}\,W_{\Phi,0}[H]\bigg|_{H=0} \tag{3.40}$$

are exactly known. Here, we defined $W_{\Phi,0}[H] := \ln Z_{\Phi,0}[H]$.

If this is the case, one possible way to proceed is to pull the interacting part of the action in front of the path integral by replacing its Φ-dependence with functional derivatives with respect to H, acting on the free generating functional $Z_{\Phi,0}[H]$,

$$Z_\Phi[H] = \mathrm{e}^{\mathrm{i}\frac{\delta}{\mathrm{i}\delta H_f}\cdot\sigma_{fB}\cdot\frac{\delta}{\mathrm{i}\delta H_B}}\,Z_{\Phi,0}[H]. \tag{3.41}$$

Expanding the exponential then yields a perturbative series that allows to calculate the interacting collective-field cumulants up to a finite order in σ_{fB}, and hence in the interaction potential v,

only requiring the computation of a finite number of free cumulants. This approach has been discussed in detail in [1, 2] and we will refer to it as the *microscopic perturbation theory*.

The reformulation of KFT that we will present in section 3.2 also requires the knowledge of the free collective cumulants. However, for that purpose it will prove more natural to work with free cumulants involving the *dressed response field*

$$\Phi_{\mathcal{F}}(1) := (\sigma_{fB} \cdot \Phi_B)(1) = \int d\bar{1} \, \sigma_{fB}(1, -\bar{1}) \, \Phi_B(\bar{1}) \tag{3.42}$$

rather than the bare response field Φ_B. The reason for this is that in the calculation of pure phase-space density cumulants $G_{f \dots f}$ every occurrence of the field Φ_B will always be dressed with an interaction matrix element σ_{fB} anyway. This is because Φ_B appears in Z_Φ only via the interaction term $S_{\psi,\mathrm{I}} = \Phi_f \cdot \sigma_{fB} \cdot \Phi_B$ once we set H_B to zero. If we further re-express $S_{\psi,\mathrm{I}}$ more abstractly in terms of $\Phi_{\mathcal{F}}$,

$$S_{\psi,\mathrm{I}}[\psi] = \Phi_f \cdot \Phi_{\mathcal{F}}, \tag{3.43}$$

it will facilitate the extension of our formalism to non-Hamiltonian systems, as we will discuss in more detail in chapter 5, where we will apply KFT to systems governed by fluid dynamics.

Let us thus define the dressed combined collective field $\tilde{\Phi} := (\Phi_f, \Phi_{\mathcal{F}})$ and its conjugate source field $\tilde{H} := (H_f, H_{\mathcal{F}})$ to construct the generating functional of dressed free collective-field correlators,

$$Z_{\tilde{\Phi},0}[\tilde{H}] := \int d\Gamma_{\mathrm{i}} \int_{x^{(\mathrm{i})}} \mathcal{D}\psi \, e^{iS_{\psi,0}[\psi] + iH \cdot \tilde{\Phi}[\psi]} . \tag{3.44}$$

The respective dressed cumulants can then be obtained either directly from $W_{\tilde{\Phi},0}[\tilde{H}] := \ln Z_{\tilde{\Phi},0}[\tilde{H}]$ or via their relation to the bare cumulants,

$$G^{(0)}_{f \dots f \mathcal{F} \dots \mathcal{F}}(1, \dots, n_f, 1', \cdots, n'_{\mathcal{F}}) := \frac{\delta}{i\delta H_f(1)} \cdots \frac{\delta}{i\delta H_f(n_f)} \frac{\delta}{i\delta H_{\mathcal{F}}(1')} \cdots \frac{\delta}{i\delta H_{\mathcal{F}}(n'_B)} W_{\tilde{\Phi},0}[\tilde{H}] \bigg|_{\tilde{H}=0} \tag{3.45}$$

$$= \prod_{r=1}^{n_{\mathcal{F}}} \left(\int d\bar{r} \, \sigma_{fB}(r', -\bar{r}) \right) G^{(0)}_{f \dots f B \dots B}(1, \dots, n_f, \bar{1}, \dots, \bar{n}_{\mathcal{F}}) . \tag{3.46}$$

3.1.3. Non-interacting theory

Before we can discuss the properties of the free collective-field cumulants in more detail we need to specify the initial phase-space probability distribution $\mathcal{P}_{\mathrm{i}}$ of the systems we want to investigate. In section 2.2 we argued that the initial conditions of cosmic structure formation are well described by a statistically homogeneous and isotropic distribution of matter with appropriately correlated Gaussian density and momentum fluctuations. This means that the initial macroscopic density contrast and momentum fields $\delta^{(\mathrm{i})}$ and $\vec{P}^{(\mathrm{i})}$ together form a Gaussian random field with zero mean and covariance matrix

$$\begin{pmatrix} C_{\delta_j \delta_k} & \vec{C}^\top_{\delta_j p_k} \\ \vec{C}_{p_j \delta_k} & C_{p_j p_k} \end{pmatrix} := \begin{pmatrix} \langle \delta^{(\mathrm{i})}(\vec{q}_j) \, \delta^{(\mathrm{i})}(\vec{q}_k) \rangle & \langle \delta^{(\mathrm{i})}(\vec{q}_j) \, \vec{P}^{(\mathrm{i})}(\vec{q}_k) \rangle^\top \\ \langle \vec{P}^{(\mathrm{i})}(\vec{q}_j) \, \delta^{(\mathrm{i})}(\vec{q}_k) \rangle & \langle \vec{P}^{(\mathrm{i})}(\vec{q}_j) \otimes \vec{P}^{(\mathrm{i})}(\vec{q}_k) \rangle \end{pmatrix} . \tag{3.47}$$

As shown in [1], the corresponding initial phase-space distribution of the microscopic particles is then obtained via a Poisson sampling of the macroscopic field distribution. It reads

$$\mathcal{P}_{\mathrm{i}}\big(\boldsymbol{x}^{(\mathbf{i})}\big) = \frac{V^{-N}}{\sqrt{(2\pi)^{dN}\det \boldsymbol{C_{pp}}}} \, C\!\left(\frac{\partial}{\mathrm{i}\partial \boldsymbol{p}^{(\mathbf{i})}}\right) \mathrm{e}^{-\frac{1}{2}\boldsymbol{p}^{(\mathbf{i})\mathsf{T}}\boldsymbol{C_{pp}}^{-1}\boldsymbol{p}^{(\mathbf{i})}}\,, \tag{3.48}$$

where V denotes the system's volume and we introduced the momentum correlation tensor $\boldsymbol{C_{pp}} = C_{p_j p_k}\otimes(\vec{e}_j\otimes\vec{e}_k)$ as well as the polynomial operator

$$C\!\left(\frac{\partial}{\mathrm{i}\partial \boldsymbol{p}^{(\mathbf{i})}}\right) = \prod_{n=1}^{N}\left(1 - \mathrm{i}\sum_{m=1}^{N}\vec{C}_{\delta_n p_m}\cdot\frac{\partial}{\mathrm{i}\vec{p}_m^{(\mathbf{i})}}\right) + \sum_{i<j}C_{\delta_i\delta_j}\prod_{\substack{n=1\\ n\neq i,j}}^{N}\left(1 - \mathrm{i}\sum_{m=1}^{N}\vec{C}_{\delta_n p_m}\cdot\frac{\partial}{\mathrm{i}\vec{p}_m^{(\mathbf{i})}}\right) + \cdots\,, \tag{3.49}$$

containing the density and density-momentum correlations.

Statistical homogeneity and isotropy imply that the covariance matrix can only depend on the spatial distance $|\vec{q}_{jk}| := |\vec{q}_j - \vec{q}_k|$ between two points. If we further use that the initial momentum field is irrotational and related to the density contrast field via the continuity equation, as argued in [1], we can express all components of the initial covariance matrix in terms of the initial density contrast power spectrum $P_\delta^{(\mathrm{i})}$,

$$C_{\delta_j\delta_k} = \int\frac{\mathrm{d}^3 k}{(2\pi)^3}\,\mathrm{e}^{\mathrm{i}\vec{k}\cdot\vec{q}_{jk}}\,P_\delta^{(\mathrm{i})}(k)\,, \tag{3.50}$$

$$\vec{C}_{p_j\delta_k} = \vec{C}_{\delta_j p_k} = \int\frac{\mathrm{d}^3 k}{(2\pi)^3}\,\mathrm{e}^{\mathrm{i}\vec{k}\cdot\vec{q}_{jk}}\,P_\delta^{(\mathrm{i})}(k)\,\frac{\mathrm{i}\vec{k}}{k^2}\,, \tag{3.51}$$

$$C_{p_j p_k} = \int\frac{\mathrm{d}^3 k}{(2\pi)^3}\,\mathrm{e}^{\mathrm{i}\vec{k}\cdot\vec{q}_{jk}}\,P_\delta^{(\mathrm{i})}(k)\,\frac{\vec{k}\otimes\vec{k}}{k^4}\,. \tag{3.52}$$

The explicit computation of the free cumulants corresponding to these initial conditions, be they dressed or bare, is rather involved. A thorough treatment of this can be found in [48], where a diagrammatic approach inspired by the Mayer cluster expansion [50] was developed to compute them systematically. In Appendix B we list the resulting expressions for the free 1- to 4-point cumulants used in this thesis. Let us further summarise their physical interpretation and a few of their general properties derived in [48], which we will make frequent use of throughout this thesis:

1. The cumulant $G_{f\cdots f}^{(0)}(1,\ldots,n_f)$ is the connected n_f-point correlation of the phase-space density observed at times $t_1,\ldots,t_{n_f}$ that emerges from the ensemble average over the initially correlated, freely evolving particles. The cumulant $G_{f\cdots f\mathcal{F}\cdots\mathcal{F}}^{(0)}(1,\ldots,n_f,1',\ldots,n'_{\mathcal{F}})$, on the other hand, is the $n_{\mathcal{F}}$-th order response of this n_f-point correlation to perturbations of the non-interacting system at times $t_{1'},\ldots,t_{n'_{\mathcal{F}}}$. If $n_{\mathcal{F}} = 1$, this is a linear response. Microscopically, these perturbations correspond to particles being deflected from their free trajectories by the forces $-\vec{\nabla}v$ acting between them and other particles. In Fourier space, this leads to the proportionality

$$G_{f\cdots f\mathcal{F}\cdots\mathcal{F}}^{(0)}(1,\ldots,n_f,1',\ldots,n'_{\mathcal{F}}) \propto -\mathrm{i}\vec{k}_{r'}\,v(k_{r'},t_{r'})\,(2\pi)^3\,\delta_{\mathrm{D}}\big(\vec{l}_{r'}\big) \quad \forall\, r'\in\{1',\ldots,n'_{\mathcal{F}}\}\,. \tag{3.53}$$

2. Causality tells us that the phase-space density $\Phi_f(u)$ evaluated at some time t_u can only respond to perturbations experienced at earlier times $t_{r'} \leq t_u$. A more detailed analysis further shows that the spatial density $\Phi_\rho(\vec{k}_u, t_u) = \Phi_f(u)\big|_{\vec{l}_u = 0}$ can in fact only respond to perturbations experienced at strictly earlier times $t_{r'} < t_u$. On the level of the free cumulants this manifests itself in the property

$$G^{(0)}_{f\cdots f\mathcal{F}\cdots\mathcal{F}}(1, \ldots, n_f, 1', \ldots, n'_{\mathcal{F}}) = 0 \quad \text{if} \quad \exists\, r' \in \{1', \ldots, n'_{\mathcal{F}}\}$$
$$\text{such that} \;\; (t_{r'} > t_u) \;\; \text{or} \;\; (t_{r'} = t_u \text{ and } \vec{l}_u = 0) \quad \forall\, u \in \{1, \ldots, n_f\}\,. \tag{3.54}$$

In particular, every free pure $\Phi_{\mathcal{F}}$-cumulant vanishes identically,

$$G^{(0)}_{\mathcal{F}\cdots\mathcal{F}}(1', \ldots, n'_{\mathcal{F}}) = 0\,. \tag{3.55}$$

3. In statistically homogeneous systems, a free collective-field cumulant containing n_f phase-space density fields is given by a sum of individual free ℓ-particle cumulants with $1 \leq \ell \leq n_f$,

$$G^{(0)}_{f\cdots f\mathcal{F}\cdots\mathcal{F}}(1, \ldots, n_f, 1', \ldots, n'_{\mathcal{F}}) = \sum_{\ell=1}^{n_f} G^{(0,\ell)}_{f\cdots f\mathcal{F}\cdots\mathcal{F}}(1, \ldots, n_f, 1', \ldots, n'_{\mathcal{F}})\,, \tag{3.56}$$

describing the contribution from correlations between ℓ particles. They satisfy

$$G^{(0,\ell)}_{f\cdots f\mathcal{F}\cdots\mathcal{F}}(1, \ldots, n_f, 1', \ldots, n'_{\mathcal{F}}) \propto \bar{\rho}^\ell (2\pi)^3 \delta_{\mathrm{D}}\big(\vec{k}_{1'} + \cdots + \vec{k}_{n'_{\mathcal{F}}} + \vec{k}_1 + \cdots + \vec{k}_{n_f}\big)\,, \tag{3.57}$$

where $\bar{\rho}$ denotes the constant mean number density and the delta function arises due to the translational invariance in statistically homogeneous systems. Note that all ℓ-particle cumulants with $\ell < n_f$ describe shot-noise contributions, arising due to the discrete nature of the density field. In the thermodynamic limit $N \to \infty$ these become negligible relative to the dominant term proportional to $\bar{\rho}^{n_f}$.

3.2. Resummed KFT

From the perspective of most quantum and statistical field theories, the KFT partition function (3.8) is rather unusual in the sense that the fields in which the path integral is expressed, i. e. the microscopic fields ψ, are different from our actual macroscopic fields of interest. This renders the application of many well-established perturbative as well as non-perturbative field theoretic tools rather difficult. Because of that, we developed in [3] a reformulation of the KFT partition function as a path integral over the macroscopic spatial density field. This additionally gave rise to a new perturbative approach to KFT which resums parts of the microscopic perturbation series.

In this section we present a substantially revised and extended derivation of this macroscopic reformulation that allows to extract cumulants of the full phase-space density. Furthermore, we demonstrate its application for a simple test system to illustrate the physical meaning of the resummation procedure involved.

3.2.1. Macroscopic action

To reformulate the partition function (3.8) as a path integral over macroscopic fields, we exploit the exact solvability of the free theory and the fact that the interacting part of the action (3.43) depends on the microscopic fields ψ only implicitly via the dressed collective fields $\tilde{\Phi}[\psi]$. We begin by introducing a functional delta distribution to replace the explicitly ψ-dependent field $\Phi_f[\psi]$ with a new formally ψ-independent field f,

$$Z = \int \mathrm{d}\Gamma_\mathrm{i} \int_{\boldsymbol{x}^{(\mathrm{i})}} \mathcal{D}\psi \int \mathcal{D}f \; \mathrm{e}^{\mathrm{i}S_{\psi,0}[\psi]+\mathrm{i}f\cdot\Phi_{\mathcal{F}}[\psi]} \, \delta_\mathrm{D}\big[f - \Phi_f[\psi]\big] \, . \tag{3.58}$$

Note that the delta distribution ensures that this new field f effectively still carries all the information of $\Phi_f[\psi]$. Most importantly, f- and Φ_f-correlation functions are precisely the same. But to emphasise the different origin we will deliberately call f the macroscopic and Φ_f the collective phase-space density field in the following.

Similar to what we did in (3.5), we can now express the delta distribution as a functional Fourier transform with respect to a new macroscopic auxiliary field β conjugate to f,

$$Z = \int \mathrm{d}\Gamma_\mathrm{i} \int_{\boldsymbol{x}^{(\mathrm{i})}} \mathcal{D}\psi \int \mathcal{D}f \int \mathcal{D}\beta \; \mathrm{e}^{\mathrm{i}S_{\psi,0}[\psi]+\mathrm{i}f\cdot\Phi_{\mathcal{F}}[\psi]-\mathrm{i}\beta\cdot(f-\Phi_f[\psi])} \, . \tag{3.59}$$

Pulling all ψ-independent parts to the front, we find that the remaining microscopic part of the path integral precisely takes the form of the free generating functional $Z_{\tilde{\Phi},0}$,

$$Z = \int \mathcal{D}f \int \mathcal{D}\beta \, \mathrm{e}^{-\mathrm{i}\beta\cdot f} \int \mathrm{d}\Gamma_\mathrm{i} \int_{\boldsymbol{x}^{(\mathrm{i})}} \mathcal{D}\psi \; \mathrm{e}^{\mathrm{i}S_{\psi,0}[\psi]+\mathrm{i}\beta\cdot\Phi_f[\psi]+\mathrm{i}f\cdot\Phi_{\mathcal{F}}[\psi]} \tag{3.60}$$

$$= \int \mathcal{D}\phi \; \mathrm{e}^{-\mathrm{i}\beta\cdot f} Z_{\tilde{\Phi},0}\big[\tilde{\phi}\big] \tag{3.61}$$

where we defined the macroscopic field vectors $\phi := (f,\beta)$ and $\tilde{\phi} = (\beta,f)$. It is $\tilde{\phi}$ which now plays the role of the dressed collective source field $\tilde{H}$ introduced in subsection 3.1.3.

Finally, using $W_{\tilde{\Phi},0} = \ln Z_{\tilde{\Phi},0}$, we arrive at our desired result,

$$Z = \int \mathcal{D}\phi \; \mathrm{e}^{\mathrm{i}S_\phi[\phi]} \tag{3.62}$$

with the macroscopic action

$$S_\phi[\phi] := -f\cdot\beta - \mathrm{i}W_{\tilde{\Phi},0}\big[\tilde{\phi}\big] \, . \tag{3.63}$$

We want to emphasise that this reformulation is *exact* and hence (3.62) still contains the complete information on the microscopic dynamics, even though S_ϕ does not depend on ψ any more. The microscopic information is now encoded in the free generating functional $W_{\tilde{\Phi},0}\big[\tilde{\phi}\big]$ and thus, by

means of a functional Taylor expansion, in the dressed free collective-field cumulants,

$$W_{\tilde{\Phi},0}[\tilde{\phi}] = \sum_{n_\beta, n_f=0}^{\infty} \frac{1}{n_\beta! \, n_f!} \prod_{u=1}^{n_\beta} \left(\int du \, \beta(-u) \frac{\delta}{\delta H_f(u)} \right) \prod_{r=1}^{n_f} \left(\int dr' \, f(-r') \frac{\delta}{\delta H_{\mathcal{F}}(r')} \right) W_{\tilde{\Phi},0}[\tilde{H}] \Big|_{\tilde{H}=0}$$

(3.64)

$$= \sum_{n_\beta, n_f=0}^{\infty} \frac{i^{n_\beta+n_f}}{n_\beta! \, n_f!} \prod_{u=1}^{n_\beta} \left(\int du \, \beta(-u) \right) \prod_{r=1}^{n_f} \left(\int dr' \, f(-r') \right) G_{f\cdots f \mathcal{F}\cdots \mathcal{F}}^{(0)}(1,\ldots,n_f,1',\ldots,n'_{\mathcal{F}}).$$

(3.65)

3.2.2. Macroscopic propagator and vertices

The path integral in the form of (3.62) allows us to set up a new perturbative approach to KFT following the standard procedure in quantum and statistical field theory, i. e. in terms of propagators and vertices. For this purpose, we first split up the action (3.63) into the parts which are quadratic in ϕ and those which are not,

$$iS_\phi[\phi] \overset{!}{=} iS_\Delta[\phi] + iS_{\mathcal{V}}[\phi] \tag{3.66}$$

$$:= -\frac{1}{2} \int d1 \int d2 \, (f,\beta)(-1) \begin{pmatrix} (\Delta^{-1})_{ff} & (\Delta^{-1})_{f\beta} \\ (\Delta^{-1})_{\beta f} & (\Delta^{-1})_{\beta\beta} \end{pmatrix}(1,2) \begin{pmatrix} f \\ \beta \end{pmatrix}(-2)$$

$$+ \sum_{\substack{n_\beta, n_f=0 \\ n_\beta+n_f \neq 2}}^{\infty} \frac{1}{n_\beta! \, n_f!} \prod_{u=1}^{n_\beta} \left(\int du \, \beta(-u) \right) \prod_{r=1}^{n_f} \left(\int dr' \, f(-r') \right) \mathcal{V}_{\beta\cdots\beta f\cdots f}(1,\ldots,n_\beta,1',\ldots,n'_f),$$

(3.67)

introducing the inverse macroscopic propagator Δ^{-1} and the macroscopic $(n_\beta + n_f)$-point vertices $\mathcal{V}_{\beta\cdots\beta f\cdots f}$.

Furthermore, we define the macroscopic generating functional Z_ϕ by introducing a source field $M = (M_f, M_\beta)$ conjugate to ϕ into the partition function,

$$Z_\phi[M] := \int \mathcal{D}\phi \; e^{iS_\phi[\phi]+iM\cdot\phi} \,. \tag{3.68}$$

Then, the vertex part of the action can be pulled in front of the path integral by replacing its ϕ-dependence with functional derivatives with respect to M, $\hat{S}_{\mathcal{V}} := S_{\mathcal{V}}\left[\frac{\delta}{i\delta M}\right]$, acting on the remaining path integral,

$$Z_\phi[M] = e^{i\hat{S}_{\mathcal{V}}} \int \mathcal{D}\phi \; e^{-\frac{1}{2}\phi\cdot\Delta^{-1}\cdot\phi+iM\cdot\phi} \tag{3.69}$$

$$= e^{i\hat{S}_{\mathcal{V}}} \, e^{\frac{1}{2}(iM)\cdot\Delta\cdot(iM)} \,. \tag{3.70}$$

Expanding the first exponential in (3.70) in orders of the vertices now gives rise to a new perturbative approach that we will refer to as the *macroscopic perturbation theory*.

Within this approach, the interacting macroscopic cumulants are obtained via

$$G_{f \cdots f \beta \cdots \beta}(1, \ldots, n_f, 1', \cdots, n'_\beta) = \frac{\delta}{\mathrm{i}\delta M_f(1)} \cdots \frac{\delta}{\mathrm{i}\delta M_f(n_f)} \frac{\delta}{\mathrm{i}\delta M_\beta(1')} \cdots \frac{\delta}{\mathrm{i}\delta M_\beta(n'_\beta)} W_\phi[M] \bigg|_{M=0},$$
$$(3.71)$$

where we defined the macroscopic cumulant-generating functional $W_\phi[M] := \ln Z_\phi[M]$. In particular, this implies that the lowest perturbative order of the 2-point phase-space density cumulant G_{ff}, is given by the ff-component of the macroscopic propagator

$$G_{ff}(1, 2) = \frac{\delta}{\mathrm{i}\delta M_f(1)} \frac{\delta}{\mathrm{i}\delta M_f(2)} W_\phi[M] \bigg|_{M=0} \tag{3.72}$$

$$= \Delta_{ff}(1, 2) + \text{terms involving vertices}, \tag{3.73}$$

For a systematic computation of the higher order contributions involving vertices, we first need to specify an explicit expansion scheme. We will return to this at the end of subsection 3.2.4 after we will have introduced a diagrammatic representation for the propagators and vertices, and investigated the general properties of the macroscopic perturbation theory in more detail.

To find explicit expressions for Δ^{-1} and $\mathcal{V}_{f \cdots f \beta \cdots \beta}$, we insert (3.65) into (3.63) and identify terms with (3.67),

$$\Delta^{-1}(1, 2) = \begin{pmatrix} (\Delta^{-1})_{ff} & (\Delta^{-1})_{f\beta} \\ (\Delta^{-1})_{\beta f} & (\Delta^{-1})_{\beta\beta} \end{pmatrix}(1, 2) = \begin{pmatrix} G^{(0)}_{\mathcal{FF}} & \mathrm{i}\,\mathcal{I} + G^{(0)}_{\mathcal{F}f} \\ \mathrm{i}\,\mathcal{I} + G^{(0)}_{f\mathcal{F}} & G^{(0)}_{ff} \end{pmatrix}(1, 2), \tag{3.74}$$

$$\mathcal{V}_{\beta \cdots \beta f \cdots f}(1, \ldots, n_\beta, 1', \ldots, n'_f) = \mathrm{i}^{n_\beta + n_f} G^{(0)}_{f \cdots f \mathcal{F} \cdots \mathcal{F}}(1, \ldots, n_\beta, 1', \ldots, n'_f). \tag{3.75}$$

Here, $\mathcal{I}$ denotes the identity 2-point function,

$$\mathcal{I}(1, 2) := (2\pi)^3\, \delta_{\mathrm{D}}\big(\vec{k}_1 + \vec{k}_2\big)\, (2\pi)^3\, \delta_{\mathrm{D}}\big(\vec{l}_1 + \vec{l}_2\big)\, \delta_{\mathrm{D}}(t_1 - t_2). \tag{3.76}$$

Note that every β-component of an inverse propagator or vertex in (3.74) and (3.75) corresponds to an f-component of a free cumulant whereas every f-component of an inverse propagator or vertex corresponds to an $\mathcal{F}$-component of a free cumulant. Together with (3.55), this directly allows us to conclude that $(\Delta^{-1})_{ff}$ and $\mathcal{V}_{f \cdots f}$ vanish identically.

The propagator Δ is then obtained by a combined matrix and functional inversion of (3.74), defined via the following matrix integral equation,

$$\int \mathrm{d}\bar{1}\, \Delta(1, -\bar{1})\, \Delta^{-1}(\bar{1}, 2) \overset{!}{=} \mathcal{I}(1, 2)\, \mathcal{I}_2. \tag{3.77}$$

The matrix part of this inversion can be performed immediately and yields

$$\Delta(1, 2) = \begin{pmatrix} \Delta_{ff} & \Delta_{f\beta} \\ \Delta_{\beta f} & \Delta_{\beta\beta} \end{pmatrix}(1, 2) = \begin{pmatrix} \Delta_{\mathrm{R}} \cdot G^{(0)}_{ff} \cdot \Delta_{\mathrm{A}} & -\mathrm{i}\Delta_{\mathrm{R}} \\ -\mathrm{i}\Delta_{\mathrm{A}} & 0 \end{pmatrix}(1, 2), \tag{3.78}$$

where we defined the abbreviations

$$\Delta_{\mathrm{R}}(1, 2) = \Delta_{\mathrm{A}}(2, 1) := \Big(\mathcal{I} - \mathrm{i}G^{(0)}_{f\mathcal{F}}\Big)^{-1}(1, 2) \tag{3.79}$$

for the remaining functional inverses. In Appendix C we describe how these as well as Δ_{ff} can be computed explicitly for a given physical system.

But even without specifying the system it is always possible to express (3.79) formally in terms of a Neumann series by expanding the functional inverse in orders of $\mathrm{i}G^{(0)}_{f\mathcal{F}}$,

$$\Delta_{\mathrm{R}}(1, 2) = \Delta_{\mathrm{A}}(2, 1) = \sum_{n=0}^{\infty} \left(\mathrm{i}G^{(0)}_{f\mathcal{F}}\right)^{n}(1, 2) \tag{3.80}$$

$$= \mathcal{I}(1, 2) + \mathrm{i}G^{(0)}_{f\mathcal{F}}(1, 2) + \int \mathrm{d}\bar{1}\ \mathrm{i}G^{(0)}_{f\mathcal{F}}(1, -\bar{1})\,\mathrm{i}G^{(0)}_{f\mathcal{F}}(\bar{1}, 2) + \cdots . \tag{3.81}$$

Recalling $G^{(0)}_{f\mathcal{F}} = G^{(0)}_{fB} \cdot \sigma_{Bf}$ from (3.46), we can see that Δ_{R} and Δ_{A} contain terms with arbitrarily high order in σ_{Bf} and hence in the interaction potential v. Inserting them into the ff-component of (3.78) yields

$$\Delta_{ff}(1, 2) = \sum_{n_{\mathrm{A}}, n_{\mathrm{R}}=0}^{\infty} \left(\left(\left(\mathrm{i}G^{(0)}_{fB} \cdot \sigma_{Bf}\right)^{n_{\mathrm{R}}} \cdot G^{(0)}_{ff} \cdot \left(\sigma_{fB} \cdot \mathrm{i}G^{(0)}_{Bf}\right)^{n_{\mathrm{A}}}\right)(1, 2) . \tag{3.82}$$

This demonstrates that the lowest perturbative order within the macroscopic approach already captures some features which could only be described at infinitely high order within the microscopic perturbation theory. Consequently, we expect the macroscopic perturbation theory to be generally more powerful than the microscopic one.

We can make this statement more precise by recalling from (3.73) that Δ_{ff} is exactly the result we get for G_{ff} by taking no vertices into account. Due to (3.67) and (3.75) this is equivalent to computing G_{ff} while ignoring all contributions involving free n-point cumulants with $n \neq 2$. Thus, the transition from the micro- to the macroscopic formulation leads to a resummation of all contributions appearing in the microscopic perturbative series that only contain free 2-point cumulants. In a statistically homogeneous system this corresponds to a resummation of all contributions that do not lead to any mode-coupling beyond that already introduced by the free evolution.

To understand what this resummation corresponds to on the level of the microscopic particle dynamics, we need to take a closer look at the meaning of the free cumulants appearing in the propagator. From the properties 1 and 2 discussed in subsection 3.1.3 we know that $\mathrm{i}G^{(0)}_{f\mathcal{F}}(1, 2)$ describes the linear response of the phase-space density $\Phi_f(1)$ at time t_1 to particles being deflected from their free trajectories by some perturbing forces acting on them at an earlier time $t_2 \leq t_1$. The product $\mathrm{i}G^{(0)}_{f\mathcal{F}}(1, -\bar{1})\,\mathrm{i}G^{(0)}_{f\mathcal{F}}(\bar{1}, 2)$ appearing under the integral in (3.81) accordingly describes the linear response of $\Phi_f(1)$ to a situation in which the forces generated by those already deflected particles perturb the trajectories of so far still freely evolving particles at an intermediate time $t_{\bar{1}}$ with $t_2 \leq t_{\bar{1}} \leq t_1$.

This process can be repeated for any possible number of iterations n, with the deflections occurring continuously at all possible intermediate times $t_{\bar{1}}, \ldots, t_{\bar{n}}$ with $t_2 \leq t_{\bar{1}} \leq \cdots \leq t_{\bar{n}} \leq t_1$, as illustrated in Figure 3.1. Δ_{R} and Δ_{A} capture this by summing over all possible numbers of linear response cumulants $\mathrm{i}G^{(0)}_{f\mathcal{F}}$ and integrating over all intermediate times. The correct time
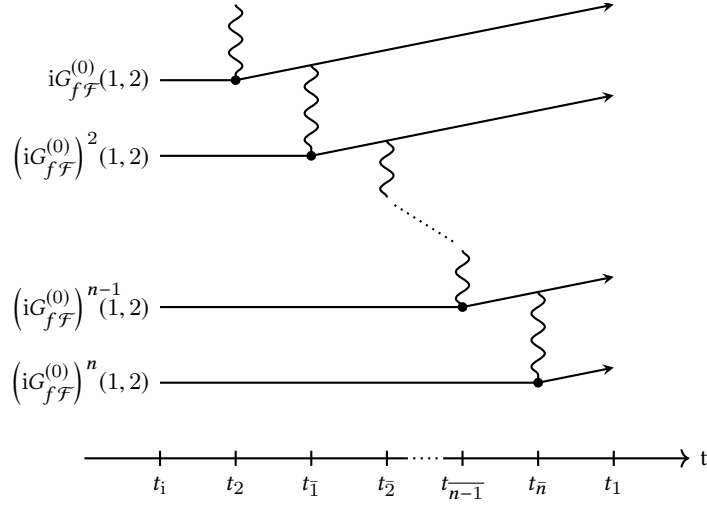
Figure 3.1.: Illustration of the microscopic particle dynamical processes resummed in the retarded propagator $\Delta_R(1,2)$. The arrows represent particle trajectories while the wavy lines depict forces acting on those particles. The different contributions to $\Delta_R(1,2)$ denoted on the left side correspond to different truncations of an iterative process where in each step particles are deflected from their free trajectories by the forces generated by the already deflected particles from the previous step. The open wavy line at the top represents the forces initiating the whole process at time t_2.

order under the integral is ensured by the property $G_{f\mathcal{F}}^{(0)}(1,2) \propto \theta(t_1 - t_2)$, following from (3.54). Consequently, we find

$$\Delta_R(1,2) = \Delta_A(2,1) = 0 \quad \text{if} \quad t_2 > t_1 \, , \tag{3.83}$$

and we will hence call Δ_R and Δ_A the *retarded and advanced (macroscopic) propagators*, respectively. If we do not want to explicitly distinguish between the two, we will refer to them more generally as the *causal (macroscopic) propagators*.

In $\Delta_{ff} = \Delta_R \cdot G_{ff}^{(0)} \cdot \Delta_A$ the forces generated by the initially correlated, freely evolving particles associated with $G_{ff}^{(0)}$ cause the perturbation needed to initiate the iterative deflection process encoded in Δ_R and Δ_A. Accordingly, it describes the connected 2-point phase-space density correlation emerging from the ensemble average over initially correlated particles that have undergone this process. We will thus call Δ_{ff} the *statistical (macroscopic) propagator* – adopting the nomenclature used in nonequilibrium quantum and statistical field theory. We want to stress that even though Δ_R and Δ_A only contain linear response cumulants, Δ_{ff} will generally contain contributions that are nonlinear in the initial phase-space density correlation, as the free-streaming of particles in $G_{ff}^{(0)}$ itself builds up those nonlinearities as long as the initial particle momenta are correlated [48].

3.2.3. A simple test system

It will prove very instructive to complement the rather abstract discussion of the macroscopic propagator's general properties in the previous subsection with an explicit example. For this,

we choose to calculate the propagator for a simple test system of N particles of mass m in static space-time, interacting via a potential v that is not explicitly time-dependent but otherwise arbitrary. The equations of motion for this system read

$$\dot{\vec{q}}_j = \frac{\vec{p}_j}{m}\,, \tag{3.84}$$

$$\dot{\vec{p}}_j = -\sum_{\substack{k=1 \\ k\neq j}}^{N} \vec{\nabla}_{q_j} v\big(|\vec{q}_j(t) - \vec{q}_k(t)|\big)\,, \tag{3.85}$$

which in the non-interacting case, $v = 0$, are solved by the Green's function (3.21) with components

$$g_{qq}(t, t') = g_{pp}(t, t') = \theta(t - t')\,, \tag{3.86}$$

$$g_{qp}(t, t') = \frac{t - t'}{m}\, \theta(t - t')\,, \tag{3.87}$$

$$g_{pq}(t, t') = 0\,, \tag{3.88}$$

as shown in Appendix A.2.

To obtain the dressed free collective-field cumulants, we further have to specify the initial conditions of our test system. The simplest non-trivial choice we can make is to consider Gaussian initial density correlations but vanishing initial momenta. The general expressions for the bare free collective-field cumulants in such a setting are listed in Appendix B.1. Inserting the interaction matrix element (3.28) and the components (3.86) to (3.88) of the Green's function into these yields

$$G_f^{(0)}(1) = (2\pi)^3\, \delta_{\mathrm{D}}\big(\vec{k}_1\big)\, \bar{\rho}\,, \tag{3.89}$$

$$G_{f\mathcal{F}}^{(0)}(1, 2) = (2\pi)^3\, \delta_{\mathrm{D}}\big(\vec{k}_1 + \vec{k}_2\big)\, (2\pi)^3\, \delta_{\mathrm{D}}\big(\vec{l}_2\big)\, \bar{\rho}\, \mathrm{i} k_1^2\, v(k_1) \left(\frac{t_1 - t_2}{m} + \frac{\vec{k}_1 \cdot \vec{l}_1}{k_1^2} \right) \theta(t_1 - t_2)\,, \tag{3.90}$$

$$G_{ff}^{(0)}(1, 2) = (2\pi)^3\, \delta_{\mathrm{D}}\big(\vec{k}_1 + \vec{k}_2\big)\, \bar{\rho}^2\, P_\delta^{(\mathrm{i})}(k_1)\,, \tag{3.91}$$

for the non-vanishing 1- and 2-point cumulants, where we further assumed to be in the thermo-dynamic limit, allowing us to neglect shot-noise contributions.

To determine the macroscopic propagator, we now first need to insert the expression (3.90) for $G_{f\mathcal{F}}^{(0)}$ into the functional inverse (3.79) defining the causal propagators Δ_{R} and Δ_{A}. In Appendix C we show how this inverse can be calculated fully analytically by means of Laplace transforms. This exploits the fact that $G_{f\mathcal{F}}^{(0)}(1, 2)$ is time-translation invariant, i.e. it only depends on t_1 and t_2 in terms of their difference. The result reads

$$\Delta_{\mathrm{R}}(1, 2) = \Delta_{\mathrm{A}}(2, 1) = \mathcal{I}(1, 2) + (2\pi)^3\, \delta_{\mathrm{D}}\big(\vec{k}_1 + \vec{k}_2\big)\, (2\pi)^3\, \delta_{\mathrm{D}}\big(\vec{l}_2\big)\, \tilde{\Delta}_{\mathrm{R}}\big(\vec{k}_1, \vec{l}_1; t_1, t_2\big)\,. \tag{3.92}$$

with

$$\tilde{\Delta}_{\mathrm{R}}\big(\vec{k}_1, \vec{l}_1; t_1, t_2\big) = -\Big[k_1 c(k_1)\, \sin\big(k_1(t_1 - t_2)\, c(k_1)\big) + m c^2(k_1)\, \vec{k}_1 \cdot \vec{l}_1\, \cos\big(k_1(t_1 - t_2)\, c(k_1)\big) \Big]\, \theta(t_1 - t_2)\,, \tag{3.93}$$

which immediately fixes the off-diagonal elements of the macroscopic propagator (3.78). The function $c(k)$ appearing here is defined as

$$c(k) := \sqrt{\frac{\bar{\rho}v(k)}{m}} \, . \tag{3.94}$$

Inserting the results for Δ_R and Δ_A as well as the expression (3.91) for $G_{ff}^{(0)}$ into the ff-component of (3.78) then yields the remaining statistical propagator,

$$\Delta_{ff}(1,2) = (2\pi)^3 \, \delta_\mathrm{D}(\vec{k}_1 + \vec{k}_2) \, \bar{\rho}^2 \, P_\delta^{(\mathrm{i})}(k_1) \, D(1) \, D(2) \, , \tag{3.95}$$

with

$$D(1) := \cos(k_1 t_1 \, c(k_1)) - mc(k_1)\frac{\vec{k}_1 \cdot \vec{l}_1}{k_1} \, \sin(k_1 t_1 \, c(k_1)) \, . \tag{3.96}$$

There are a number of things we would like to point out about this result for the propagator. First of all, we note that the sign of the Fourier transformed interaction potential $v(k)$ is crucial since it appears under a square root in the function $c(k)$. If $v(k) > 0$, then $c(k)$ is real and the time-dependence of the propagator is described by the trigonometric sine and cosine functions. If $v(k) < 0$, however, $c(k)$ is imaginary and the time-dependence is actually described by the hyperbolic sine and cosine functions $\sinh(y) = -\mathrm{i}\sin(\mathrm{i}y)$ and $\cosh(y) = \cos(\mathrm{i}y)$. In other words, $v(k) > 0$ yields oscillating modes, whereas $v(k) < 0$ yields exponentially growing modes.[3]

To interpret this behaviour from a physical perspective, we first recall from (3.73) that the statistical propagator Δ_{ff} is the lowest order perturbative result of the 2-point phase-space density cumulant G_{ff}. Hence, it describes the evolution of macroscopic structures in the regime where mode-coupling due to interactions is negligible. We further note that a positive sign of the Fourier transformed potential corresponds to an repulsive interaction, which should indeed lead to an oscillatory evolution of structures. A negative sign, on the other hand, corresponds to an attractive interaction, leading to the growth of structures. Remarkably, the macroscopic propagator is thus able to capture the characteristic general behaviour of structure formation in both of these very different types of interacting system.

This clearly demonstrates an important advantage of the macroscopic perturbation theory over the microscopic one. In the latter approach, cumulants can only be calculated up to a finite order in the interaction potential v. Expanding the result (3.95) of Δ_{ff} as a series in v and truncating this series at a finite order would only yield a very crude approximation to the full exponential or trigonometric behaviour. We thus expect a plain perturbative expansion to any feasible order in the microscopic approach to only be able to describe the evolution of the system for early times when the argument $ktc(k)$ is still small. For later times the truncated result should start to underpredict the growth of structures in systems with attractive interaction, and overpredict it in systems with repulsive interactions.[4]

---

[3]Technically, the hyperbolic functions are each given by a sum of a growing and a decaying mode. But since the decaying modes quickly become negligible compared to the growing ones, we will always just speak of growing modes.

[4]In [1, 2], where we applied the microscopic perturbation theory to cosmic structure formation, this problem is bypassed by replacing the Hamiltonian free trajectories with the modified Zel'dovich trajectories introduced in [51], which already contain part of the gravitational interaction.

3.2.4. Feynman diagrams

Now that we have gained a good understanding of the properties of the macroscopic propagator, let us discuss some general properties of the macroscopic perturbation theory as a whole. For this purpose, it is convenient to introduce diagrammatic representations for the propagators and vertices. We want to do this in such a way that the diagrams indicate the causal structure inherited from the free collective-field cumulants. Combining (3.54) and (3.75) yields

$$\mathcal{V}_{\beta\cdots\beta f\cdots f}(1,\ldots,n_\beta,1',\ldots,n_f') = 0 \quad \text{if} \quad \exists\, r' \in \{1',\ldots,n_f'\}$$
$$\text{such that} \ \left(t_{r'} > t_u\right) \ \text{or} \ \left(t_{r'} = t_u \text{ and } \vec{l}_u = 0\right) \quad \forall\, u \in \{1,\ldots,n_\beta\}. \tag{3.97}$$

meaning that every f-argument of a vertex must always be evaluated at an earlier time than at least one of its β-arguments. We visualise this by placing incoming arrowheads on the ends of f-legs and outgoing arrowheads on the ends of β-legs, indicating the direction of time. A general vertex is then represented as

$$\mathcal{V}_{\beta\cdots\beta f\cdots f}(1,\ldots,n_\beta,1',\ldots,n_f') \cong \quad \text{if } n_\beta \geq 1, \tag{3.98}$$

and $\mathcal{V}_{f\cdots f} = 0$.

The propagator (3.78) contains the building blocks $G_{ff}^{(0)}$, Δ_R and Δ_A. For the first one of these we can directly adopt the representation (3.98) by means of $G_{ff}^{(0)} = -\mathcal{V}_{\beta\beta}$,

$$- G_{ff}^{(0)}(1,2) \cong \quad 1 \longleftarrow\!\!\bullet\!\!\longrightarrow 2 \ . \tag{3.99}$$

But Δ_R and Δ_A require a new kind of diagram. In accordance with their respective retarded or advanced causal structure we represent them as a line with an arrowhead in the middle, pointing towards the later time,

$$- \mathrm{i}\Delta_\mathrm{R}(1,2) = -\mathrm{i}\Delta_\mathrm{A}(2,1) \cong \quad 1 \longrightarrow\!\!\!\!\leftarrow\!\!\longrightarrow 2 \ , \tag{3.100}$$

additionally introducing a conventional factor $-\mathrm{i}$. Whenever we connect the diagrams (3.98), (3.99) and (3.100) in such a way that there are consecutive arrowheads on a line pointing into the same direction, we further choose to join these into one. This yields the following diagrammatic representations for the different components of the propagator,

$$\Delta(1,2) \cong \begin{pmatrix} 1 \longrightarrow\!\!\bullet\!\!\longrightarrow 2 & 1 \longleftarrow 2 \\ 1 \longrightarrow 2 & 0 \end{pmatrix} . \tag{3.101}$$

Every term in the macroscopic perturbative expansion (3.70) can now be represented by combining the diagrammatic expressions (3.98) and (3.101) for the vertices and propagators appearing in that term. Furthermore, it is a well-established fact in quantum and statistical

field theory that the terms appearing in the cumulant-generating functional $W_\phi[M] := \ln Z_\phi[M]$ always correspond to connected diagrams. We will thus only consider those in the following.

In such a diagram every f-leg of each vertex will be attached to an f-end of a propagator and every β-leg of each vertex will be attached to a β-end of a propagator. This allows some immediate conclusions. First, one notices that the arrow directions of propagator-ends and vertex-legs being connected in this way will always agree. There will thus be a consistent and continuous *time-flow* throughout the complete diagram. Second, the fact that there are no propagators or vertices with incoming arrows only means that the time-flow has no sinks. In Appendix D.1 we demonstrate how these two properties can be used to derive the following

Causality rule A diagram is causally forbidden and vanishes identically if it has only incoming arrows on its outer legs or contains a subdiagram which does so.

The overall time-flow behaviour in a general diagram nicely illustrates the characteristics of the initial-value problem we are dealing with when calculating a phase-space density correlation within the macroscopic perturbation theory:

- The time-flow is sourced by the free collective-field cumulants within the propagators and vertices since they encode the initial conditions of the system.

- Time-flows can merge and split, as a single event can be influenced by several preceding ones and it can itself also affect several subsequent ones.

- Time-flows can only end at the outer legs of the diagram since this is where we read off the cumulant of interest evolved to some final points in time.

If the system of interest is statistically homogeneous, the macroscopic perturbation theory has some additional very convenient properties. First of all, we recall from (3.57) that the free cumulants conserve spatial Fourier modes in this case. This property is translated to the propagator and vertices,

$$\Delta(1,2) \propto (2\pi)^3 \, \delta_{\mathrm{D}}\!\left(\vec{k}_1 + \vec{k}_2\right), \tag{3.102}$$

$$\mathcal{V}_{\beta\cdots\beta f\cdots f}(1,\ldots,n_\beta,1',\ldots,n'_f) \propto (2\pi)^3 \, \delta_{\mathrm{D}}\!\left(\vec{k}_1 + \cdots + \vec{k}_{n_\beta} + \vec{k}_2 + \cdots + \vec{k}_{n'_f}\right), \tag{3.103}$$

as can be checked by inserting (3.28) and (3.76) into (3.74) and (3.75). Consequently, any connected diagram has to conserve spatial Fourier modes as well.

Furthermore, we show in Appendix D.2 how this property allows to prove the following

Homogeneity rule In statistically homogeneous systems, a diagram vanishes identically if it contains a so-called tadpole subdiagram, i.e. a subdiagram which is connected to the rest of the diagram solely via a single propagator.

The physical interpretation of this rule is straightforward. The only information carried by a diagram with only one external leg is the value of the mean phase-space density. But a homogeneous background density can not affect the dynamics of the particles, as this depends on potential gradients only.

The two Feynman rules will enable us to drastically reduce the number of contributions to the macroscopic perturbative expansion that have to be taken into account. The Homogeneity rule further implies the applicability of the conventional loop expansion scheme when considering statistically homogeneous systems, as this rule ensures that there will always only be a finite number of non-vanishing diagrams with a given number of loops. The complete procedure for calculating the L-loop expression for an interacting n_f-point phase-space density cumulant of a statistically homogeneous system within the macroscopic perturbation theory is then as follows:

1. Draw n_f points and label these with the Fourier space arguments 1 to n_f.

2. By combining the propagators (3.101) and vertices (3.98) such that the arrow directions of joint legs always agree, draw all possible connected diagrams with n_f outgoing external propagators ending at the labelled points that are allowed by the Causality as well as the Homogeneity rule and contain exactly L loops.

3. Divide each diagram by its respective symmetry factor, i. e. the number of possible permutations of internal propagators and vertices which leave the labelled diagram invariant.

4. Translate each diagram into its respective functional expression, taking into account that every link between a propagator and a vertex corresponds to a Fourier space integral over the argument at their joint legs, and sum up all resulting expressions.

In this sense, Δ_{ff} is the 0-loop or – adopting the usual field theoretical nomenclature – tree-level result of the 2-point phase-space cumulant G_{ff}. Two examples of diagrams appearing in the 1-loop result of G_{ff} are

$$
1 \longrightarrow \bullet \bigcirc \bullet \longrightarrow 2 \; \cong \int \mathrm{d}\bar{1}\cdots\mathrm{d}\bar{6}\; \Delta_{f\beta}(1,-\bar{1})\,\mathcal{V}_{\beta ff}(\bar{1},-\bar{2},-\bar{3})\,\Delta_{ff}(\bar{2},-\bar{4})
$$
$$
\times \Delta_{f\beta}(\bar{3},-\bar{5})\,\mathcal{V}_{f\beta\beta}(\bar{4},\bar{5},-\bar{6})\,\Delta_{\beta f}(\bar{6},2)\,,
\tag{3.104}
$$

$$
1 \longrightarrow \bullet\bullet \longrightarrow 2 \quad \cong \int \mathrm{d}\bar{1}\cdots\mathrm{d}\bar{4}\; \Delta_{f\beta}(1,-\bar{1})\,\mathcal{V}_{\beta f\beta f}(\bar{1},-\bar{2},\bar{3},-\bar{4})
$$
$$
\times \Delta_{f\beta}(\bar{2},-\bar{3})\,\Delta_{ff}(\bar{4},2)\,.
\tag{3.105}
$$

4. Dark matter structure formation

In this chapter we use the resummed KFT framework introduced in section 3.2 to describe the formation of structures in pure dark matter. We will begin by deriving the free collective-field cumulants obtained from the dynamics of gravitating particles in an expanding space-time. Using these, we then compute the tree-level and 1-loop contributions to the macroscopic propagator, which allows us to obtain the first nonlinear corrections to the dark matter power spectrum. Finally, we compare these to results from numerical simulations and Eulerian perturbation theory, and discuss the differences and similarities.

4.1. Dark matter dynamics

To describe the dynamics of classical particles in an expanding space-time, we first need to specify our choice of coordinates. Following [31], we use

$$\eta(t) := \ln \frac{D_+(t)}{D_+(t_i)} \tag{4.1}$$

as our time coordinate, with D_+ being the usual linear growth factor defined in (2.26). Note that this definition implies $\eta_i = 0$. The spatial coordinate is chosen to be comoving with the homogenous expansion of the background space-time, $\vec{q} := \vec{r}/a$, where $\vec{r}$ denotes the physical coordinate and a the cosmological scale factor. As the momentum variable we use $\vec{p} := \mathrm{d}\vec{q}/\mathrm{d}\eta$, i. e. the peculiar comoving velocity with respect to the coordinate time η.

In Appendix E we show that the resulting equations of motion for the phase-space trajectories of dark matter particles read

$$\frac{\mathrm{d}\vec{q}_j}{\mathrm{d}\eta} = \vec{p}_j \,, \tag{4.2}$$

$$\frac{\mathrm{d}\vec{p}_j}{\mathrm{d}\eta} = -\left(\frac{3}{2}\frac{\Omega_{\mathrm{m}}}{f_+^2} - 1\right)\vec{p}_j - \vec{\nabla}_{q_j}\tilde{V}_G \approx -\frac{1}{2}\vec{p}_j - \vec{\nabla}_{q_j}\tilde{V}_G \,, \tag{4.3}$$

with the dimensionless matter density parameter Ω_{m}, the growth function $f_+ := \mathrm{d}\ln D_+/\mathrm{d}\ln a$ and the effective gravitational potential $\tilde{V}_G$ satisfying the Poisson equation

$$\nabla_q^2 \tilde{V}_G = \frac{3}{2}\frac{\Omega_{\mathrm{m}}}{f_+^2}\frac{\Phi_\rho - \bar{\rho}}{\bar{\rho}} \approx \frac{3}{2}\frac{\Phi_\rho - \bar{\rho}}{\bar{\rho}} \,, \tag{4.4}$$

where $\bar{\rho}$ denotes the mean comoving number density of dark matter particles. Here, we additionally used $\Omega_{\mathrm{m}}/f_+^2 \approx 1$, which is a very good approximation during the matter- and Λ-dominated cosmological epochs that we are interested in [5, 52].

The single-particle Green's function $\mathcal{G}$ (3.21) that solves the equations of motion (4.2) and (4.3) in the non-interacting case, $\tilde{V}_G = 0$, has the components

$$g_{qq}(\eta, \eta') = \theta(\eta - \eta'), \tag{4.5}$$

$$g_{qp}(\eta, \eta') = \theta(\eta - \eta') \, 2 \left(1 - e^{-\frac{1}{2}(\eta - \eta')} \right), \tag{4.6}$$

$$g_{pq}(\eta, \eta') = 0, \tag{4.7}$$

$$g_{pp}(\eta, \eta') = \theta(\eta - \eta') \, e^{-\frac{1}{2}(\eta - \eta')}, \tag{4.8}$$

as shown in Appendix A.3. Furthermore, the Poisson equation (4.4) is solved by

$$\tilde{V}_G(\vec{q}, t) = \sum_{j=1}^{N} \tilde{v}_G \left(|\vec{q} - \vec{q}_j(t)| \right) \tag{4.9}$$

with the effective single-particle gravitational potential reading

$$\tilde{v}_G(k) := -\frac{3}{2} \frac{1}{\bar{\rho} \, k^2} \tag{4.10}$$

in Fourier space. It replaces the generic potential v in the definition (3.28) of the interaction matrix element σ_{fB}.

We further choose to fix the initial time to some point early in the matter-dominated epoch, when the cosmic density and momentum fields were still well-described by Gaussian random fields. As described in subsection 3.1.3, the initial conditions are then completely fixed by specifying the initial density contrast power spectrum $P_\delta^{(i)}$. Since we are considering the structure formation in pure dark matter here, we choose to neglect the effects of baryonic matter in the early universe and assume an initial BBKS spectrum [12], described in subsection 2.2.2.

General expressions for the free collective-field cumulants resulting from this choice of initial conditions have been derived in [48], and in Appendix B we listed these for the 1- to 4-point cumulants used in this thesis. Inserting the Green's function components (4.5) to (4.8) as well as the interaction matrix element (3.28) with the potential (4.10) into these yields the specific expressions needed for our application to dark matter structure formation. In particular, the resulting non-vanishing 1-and 2-point cumulants read

$$G_f^{(0)}(1) = (2\pi)^3 \, \delta_{\mathrm{D}}(\vec{k}_1) \, \bar{\rho} \, e^{-\frac{\sigma_p^2}{2} \tilde{T}_1^2 l_1^2}, \tag{4.11}$$

$$\begin{aligned} G_{f\mathcal{F}}^{(0)}(1, 2) = (2\pi)^3 \, \delta_{\mathrm{D}}(\vec{k}_1 + \vec{k}_2) \, (2\pi)^3 \, \delta_{\mathrm{D}}(\vec{l}_2) \; \theta(\eta_1 - \eta_2) \\ \times \frac{-3\,\mathrm{i}}{2} \left(T_{12} + \tilde{T}_{12} \frac{\vec{k}_1 \cdot \vec{l}_1}{k_1^2} \right) e^{-\frac{\sigma_p^2}{2} \left((T_1 - T_2)\vec{k}_1 + \tilde{T}_1 \vec{l}_1 \right)^2}, \end{aligned} \tag{4.12}$$

$$G_{ff}^{(0)}(1, 2) = (2\pi)^3 \, \delta_{\mathrm{D}}(\vec{k}_1 + \vec{k}_2) \, \bar{\rho}^2 \, C_2(1, 2) \, e^{-\frac{\sigma_p^2}{2} \left[\left(T_1 \vec{k}_1 + \tilde{T}_1 \vec{l}_1 \right)^2 + \left(-T_2 \vec{k}_1 + \tilde{T}_2 \vec{l}_2 \right)^2 \right]}, \tag{4.13}$$

where we neglected contributions due to shot noise by taking the thermodynamic limit, as discussed in item 3 of subsection 3.1.3. This is an excellent approximation on all scales relevant

for cosmic structure formation, as the number of dark matter particles contained in any volume of interest is huge.

We also already imposed the constraints on $\vec{k}_2$ and $\vec{l}_2$ set by the delta functions, and defined the short-hand notations

$$\tilde{T}_u := \mathrm{e}^{-\frac{1}{2}\eta_u}, \qquad \tilde{T}_{ur} := \mathrm{e}^{-\frac{1}{2}(\eta_u - \eta_r)}, \tag{4.14}$$

$$T_u := 2\left(1 - \tilde{T}_u\right), \quad T_{ur} := 2\left(1 - \tilde{T}_{ur}\right) \tag{4.15}$$

for the time-dependencies introduced by the Green's function. Furthermore, σ_p^2 denotes the 1-point variance of the initial momentum field,

$$\sigma_p^2 = \frac{1}{3}\operatorname{tr} C_{p_j p_j} = \frac{1}{3}\int \frac{\mathrm{d}^3 k}{(2\pi)^3} \frac{P_\delta^{(\mathrm{i})}(k)}{k^2}, \tag{4.16}$$

and C_2 describes the 2-point phase-space density correlations emerging from the free-streaming of particles. Expanding the latter to second order in $P_\delta^{(\mathrm{i})}$ yields

$$
\begin{aligned}
C_2(1,2) = {}& P_\delta^{(\mathrm{i})}(k_1)\left(1 + \frac{\vec{k}_1 \cdot (T_1\vec{k}_1 + \tilde{T}_1\vec{l}_1)}{k_1^2}\right)\left(1 - \frac{\vec{k}_1 \cdot (-T_1\vec{k}_1 + \tilde{T}_2\vec{l}_2)}{k_1^2}\right) \\
& + \int \frac{\mathrm{d}^3 k'}{(2\pi)^3} P_\delta^{(\mathrm{i})}(k') P_\delta^{(\mathrm{i})}(|\vec{k}_1 + \vec{k}'|)\left[\frac{\left(\vec{k}' \cdot (T_1\vec{k}_1 + \tilde{T}_1\vec{l}_1)\right)\left(\vec{k}' \cdot (-T_2\vec{k}_1 + \tilde{T}_2\vec{l}_2)\right)}{k'^4}\right. \\
& \times \left(1 + \frac{(\vec{k}_1 + \vec{k}') \cdot \left((T_1 - T_2)\vec{k}_1 + \tilde{T}_1\vec{l}_1 + \tilde{T}_2\vec{l}_2\right)}{|\vec{k}_1 + \vec{k}'|^2}\right. \\
& + \frac{1}{2}\frac{\left((\vec{k}_1 + \vec{k}') \cdot (T_1\vec{k}_1 + \tilde{T}_1\vec{l}_1)\right)\left((\vec{k}_1 + \vec{k}') \cdot (-T_2\vec{k}_1 + \tilde{T}_2\vec{l}_2)\right)}{|\vec{k}_1 + \vec{k}'|^4}\right) \\
& \left. - \frac{\left(\vec{k}' \cdot (T_1\vec{k}_1 + \tilde{T}_1\vec{l}_1)\right)\left((\vec{k}_1 + \vec{k}') \cdot (-T_2\vec{k}_1 + \tilde{T}_2\vec{l}_2)\right)}{k'^2 |\vec{k}_1 + \vec{k}'|^2}\right] + O\left(\left(P_\delta^{(\mathrm{i})}\right)^3\right).
\end{aligned}
\tag{4.17}
$$

As pointed out in [48], the full nonlinear expression for C_2 given in (B.10) has to be evaluated numerically. The same is true for the analogous functions C_{n_f} with $n_f \geq 3$ which appear in the free collective-field cumulants involving n_f phase-space density fields and characterise the n_f-point phase-space density correlations emerging from free-streaming. So far, implementing this in a sufficiently numerically stable manner has unfortunately only been achieved specifically for the function $C_2(1,2)$ evaluated at $\vec{k}_2 = -\vec{k}_1$ and $\vec{l}_1 = \vec{l}_2 = 0$. Hence, the only free collective-field cumulant whose full nonlinear form is currently accessible is the free 2-point cumulant of spatial densities $G_{\rho\rho}^{(0)}$.

It turns out that its numerical result is exceptionally well-described by the analytic expression

$$G_{\rho\rho}^{(0)}(1,2) = (2\pi)^3 \, \delta_{\mathrm{D}}(\vec{k}_1 + \vec{k}_2) \, \bar{\rho}^2 \, P_\delta^{(\mathrm{i})}(k_1) \, \mathrm{e}^{-\frac{\sigma_p^2}{2}(T_1 - T_2)^2 k_1^2} , \qquad (4.18)$$

at least up to wavenumbers of $k = 10^5 \, h/\mathrm{Mpc}$ which easily covers all scales relevant for cosmic structure formation. As we can see, the only difference between this expression and the one obtained when using the linearised result for C_2 is the form of their damping factors. In particular, the full nonlinear result does not experience any damping at all when evaluated at equal times. Apparently, the influence of the complete hierarchy of initial correlations thus mainly manifests itself in compensating the dissolution of small-scale structures caused by the particles' momentum dispersion. A similar result was found in [2] for Zel'dovich dynamics.

4.2. Tree-level propagator

4.2.1. Analytical large-scale solution

To determine the macroscopic propagator for cosmic structure formation, we first insert the expression (4.12) for $G_{f\mathcal{F}}^{(0)}$ into the functional inverse (3.79) defining the causal propagators Δ_{R} and Δ_{A}. In Appendix C we show how this inverse can be computed fully analytically if $G_{f\mathcal{F}}^{(0)}(1,2)$ evaluated at $\vec{l}_1 = \vec{l}_2 = 0$ is time-translation invariant, i. e. if it only depends on η_1 and η_2 in terms of their difference $\eta_{12} := \eta_1 - \eta_2$. While this is generally not the case for (4.12), we can see that it is only the remaining k_1-dependent part of the Gaussian damping factor, $\mathrm{e}^{-\frac{\sigma_p^2}{2}(T_1 - T_2)^2 k_1^2}$, which breaks this invariance. For the moment, let us thus consider the large-scale limit $k_1^2 \ll \sigma_p^{-2}$ in which this part of the damping factor becomes negligible and we can follow the steps outlined in Appendix C to find the analytic solution

$$\Delta_{\mathrm{R}}^{(\mathrm{ls})}(1,2) = \Delta_{\mathrm{A}}^{(\mathrm{ls})}(2,1) = \mathcal{I}(1,2) + (2\pi)^3 \, \delta_{\mathrm{D}}(\vec{k}_1 + \vec{k}_2) \, (2\pi)^3 \, \delta_{\mathrm{D}}(\vec{l}_2) \, \tilde{\Delta}_{\mathrm{R}}^{(\mathrm{ls})}(\vec{k}_1, \vec{l}_1; \eta_1, \eta_2) . \qquad (4.19)$$

with

$$\tilde{\Delta}_{\mathrm{R}}^{(\mathrm{ls})}(\vec{k}_1, \vec{l}_1; \eta_1, \eta_2) = \frac{3}{5}\left[\left(1 + \frac{\vec{k}_1 \cdot \vec{l}_1}{k_1^2}\right) \mathrm{e}^{\eta_{12}} - \left(1 - \frac{3}{2}\frac{\vec{k}_1 \cdot \vec{l}_1}{k_1^2}\right) \mathrm{e}^{-\frac{3}{2}\eta_{12}}\right] \theta(\eta_{12}) \, \mathrm{e}^{-\frac{\sigma_p^2}{2}\tilde{T}_1^2 l_1^2} . \qquad (4.20)$$

This immediately fixes the off-diagonal elements of the macroscopic propagator (3.78).

In this limit, the damping factor in the expression (4.13) for $G_{ff}^{(0)}$ simplifies as well, and restricting C_2 to its linear part becomes a very good approximation, as the nonlinear contributions are expected to be sub-dominant on large scales. Hence, the large-scale limit of $G_{ff}^{(0)}$ reads

$$\begin{aligned}
G_{ff}^{(0,\mathrm{ls})}(1,2) = {} & (2\pi)^3 \, \delta_{\mathrm{D}}(\vec{k}_1 + \vec{k}_2) \, \bar{\rho}^2 \, P_\delta^{(\mathrm{i})}(k_1) \, \mathrm{e}^{-\frac{\sigma_p^2}{2}\left(\tilde{T}_1^2 l_1^2 + \tilde{T}_2^2 l_2^2\right)} \\
& \times \left(1 + \frac{\vec{k}_1 \cdot \left(T_1 \vec{k}_1 + \tilde{T}_1 \vec{l}_1\right)}{k_1^2}\right)\left(1 - \frac{\vec{k}_1 \cdot \left(-T_1 \vec{k}_1 + \tilde{T}_2 \vec{l}_2\right)}{k_1^2}\right) .
\end{aligned} \qquad (4.21)$$

Inserting (4.19) and (4.21) into the ff-component of (3.78) then yields the remaining statistical propagator,

$$\Delta_{ff}^{(\mathrm{ls})}(1,2) = (2\pi)^3\,\delta_{\mathrm{D}}\big(\vec{k}_1+\vec{k}_2\big)\,\bar{\rho}^2\,P_\delta^{(\mathrm{i})}(k_1)\,\mathrm{e}^{\eta_1+\eta_2}\left(1+\frac{\vec{k}_1\cdot\vec{l}_1}{k_1^2}\right)\left(1+\frac{\vec{k}_2\cdot\vec{l}_2}{k_2^2}\right)\mathrm{e}^{-\frac{\sigma_p^2}{2}\left(\tilde{T}_1^2 l_1^2+\tilde{T}_2^2 l_2^2\right)}\,,\quad(4.22)$$

as shown in detail in Appendix C.

From (4.22) we can infer the large-scale solution of the density contrast power spectrum,

$$P_\delta^{(\Delta,\mathrm{ls})}(k_1,\eta_1) = \left.\frac{\Delta_{ff}^{(\mathrm{ls})}(1,2)}{(2\pi)^3\,\delta_{\mathrm{D}}\big(\vec{k}_1+\vec{k}_2\big)\,\bar{\rho}^2}\right|_{\substack{\vec{k}_2=-\vec{k}_1\\\vec{l}_1=\vec{l}_2=0\\\eta_2=\eta_1}} = P_\delta^{(\mathrm{i})}(k_1)\,\mathrm{e}^{2\eta_1} = P_\delta^{(\mathrm{i})}(k_1)\,\frac{D_+^2(\eta_1)}{D_+^2(0)} = P_\delta^{(\mathrm{lin})}(k_1,\eta_1)\,.$$

$$(4.23)$$

We see that we are precisely recovering the well-known linear growth of structures on the very largest scales. It can not be stressed enough that at no point in the derivation did we have to employ the Zel'dovich approximation or assume fluid dynamics. Instead, this result was derived completely analytically from *Hamiltonian* particle dynamics alone, which, to our knowledge, is the first time that this has been achieved.

If we compare (4.23) with the large-scale limit of the freely evolved power spectrum,

$$P_\delta^{(0,\mathrm{ls})}(k_1,\eta_1) = \left.\frac{G_{ff}^{(0,\mathrm{ls})}(1,2)}{(2\pi)^3\,\delta_{\mathrm{D}}\big(\vec{k}_1+\vec{k}_2\big)\,\bar{\rho}^2}\right|_{\substack{\vec{k}_2=-\vec{k}_1\\\vec{l}_1=\vec{l}_2=0\\\eta_2=\eta_1}} = P_\delta^{(\mathrm{i})}(k_1)\left(3-2\,\mathrm{e}^{-\frac{1}{2}\eta_1}\right)^2\qquad(4.24)$$

we can see that the growth of the latter is drastically slower and even bounded from above for late times. The reason for this is that, relative to the expanding space-time, freely evolving particles slow down in comoving coordinates since their initial momentum falls behind the cosmic expansion [51]. We conclude that the particle interactions resummed in the macroscopic propagator, as discussed in subsection 3.2.2, precisely compensate the significant lack of large-scale structure growth caused by this deceleration. Not only does this demonstrate the power of our resummation procedure, but it also provides a novel insight into the connection between the formation of structures on cosmic scales and the underlying microscopic Hamiltonian particle dynamics.

Having the full phase-space information at hand, we can also directly deduce correlations of, for example, the first momentum moment of the phase-space density,

$$\vec{\pi}(\vec{q},\eta) := \int\mathrm{d}^3 p\,\vec{p}\,f(\vec{q},\vec{p},\eta)\,,\qquad \vec{\pi}(\vec{k},\eta) = \left.\mathrm{i}\frac{\partial}{\partial\vec{l}}\,f(\vec{k},\vec{l},\eta)\right|_{\vec{l}=0}.\qquad(4.25)$$

Here, we used (3.37) to obtain the expression in Fourier space. Its power spectrum is defined via

$$(2\pi)^3\,\delta_{\mathrm{D}}\big(\vec{k}_1+\vec{k}_2\big)\,P_\pi(k_1,\eta) := (\bar{\rho})^{-2}\left\langle\vec{\pi}(\vec{k}_1,\eta)\cdot\vec{\pi}(\vec{k}_2,\eta)\right\rangle_{\mathrm{c}}\,,\qquad(4.26)$$

and has the large-scale limit

$$
P_\pi^{(\Delta,\mathrm{ls})}(k_1,\eta_1) = \frac{\mathrm{i}\frac{\partial}{\partial \vec{l}_1} \cdot \mathrm{i}\frac{\partial}{\partial \vec{l}_2}\,\Delta_{ff}^{(\mathrm{ls})}(1,2)}{(2\pi)^3\,\delta_{\mathrm{D}}\big(\vec{k}_1 + \vec{k}_2\big)\,\bar\rho^2}\Bigg|_{\substack{\vec{k}_2=-\vec{k}_1 \\ \vec{l}_1=\vec{l}_2=0 \\ \eta_2=\eta_1}} = \frac{P_\delta^{(\mathrm{i})}(k_1)}{k_1^2}\,\frac{D_+^2(\eta_1)}{D_+^2(0)} = \frac{P_\delta^{(\mathrm{lin})}(k_1,\eta_1)}{k_1^2}\,, \qquad (4.27)
$$

which agrees with the solution of the linearised Eulerian fluid equations [53].

4.2.2. Numerical solution on all scales

Going beyond the large-scale limit requires a numerical evaluation of the macroscopic propagator. We have shown in Appendix C how this can be reduced to solving a simple matrix equation and computing one- and two-dimensional integrals over time arguments. Performing these steps is in itself computationally cheap and numerically stable. In practice, however, we are of course limited by the more challenging numerical evaluation of the free 2-point cumulant $G_{ff}^{(0)}$ entering this computation. In this thesis, we will thus only consider the numerical evaluation of the tree-level density contrast power spectrum $P_\delta^{(\Delta)}$, as this just requires the spatial density cumulant $G_{\rho\rho}^{(0)}$ as an ingredient, which allows us to use the analytic approximation (4.18). The numerical evaluation of $P_\pi^{(\Delta)}$, which requires to evaluate $G_{ff}^{(0)}(1,2)$ also for non-vanishing $\vec{l}_1$ and $\vec{l}_2$, will be the subject of future work.

In Figure 4.1 we show the result found for $P_\delta^{(\Delta)}$ evolved from the time of CMB decoupling until today and compare it to the freely evolved spectrum $P_\delta^{(0)}$ as well as the linear result $P_\delta^{(\mathrm{lin})}$. At small wavenumbers, the full tree-level result follows the linear spectrum before it starts to fall below the linear prediction on wavenumbers $k \gtrsim 20\,h/\mathrm{Mpc}$ where the influence of the particles' momentum dispersion starts to become relevant. When going to even higher wavenumbers it eventually approaches and follows the freely evolved spectrum for $k \gtrsim 10^4\,h/\mathrm{Mpc}$. The overall shape of the tree-level spectrum thus interpolates between linear growth on large scales and free evolution of structures on small scales.

There are two important conclusions that can be drawn from this result. First of all, it suggests that the partial resummation of gravitational interactions described by the macroscopic tree-level propagator is not able to capture the full nonlinear hierarchy of initial correlations encoded in the free 2-point cumulant $G_{\rho\rho}^{(0)}$. Otherwise we would expect to see a similar compensation of the dispersion-induced damping as observed in $P_\delta^{(0)}$. This is not surprising, though, since the propagator only takes the linear response of the phase-space density to particle interactions into account, as discussed in subsection 3.2.2. Consequently, any compensation of the damping effect is only expected to be captured by higher-order corrections within the macroscopic perturbation theory.

At the same time, however, we can also infer that the resummed interactions do not enhance the damping effect either, as the tree-level result never drops below the structure growth found in the freely evolving system. This differs from the behaviour found in Zel'dovich dynamics which overpredicts the dissolution of small-scale structures [2, 5].

Altogether, the full tree-level result for the density contrast power spectrum is thus found to capture the linear effects introduced by gravitational interactions in a way that is fully consistent
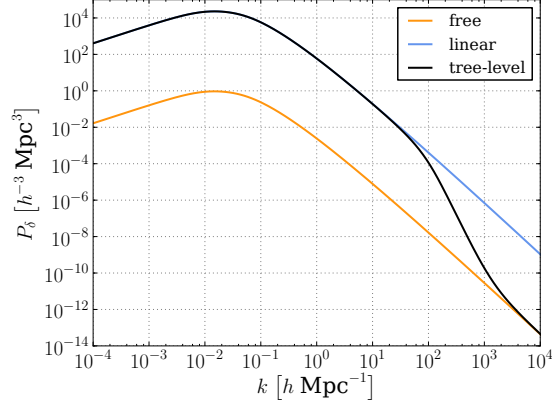
Figure 4.1.: Density contrast power spectra obtained from the macroscopic tree-level propagator, the free theory and the linear theory, respectively, evolved from the time of CMB decoupling to redshift zero. The tree-level result follows the linear growth on large scales, but drops down to the free-streaming growth on small scales where the particles' momentum dispersion becomes relevant.

with the underlying free Hamiltonian particle dynamics.

4.3. Loop corrections

4.3.1. 1-Loop diagrams

Describing the structure formation on scales below approximately $10\,\mathrm{Mpc}/h$ requires to also take the nonlinear dynamical effects introduced by the interactions between dark matter particles into account. Within the macroscopic perturbation theory, this amounts to the inclusion of loop corrections, as discussed in subsection 3.2.4. In this thesis, we will focus on the computation of 1-loop corrections to the macroscopic propagator.

Let us start by defining the *exact macroscopic propagator G* as the matrix of all fully interacting macroscopic 2-point cumulants introduced in (3.71),

$$G(1,2) := \begin{pmatrix} G_{ff} & G_{f\beta} \\ G_{\beta f} & G_{\beta\beta} \end{pmatrix} (1,2)\,. \tag{4.28}$$

To organise the different loop contributions to G, we follow the conventional approach in quantum and statistical field theory and introduce the *macroscopic self-energy Σ*, defined via

$$G(1,2) =: \Delta(1,2) + \left(\Delta \cdot \Sigma \cdot \Delta\right)(1,2)\,. \tag{4.29}$$

It corresponds to the sum of all 2-point loop contributions with both their external tree-level propagators stripped off and thus acts like an effective 2-point vertex. As such it inherits the causal structure of the tree-level vertices, meaning that $\Sigma_{\beta\beta}$ is symmetric in its time arguments, $\Sigma_{\beta f}$ and $\Sigma_{f\beta}$ have a retarded and advanced time-dependence, respectively, and Σ_{ff} vanishes

identically. We choose to adopt the nomenclature introduced for the propagator and refer to $\Sigma_{\beta\beta}$, $\Sigma_{\beta f}$ and $\Sigma_{f\beta}$ as the statistical, retarded and advanced self-energies, respectively.

When computing the propagator corrections to some given loop order, it is then convenient to first compute the respective loop contributions to the statistical and causal self-energies, and afterwards use

$$
\begin{aligned}
G_{ff}(1,2) = \Delta_{ff}(1,2) &+ \left(\Delta_{f\beta} \cdot \Sigma_{\beta\beta} \cdot \Delta_{\beta f}\right)(1,2) \\
&+ \left(\Delta_{f\beta} \cdot \Sigma_{\beta f} \cdot \Delta_{ff}\right)(1,2) \\
&+ \left(\Delta_{ff} \cdot \Sigma_{f\beta} \cdot \Delta_{\beta f}\right)(1,2),
\end{aligned}
\tag{4.30}
$$

$$
G_{f\beta}(1,2) = G_{\beta f}(2,1) = \Delta_{f\beta}(1,2) + \left(\Delta_{f\beta} \cdot \Sigma_{\beta f} \cdot \Delta_{f\beta}\right)(1,2)
\tag{4.31}
$$

to obtain the resulting expressions for the statistical and off-diagonal propagators. This way we can avoid some redundancy in our calculations. For later convenience, we will also define the exact retarded and advanced propagators $G_{\mathrm{R}} \coloneqq \mathrm{i}G_{f\beta}$ and $G_{\mathrm{A}} \coloneqq \mathrm{i}G_{\beta f}$.

Using the diagrammatic language introduced in subsection 3.2.4, the 1-loop contributions to the self-energy are given by

$$
\tag{4.32}
$$

$$
\tag{4.33}
$$

After exploiting all the Dirac delta functions appearing in the propagators and vertices, we find that there are between 4 and 6 non-trivial integrals left in each diagram: 2 integrals for the modulus and angle of the loop wavevector, and 2 to 4 time integrals – one for each joint between a propagator and a vertex – all of which have to be performed numerically. While being computationally quite demanding, this in itself is no fundamental obstacle. However, the fact that the free collective-field cumulants of two or more phase-space density fields themselves have to be evaluated numerically poses a problem since we have only been able to implement this in a sufficiently stable manner for the 2-point spatial density cumulant $G_{\rho\rho}^{(0)}$, as discussed in the

previous section. Hence, we currently do not have a way of evaluating the full 3- and 4-point vertices with 2 or more β-legs, appearing in every diagram except for diagram 1 in (4.32) and diagrams 1 and 4 in (4.33).

While in principle we could compute only these three diagrams and ignore or approximate the rest, this would break the loop expansion scheme of the macroscopic perturbation theory in a rather arbitrary fashion and thus render the interpretation of the results very difficult. In this thesis, we will instead consider an approximation that treats all 1-loop diagrams consistently, allowing us to investigate the properties of the 1-loop correction in a more well-defined manner.

4.3.2. Expansion in the initial power spectrum

Given the current numerical limitations, we are specifically not able to evaluate the full nonlinear expressions for the functions C_2 and C_3 appearing in the free collective field cumulants (B.3) to (B.7). A minimal approximation scheme would thus consist in expanding these two functions to some finite order in the initial power spectrum and leaving the remaining expressions for the cumulants unchanged. In particular, this would take the full exponential damping caused by the initial 1-point momentum variance σ_p^2 into account. However, our discussions of the tree-level density contrast power spectrum in subsection 4.2.2 showed that the effects of the full nonlinear correlations and σ_p^2 on the free-streaming of particles are actually strongly linked and partially cancel each other. Choosing different expansions for these two quantities is thus expected to generally lead to inconsistencies.

To treat them on equal footing, we will instead consider an expansion of the free cumulants in orders of the initial covariance matrix (3.47). In the case of cosmic structure formation, (3.50) to (3.52) imply that this is equivalent to a strict expansion in orders of the initial power spectrum $P_\delta^{(i)}$ and thus also σ_p^2, due to (B.16). To keep track of the order in $P_\delta^{(i)}$, it will be useful to denote the n-th term in this expansion by a subscript n, e.g. $G_{ff,2}^{(0)}$ denotes the contribution to $G_{ff}^{(0)}$ that is quadratic in $P_\delta^{(i)}$. As shown in [48], the lowest-order non-shot-noise contribution to a free collective-field cumulant involving n_f phase-space density fields is of order $n_f - 1$ in $P_\delta^{(i)}$, i.e.

$$G_{f\cdots f\mathcal{F}\cdots\mathcal{F}}^{(0)}(1,\ldots,n_f,1',\ldots,n_{\mathcal{F}}') = \sum_{n=n_f-1}^{\infty} G_{f\cdots f\mathcal{F}\cdots\mathcal{F},n}^{(0)}(1,\ldots,n_f,1',\ldots,n_{\mathcal{F}}'). \qquad (4.34)$$

Recalling the definition (3.75) of the macroscopic vertices, we infer that a vertex with n_β β-legs is thus at least of order $n_\beta - 1$,

$$\mathcal{V}_{\beta\cdots\beta f\cdots f}(1,\ldots,n_\beta,1',\ldots,n_f') = \sum_{n=n_\beta-1}^{\infty} \mathcal{V}_{\beta\cdots\beta f\cdots f,n}(1,\ldots,n_\beta,1',\ldots,n_f'). \qquad (4.35)$$

Since the macroscopic self-energies $\Sigma_{\beta\beta}$, $\Sigma_{\beta f}$ and $\Sigma_{f\beta}$ behave as effective 2-point vertices, their expansions are defined analogously.

From (3.78) and (3.79) it further follows that the the statistical propagator Δ_{ff} is at least linear

in $P_\delta^{(i)}$ while the causal propagators Δ_R and Δ_A have a minimal order of 0,

$$\Delta_{ff}(1,2) = \sum_{n=1}^{\infty} \Delta_{ff,n}(1,2), \tag{4.36}$$

$$\Delta_R(1,2) = \sum_{n=0}^{\infty} \Delta_{R,n}(1,2), \tag{4.37}$$

$$\Delta_A(1,2) = \sum_{n=0}^{\infty} \Delta_{A,n}(1,2). \tag{4.38}$$

The expansions of the exact macroscopic propagators G_{ff}, G_R and G_A are defined analogously.

By construction, the lowest order in this expansion scheme corresponds to the linear theory. Hence, the lowest-order results for the propagators are precisely given by the large-scale solutions (4.19) and (4.22) found in subsection 4.2.1 if we set the initial momentum variance σ_p^2 appearing in these expressions to zero,

$$G_{ff,1}(1,2) = \Delta_{ff,1}(1,2) = \Delta_{ff}^{(ls)}(1,2)\Big|_{\sigma_p^2=0}, \tag{4.39}$$

$$G_{R,0}(1,2) = \Delta_{R,0}(1,2) = \Delta_R^{(ls)}(1,2)\Big|_{\sigma_p^2=0}. \tag{4.40}$$

To obtain the next order, we have to add contributions from two different origins. On the one hand, the statistical and causal tree-level propagators have to be expanded to second and first order in $P_\delta^{(i)}$, respectively. On the other hand, we also have to take the 1-loop contributions to the propagator into account, using the lowest-order expressions for the propagators and vertices inside each loop-diagram. The respective contributions to the exact propagators thus read

$$G_{ff,2}(1,2) = \Delta_{ff,2}(1,2) + \left(\Delta_{f\beta,0} \cdot \Sigma_{\beta\beta,2}^{(1)} \cdot \Delta_{\beta f,0}\right)(1,2)$$
$$+ \left(\Delta_{f\beta,0} \cdot \Sigma_{\beta f,1}^{(1)} \cdot \Delta_{ff,1}\right)(1,2) \tag{4.41}$$
$$+ \left(\Delta_{ff,1} \cdot \Sigma_{f\beta,1}^{(1)} \cdot \Delta_{\beta f,0}\right)(1,2),$$

$$G_{f\beta,1}(1,2) = G_{\beta f,1}(2,1) = \Delta_{f\beta,1}(1,2) + \left(\Delta_{f\beta,0} \cdot \Sigma_{\beta f,1}^{(1)} \cdot \Delta_{f\beta,0}\right)(1,2). \tag{4.42}$$

Let us first consider the expansion of the tree-level propagators. To find the first-order contribution to the causal propagators, we insert the expansion (4.34) of $G_{f\mathcal{F}}^{(0)}$ into their Neumann series expression (3.80) and collect all terms linear in $P_\delta^{(i)}$. Omitting the functional arguments for

brevity, this reads

$$\Delta_{\mathrm{R},1} = \sum_{n=1}^{\infty} \sum_{m=1}^{n} \left(\mathrm{i}G^{(0)}_{f\mathcal{F},0}\right)^{m-1} \cdot \mathrm{i}G^{(0)}_{f\mathcal{F},1} \cdot \left(\mathrm{i}G^{(0)}_{f\mathcal{F},0}\right)^{n-m} \tag{4.43}$$

$$= \sum_{m=1}^{\infty} \sum_{n=m}^{\infty} \left(\mathrm{i}G^{(0)}_{f\mathcal{F},0}\right)^{m-1} \cdot \mathrm{i}G^{(0)}_{f\mathcal{F},1} \cdot \left(\mathrm{i}G^{(0)}_{f\mathcal{F},0}\right)^{n-m} \tag{4.44}$$

$$= \sum_{m=0}^{\infty} \left(\mathrm{i}G^{(0)}_{f\mathcal{F},0}\right)^{m} \cdot \mathrm{i}G^{(0)}_{f\mathcal{F},1} \cdot \sum_{n=0}^{\infty} \left(\mathrm{i}G^{(0)}_{f\mathcal{F},0}\right)^{n} \tag{4.45}$$

$$= \Delta_{\mathrm{R},0} \cdot \mathrm{i}G^{(0)}_{f\mathcal{F},1} \cdot \Delta_{\mathrm{R},0} \tag{4.46}$$

for the retarded propagator. In the second line we exchanged the order of the two sums, in the third line we shifted their summation indices, and in the last line we identified the zeroth-order retarded propagator. The expression for the advanced propagator is obtained analogously and reads

$$\Delta_{\mathrm{A},1} = \Delta_{\mathrm{A},0} \cdot \mathrm{i}G^{(0)}_{\mathcal{F}f,1} \cdot \Delta_{\mathrm{A},0} \, . \tag{4.47}$$

To find the second-order expression for the statistical propagator, we insert the expansions (4.34), (4.37) and (4.38) for $G^{(0)}_{ff}$, Δ_{R} and Δ_{A} into its definition (3.78) and add all the terms quadratic in $P^{(\mathrm{i})}_{\delta}$,

$$\Delta_{ff,2} = \Delta_{\mathrm{R},0} \cdot G^{(0)}_{ff,2} \cdot \Delta_{\mathrm{A},0} \; + \; \Delta_{\mathrm{R},1} \cdot G^{(0)}_{ff,1} \cdot \Delta_{\mathrm{A},0} \; + \; \Delta_{\mathrm{R},0} \cdot G^{(0)}_{ff,1} \cdot \Delta_{\mathrm{A},1} \tag{4.48}$$

$$\begin{aligned} = \; & \Delta_{\mathrm{R},0} \cdot G^{(0)}_{ff,2} \cdot \Delta_{\mathrm{A},0} \; + \; \Delta_{\mathrm{R},0} \cdot \mathrm{i}G^{(0)}_{f\mathcal{F},1} \cdot \Delta_{\mathrm{R},0} \cdot G^{(0)}_{ff,1} \cdot \Delta_{\mathrm{A},0} \\ & + \; \Delta_{\mathrm{R},0} \cdot G^{(0)}_{ff,1} \cdot \Delta_{\mathrm{A},0} \cdot \mathrm{i}G^{(0)}_{\mathcal{F}f,1} \cdot \Delta_{\mathrm{A},0} \end{aligned} \tag{4.49}$$

$$= \Delta_{\mathrm{R},0} \cdot G^{(0)}_{ff,2} \cdot \Delta_{\mathrm{A},0} \; + \; \Delta_{\mathrm{R},0} \cdot \mathrm{i}G^{(0)}_{f\mathcal{F},1} \cdot \Delta_{ff,1} \; + \; \Delta_{ff,1} \cdot \mathrm{i}G^{(0)}_{\mathcal{F}f,1} \cdot \Delta_{\mathrm{A},0} \, , \tag{4.50}$$

where we inserted $\Delta_{\mathrm{R},1}$ and $\Delta_{\mathrm{A},1}$ in the second line, and identified the first-order statistical propagator in the last step.

Inserting $\Delta_{ff,2}$ and $\Delta_{f\beta,1} = -\mathrm{i}\Delta_{\mathrm{R},1}$ into the expressions (4.41) and (4.42) for $G_{ff,2}$ and $G_{f\beta,1}$ then shows that we can effectively consider $-G^{(0)}_{ff,2}$ and $-G^{(0)}_{f\mathcal{F},1}$ as additional contributions to the self-energy,

$$\Sigma^{(1)}_{\beta\beta,2} \quad \rightarrow \quad \Sigma_{\beta\beta,2} \coloneqq \Sigma^{(1)}_{\beta\beta,2} - G^{(0)}_{ff,2} \, , \tag{4.51}$$

$$\Sigma^{(1)}_{\beta f,1} \quad \rightarrow \quad \Sigma_{\beta f,1} \coloneqq \Sigma^{(1)}_{\beta f,1} - G^{(0)}_{f\mathcal{F},1} \, , \tag{4.52}$$

such that

$$G_{ff,2} = \Delta_{f\beta,0} \cdot \Sigma_{\beta\beta,2} \cdot \Delta_{\beta f,0} \; + \; \Delta_{f\beta,0} \cdot \Sigma_{\beta f,1} \cdot \Delta_{ff,1} \; + \; \Delta_{ff,1} \cdot \Sigma_{f\beta,1} \cdot \Delta_{\beta f,0} \, , \tag{4.53}$$

$$G_{f\beta,1} = \Delta_{f\beta,0} \cdot \Sigma_{\beta f,1} \cdot \Delta_{f\beta,0} \, . \tag{4.54}$$

The next step is now to compute the 1-loop self-energy contributions $\Sigma^{(1)}_{\beta\beta,2}$ and $\Sigma^{(1)}_{\beta f,1}$. In contrast to the full 1-loop expressions, all time integrals involved in these can be calculated

analytically, leaving us only with a two-dimensional integration over the loop wavevector that has to be performed numerically. In this thesis, we restrict ourselves to the spatial-density information contained in the 1-loop diagrams, obtained by evaluating all momentum Fourier vectors $\vec{l}$ at zero, which allows to simplify the calculations considerably. The explicit expressions obtained for individual diagrams after performing the time integrations are nonetheless generally very lengthy and not particularly insightful. But they all share similar structures and it turns out that a large number of terms cancel when adding all diagrams belonging to the same component of the self-energy. Rather than showing the resulting expressions for all diagrams individually, we will thus only discuss their general structure and physical interpretation, and give the result for the sum of all diagrams in the end.

Let us first have a look at the statistical 1-loop self-energy $\Sigma^{(1)}_{\beta\beta,2}$. We find that the expressions for all of its contributing diagrams, and thus also for $\Sigma^{(1)}_{\beta\beta,2}$ as a whole, split into two parts with different types of remaining wavevector integrals,

$$\Sigma^{(1)}_{\beta\beta,2}(1,2) = \Sigma^{(1,\mathrm{P})}_{\beta\beta,2}(1,2) + \Sigma^{(1,\mathrm{C})}_{\beta\beta,2}(1,2) \tag{4.55}$$

where

$$\left.\Sigma^{(1,\mathrm{P})}_{\beta\beta,2}(1,2)\right|_{\vec{l}_1=\vec{l}_2=0} = (2\pi)^3\,\delta_{\mathrm{D}}\!\left(\vec{k}_1+\vec{k}_2\right)P^{(\mathrm{i})}_{\delta}(k_1)\int\frac{\mathrm{d}^3k'}{(2\pi)^3}\,P^{(\mathrm{i})}_{\delta}(k')\,K^{(1,\mathrm{P})}_{\beta\beta,2}\!\left(\vec{k}_1,\vec{k}',\eta_1,\eta_2\right), \tag{4.56}$$

$$\left.\Sigma^{(1,\mathrm{C})}_{\beta\beta,2}(1,2)\right|_{\vec{l}_1=\vec{l}_2=0} = (2\pi)^3\,\delta_{\mathrm{D}}\!\left(\vec{k}_1+\vec{k}_2\right)\int\frac{\mathrm{d}^3k'}{(2\pi)^3}\,P^{(\mathrm{i})}_{\delta}(k')\,P^{(\mathrm{i})}_{\delta}\!\left(|\vec{k}_1+\vec{k}'|\right)K^{(1,\mathrm{C})}_{\beta\beta,2}\!\left(\vec{k}_1,\vec{k}',\eta_1,\eta_2\right), \tag{4.57}$$

with some kernel functions $K^{(1,\mathrm{P})}_{\beta\beta,2}$ and $K^{(1,\mathrm{C})}_{\beta\beta,2}$. The first contribution is a product of one initial power spectrum with the weighted integral of the other one, while the second one is a weighted convolution of both spectra. In the following, we will hence refer to them as the product- and convolution-contributions to $\Sigma^{(1)}_{\beta\beta,2}$, respectively. Both types of integrals can be performed numerically stably and fast.

To investigate their impact on the nonlinear dark matter structure formation, we compute their contributions to the density-contrast power spectrum at redshift zero, obtained via

$$P_{\delta,2}(k_1,\eta_1)\Big|_{\Sigma^{(1,\mathrm{P/C})}_{\beta\beta,2}} = \left.\frac{\left(\Delta_{f\beta,0}\cdot\Sigma^{(1,\mathrm{P/C})}_{\beta\beta,2}\cdot\Delta_{\beta f,0}\right)(1,2)}{(2\pi)^3\,\delta_{\mathrm{D}}\!\left(\vec{k}_1+\vec{k}_2\right)\bar{\rho}^2}\right|_{\substack{\vec{k}_2=-\vec{k}_1\\\vec{l}_1=\vec{l}_2=0\\\eta_2=\eta_1}}, \tag{4.58}$$

for one exemplary diagram and plot these in Figure 4.2. For this, we chose the 4$^{\text{th}}$ diagram in (4.32), as it contains all characteristic features found in the different $\Sigma_{\beta\beta}$-diagrams. Negative contributions are plotted as dashed lines, and for reference we also show the linear power spectrum $P^{(\mathrm{lin})}_{\delta}$. In addition, the explicit expressions for the kernels of this particular diagram can be found in Appendix F.

We first note that this diagram appears to describe only a subdominant contribution to the 1-loop correction, as its amplitude only becomes comparable to the linear result on very large
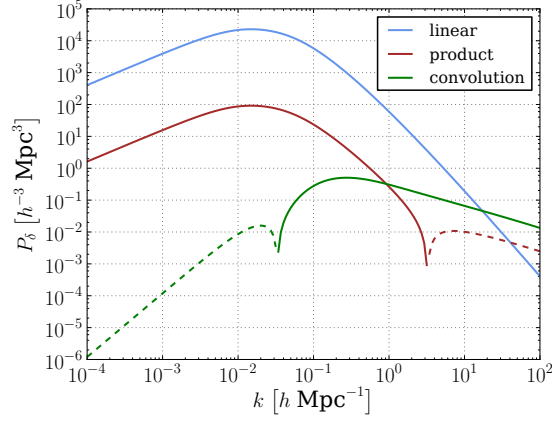
Figure 4.2.: Contributions of one exemplary 1-loop diagram to the density contrast power spectrum evaluated at redshift zero. For reference, the linear power spectrum is shown as well. The convolution-contribution describes a transport of power from large to small scales. The product-contribution, on the other hand, reduces power on small scales and shows an enhancement of power on arbitrarily large scales.

wavenumbers. But let us ignore this for the moment, and rather focus on its shape, which shows a number of interesting features also found in other, more dominant diagrams. We see that the convolution-contribution shows a reduction of power on small wavenumbers whose relative effect compared to the linear result is strongest around the peak of $P_\delta^{(\mathrm{lin})}(k)$ and becomes weaker when going to smaller k. On large wavenumbers, on the other hand, it shows an increase in power whose relative effect becomes ever stronger when going to larger k. Overall, it thus describes the transport of power from large to small scales, similar to our findings in [2].

The product-contribution shows more or less the opposite behaviour: It adds power on small wavenumbers and subtracts it on large ones. However, while on large k it shows the same slope as the convolution term, its slope on small k is shallower than that of the convolution term and appears to match the slope of the linear spectrum instead. Hence, its relative effect compared to the linear spectrum does not decrease when going to smaller k, which seems unphysical, as those small wavenumbers should be fully described by the linear theory.

To understand this better, let us investigate the limiting behaviour of (4.56) and (4.57) for small and large wavenumbers k_1. To do so, we exploit the fact that most of the integrand's weight comes from the region around the peak of the power spectrum, which can be explicitly checked by varying the integration boundaries. This implies that taking the limits of small and large values of k_1 corresponds in good approximation to taking the limits $k_1 \ll k'$ and $k_1 \gg k'$ under the

integrals, respectively. For our exemplary diagram we then find

$$
\Sigma_{\beta\beta,2}^{(1,\mathrm{P})}(1,2)\Big|_{\vec{l}_1=\vec{l}_2=0} \propto
\begin{cases}
P_\delta^{(\mathrm{i})}(k_1)\,\sigma_\delta^2 & \text{for small } k_1, \\[2mm]
P_\delta^{(\mathrm{i})}(k_1)\,k_1^2\sigma_p^2 & \text{for large } k_1,
\end{cases}
\tag{4.59}
$$

$$
\Sigma_{\beta\beta,2}^{(1,\mathrm{C})}(1,2)\Big|_{\vec{l}_1=\vec{l}_2=0} \propto
\begin{cases}
k_1^2\int\frac{\mathrm{d}^3 k'}{(2\pi)^3}\frac{\left(P_\delta^{(\mathrm{i})}(k')\right)^2}{k'^2} & \text{for small } k_1, \\[2mm]
P_\delta^{(\mathrm{i})}(k_1)\,k_1^2\sigma_p^2 & \text{for large } k_1,
\end{cases}
\tag{4.60}
$$

where we omitted the explicit time-dependencies and defined the initial 1-point density contrast variance

$$
\sigma_\delta^2 := C_{\delta_j\delta_j} = \int\frac{\mathrm{d}^3 k'}{(2\pi)^3}\,P_\delta^{(\mathrm{i})}(k')\,.
\tag{4.61}
$$

Note that the contributions of $\Sigma_{\beta\beta,2}^{(1,\mathrm{P/C})}$ to the power spectrum, given by (4.58), show exactly the same scaling behaviour since the zeroth-order tree-level propagators $\Delta_{f\beta,0}$ and $\Delta_{\beta f,0}$ are scale-independent.

We see that on large wavenumbers both terms are dominated by contributions proportional to the initial 1-point momentum variance σ_p^2. We expect this to be related to the fact that small-scale structures are washed out by the particles' momentum dispersion, as discussed in subsection 4.2.1. This effect should actually be described by a Gaussian damping factor. But owing to the fact that we are currently considering an expansion to second order in $P_\delta^{(\mathrm{i})}$ and σ_p^2, only the linear contribution to such a Gaussian can show up.

On small wavenumbers, the convolution term scales like k_1^2 and is thus subdominant compared to the linear spectrum $P_\delta^{(\mathrm{lin})}(k_1)$. This is because the latter scales like $k_1^{n_{\mathrm{s}}}$ with a spectral index of $n_{\mathrm{s}} = 0.967$ on small wavenumbers, as described in (2.25). The product term, however, has in this limit exactly the same k_1 dependence as $P_\delta^{(\mathrm{i})}(k_1)$ and thus also $P_\delta^{(\mathrm{lin})}(k_1)$, confirming the behaviour seen in Figure 4.2. Furthermore, we note that the latter is proportional to the initial density contrast variance σ_δ^2. This reveals another problem, as the integral in (4.61) is divergent for initial power spectra that scale like k_1^n with a slope $n \geq -3$ in the limit of k_1 going to infinity. According to (2.25), our initial power spectrum has a large-wavenumber slope of $n = n_{\mathrm{s}} - 4 = -3.033$, which is just barely within the convergent regime. Nevertheless, this still means that the value of this large-scale correction is very sensitive to the power of small-scale fluctuations, rendering this contribution even more implausible.

The crucial question is now if this seemingly unphysical behaviour is only a spurious effect of individual 1-loop diagrams or if it actually survives when summing up all of them? If the latter was true, this might imply a serious problem for the macroscopic perturbation theory. Before we can answer this question, though, a few words have to be said on how the properties of the other statistical as well as causal 1-loop self-energy diagrams compare to those found for our exemplary diagram.

First of all, performing the same analysis for the remaining statistical self-energy diagrams reveals that their small- and large-wavenumber limits have scaling behaviours that either agree with those found in (4.59) and (4.60) or are less relevant in the respective limit. In particular, this means that there is no $\Sigma_{\beta\beta,2}^{(1)}$-contribution whose small-k limit scales like $P_\delta^{(\mathrm{i})}(k)\,k^n$ with $n < 0$,

and thus they do not introduce any new type of problematic behaviour other than that already mentioned.

Examining the causal self-energy diagrams (4.33) shows that they can all be expressed as a weighted integral over a single initial power spectrum,

$$\Sigma_{\beta f,1}^{(1)}(1,2)\Big|_{\vec{l}_1=\vec{l}_2=0} = (2\pi)^3\,\delta_{\mathrm{D}}\big(\vec{k}_1+\vec{k}_2\big)\,\int\frac{\mathrm{d}^3k'}{(2\pi)^3}\,P_\delta^{(\mathrm{i})}(k')\,K_{\beta f,1}^{(1)}\big(\vec{k}_1,\vec{k}',\eta_1,\eta_2\big)\,,\qquad (4.62)$$

with some kernel $K_{\beta f,1}^{(1)}$, and that their scaling behaviours are either given by

$$\Sigma_{\beta f,1}^{(1)}(1,2)\Big|_{\vec{l}_1=\vec{l}_2=0} \propto \begin{cases} \sigma_\delta^2 & \text{for small } k_1, \\ k_1^2\sigma_P^2 & \text{for large } k_1 \end{cases} \qquad (4.63)$$

or are less relevant than this in the respective limit. It further turns out that their contributions to the power spectrum,

$$P_{\delta,2}(k_1,\eta_1)\Big|_{\Sigma_{\beta f,1}^{(1)}} = \frac{\Big(\Delta_{f\beta,0}\cdot\Sigma_{\beta f,1}^{(1)}\cdot\Delta_{ff,1}\Big)(1,2) + \Big(\Delta_{ff,1}\cdot\Sigma_{f\beta,1}^{(1)}\cdot\Delta_{\beta f,0}\Big)(1,2)}{(2\pi)^3\,\delta_{\mathrm{D}}\big(\vec{k}_1+\vec{k}_2\big)\,\bar\rho^2}\Bigg|_{\substack{\vec{k}_2=-\vec{k}_1\\ \vec{l}_1=\vec{l}_2=0\\ \eta_2=\eta_1}},\qquad (4.64)$$

show the same scaling behaviour as those of the product-contributions to the statistical self-energy, due the first-order statistical tree-level propagator $\Delta_{ff,1}$ being linear in the initial power spectrum. This means that the causal self-energy diagrams do not introduce any new type of problematic behaviour either.

We conclude that it suffices to check if there are any terms proportional to σ_δ^2 in the small-k limit remaining when summing up all 1-loop contributions to the statistical and causal self-energies, respectively. Performing this analysis shows that this is not the case, as all appearing σ_δ^2-contributions, including their full time-dependencies, cancel precisely. Thus, both self-energy components as well as the 1-loop correction as a whole are physically consistent in the sense that their large-scale limit is subdominant compared to the linear result and insensitive to the power of small-scale fluctuations. While this is very reassuring, it also suggests that individual 1-loop diagrams on their own might generally not describe a physical process. We will always have to keep this in mind when interpreting results within the macroscopic perturbation theory.

However, it turns out that there are in fact three subsets of $\Sigma_{\beta\beta,2}^{(1)}$-diagrams in (4.32) whose sums are free of σ_δ^2-contributions on their own. One set just contains diagram 1, the second set consists of the diagrams 2, 3, 4 and 7, and the remaining diagrams 5, 6 and 8 form the third set. We note that these three sets differ in the number of β-legs of their vertices. Set 1 is given by the only diagram whose vertices have only a single β-leg. All diagrams in set 2 contain vertices with two β-legs but no vertices with more β-legs than that. And set 3 collects all diagrams containing vertices with three β-legs. If this was indeed a general pattern, one would also expect the $\Sigma_{\beta f,1}^{(1)}$-diagrams in (4.33) to split into two subsets that are physically consistent on their own: diagrams 1 and 4, and diagrams 2, 3 and 5, respectively. This is not the case, though, as only the sum of all $\Sigma_{\beta f,1}^{(1)}$-diagrams together is free of σ_δ^2-contributions.

Instead, we suspect a slightly different pattern by recalling from (3.75) that a vertex with n β-legs involves a free connected n-point phase-space density correlation. Hence, the diagrams in set 3 of $\Sigma^{(1)}_{\beta\beta,2}$ are the only diagrams involving a connected 3-point correlation, whereas all other 1-loop diagrams contain connected 2-point correlators – if not via the vertices then at least via the statistical propagators. This suggests the following refinement of the perturbative expansion scheme proposed in subsection 3.2.4: In addition to fixing a number of loops, one might also restrict the maximal order of free connected n-point correlations involved in a diagram without loosing physical consistency. However, this is just a conjecture that still has to be proven or at least be tested in higher loop orders and in the computation of other macroscopic cumulants than the propagator. Furthermore, it still has to be investigated if the cancellations of σ_δ^2-contributions found here for the expansion to second order in the initial power spectrum holds in the same way for the full 1-loop corrections containing the complete hierarchy of initial momentum correlations.

Finally, the expressions for the complete next-to-lowest-order self-energies $\Sigma_{\beta\beta,2}$ and $\Sigma_{\beta f,1}$ as well as propagators $G_{ff,2}$ and $G_{R,1}$, including the tree-level- and loop-contributions, and all evaluated at $\vec{l}_1 = \vec{l}_2 = 0$, are listed in Appendix F. Considering the large number of individual contributions entering this calculation, the resulting expressions are surprisingly compact. Beyond that, the results for the propagators also show some remarkable symmetries in their time-dependencies. In contrast, some of the terms in the expressions for the self-energies show a rather unusual time-dependence. Unlike all other terms they do not only depend exponentially on η, but also polynomially. Given the definition (4.1) of η, this corresponds to a spurious logarithmic dependence on the linear growth factor D_+. This might indicate that the self-energies themselves are not a natural quantity to compute in this expansion scheme, and should only be considered as an intermediate result during the computation of the propagators.

In Figure 4.3a we plot the different contributions to the density contrast power spectrum as well as their sum at redshift zero. For comparison we also show the linear result. We first want to point out that this plot nicely illustrates how all three contributions are indeed free of the unphysical small-k behaviour found in individual diagrams. Beyond that, we also observe some remarkable cancellations on large wavenumbers. While all three contributions on their own show the same large-k scaling behaviour found in individual diagrams, this is not the case for their sum which appears to have the same slope as the linear power spectrum on these wavenumbers instead. In fact, this can be confirmed analytically by taking the respective limit of the expression found for $G_{\rho\rho,2}$, which further reveals that the cancellation only occurs if $G_{\rho\rho,2}$ is evaluated at equal times.

To understand this, we have to recall that the large-k limit of individual diagrams scales like $P^{(i)}_\delta(k_1)\,k_1^2\sigma_p^2$ and is hence associated with the momentum dispersion of the particles. The cancellation of these contributions at equal times is thus reminiscent of the compensation of damping effects found in (4.18) for the full nonlinear free 2-point cumulant $G^{(0)}_{\rho\rho}$. This is a first hint at the preservation of this property in the interacting theory.

In Figure 4.3b we compare the sum of the first- and second-order results for the power spectrum with a fit to numerical simulations provided by [54]. Both agree in the wavenumber above which the nonlinear evolution sets in, and also their overall shapes show a good match. Considering that we are currently only investigating the next-to-lowest order expansion in the initial power spectrum, this is already quite remarkable. The fact that our results overpredict the growth of

(a) Individual contributions

(b) Comparison with simulation
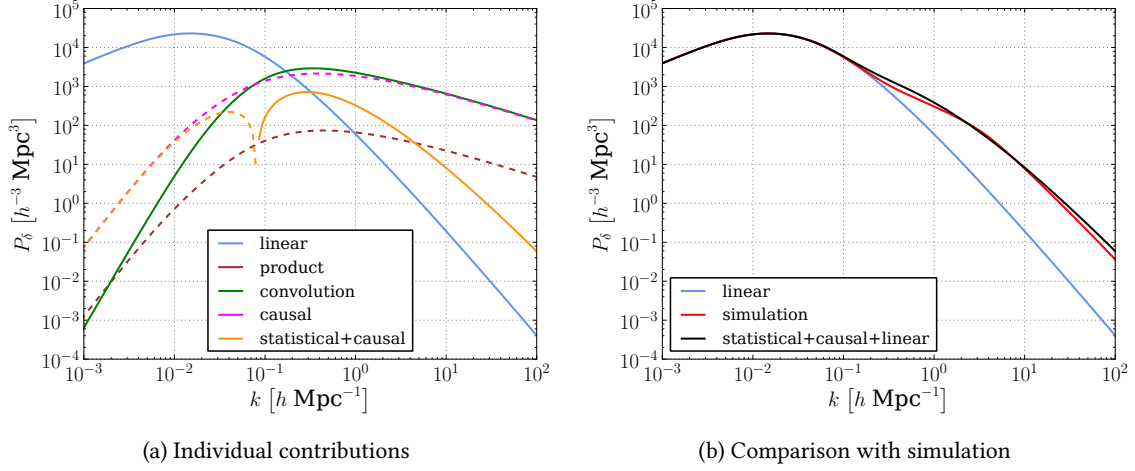
Figure 4.3.: First- and second-order contributions to the density contrast power spectrum evaluated at redshift zero. In (a) the individual second-order contributions as well as their sum are shown next to the linear power spectrum. Their sum yields an overall transport of power from large to small scales. Furthermore, a cancellation of the small-scale effects associated with the particles' momentum dispersion is seen. In (b) the sum of all first- and second-order contributions is compared to the nonlinear power spectrum obtained from numerical simulations by [54].

structures on mildly non-linear scales, though, also demonstrates that it will be necessary to take higher-order corrections into account if we want to achieve a more accurate agreement with numerical simulations.

4.3.3. Comparison to standard Eulerian perturbation theory

To fully understand the implications of the results found in the previous subsection, it will prove very useful to compare them to the respective results found in standard Eulerian perturbation theory (SPT). We will start by providing a short summary of the general formalism of SPT, focussing on the main aspects only. For more details on this we refer the reader to [5, 55].

In SPT, dark matter is assumed to be described by a collisionless self-gravitating fluid. Its dynamics is thus governed by the collisionless Boltzmann equation, also referred to as Vlasov equation,

$$0 = \frac{\mathrm{d}f}{\mathrm{d}\eta} = \frac{\partial f}{\partial \eta} + \vec{p} \cdot \frac{\partial f}{\partial \vec{q}} - \vec{\nabla}_q \tilde{V}_G \cdot \frac{\partial f}{\partial \vec{p}} \,, \tag{4.65}$$

where the effective gravitational potential $\tilde{V}_G$ is satisfying the Poisson equation (4.4). Rather than trying to solve this evolution equation for the phase-space density f as a whole, though, SPT deals with the dynamics of the momentum moments of f. Of particular interest are the zeroth,

first and second moments,

$$\int \mathrm{d}^3 p \; f(\vec{q}, \vec{p}, \eta) = \rho(\vec{q}, \eta) \,, \tag{4.66}$$

$$\int \mathrm{d}^3 p \; \vec{p} \; f(\vec{q}, \vec{p}, \eta) = \rho(\vec{q}, \eta) \, \vec{u}(\vec{q}, \eta) \,, \tag{4.67}$$

$$\int \mathrm{d}^3 p \; \vec{p} \otimes \vec{p} \; f(\vec{q}, \vec{p}, \eta) = \rho(\vec{q}, \eta) \, \vec{u}(\vec{q}, \eta) \otimes \vec{u}(\vec{q}, \eta) + \sigma_u(\vec{q}, \eta) \,, \tag{4.68}$$

where $\vec{u}$ denotes the peculiar comoving velocity field with respect to the coordinate time η and σ_u the stress tensor of the fluid. Their evolution equations are then obtained by taking the respective moments of the Vlasov equation (4.65). For ρ and $\vec{u}$ this yields

$$0 = \frac{\partial \rho}{\partial \eta} + \vec{\nabla}_q \cdot \left(\rho \vec{u} \right) \,, \tag{4.69}$$

$$0 = \frac{\partial \vec{u}}{\partial \eta} + \frac{1}{2} \vec{u} + \vec{u} \cdot \vec{\nabla}_q \vec{u} + \vec{\nabla}_q \tilde{V}_G + \frac{1}{\rho} \, \vec{\nabla}_q \sigma_u \,. \tag{4.70}$$

As already hinted at by these two equations, this procedure leads to an infinite hierarchy of evolution equations since the equation for the n-th moment always couples to the $(n+1)$-th moment. To get a closed set of equations, this hierarchy has to be truncated at some point, which is usually achieved by making some approximation for the stress tensor σ_u. The approach taken in SPT is to assume it to vanish identically, $\sigma_u = 0$, which corresponds to the assumption of particle trajectories following a single coherent stream [5]. While this is expected to be a good approximation in the early stages of cosmic structure formation, it will eventually break down when streams of particles start to cross during the collapse of structures, usually referred to as shell-crossing.

Conventionally, the equations of motion (4.69) and (4.70) are then expressed in terms of the density contrast δ and the velocity divergence $\theta := \vec{\nabla} \cdot \vec{u}$. If we further define their joint field vector $\Psi := (\delta, -\theta)$, insert the Poisson equation (4.4) and transform to Fourier space, the resulting equations of motion can be written in the compact form

$$\left(\delta_{ab} \partial_\eta + \omega_{ab} \right) \Psi_b(\vec{k}, \eta) = \int \frac{\mathrm{d}^3 k_1}{(2\pi)^3} \int \frac{\mathrm{d}^3 k_2}{(2\pi)^3} \, \gamma_{abc}(\vec{k}, -\vec{k}_1, -\vec{k}_2) \, \Psi_b(\vec{k}_1, \eta) \, \Psi_c(\vec{k}_2, \eta) \,, \tag{4.71}$$

where the summation over repeated indices is implied. Here, the linear evolution is characterised by the matrix

$$\omega := \begin{pmatrix} 0 & -1 \\ -\frac{3}{2} & \frac{1}{2} \end{pmatrix} \,, \tag{4.72}$$

and the nonlinearities are collected in the vertices γ_{abc} whose only non-vanishing entries are

$$\gamma_{112}(\vec{k}, \vec{k}_1, \vec{k}_2) = \gamma_{121}(\vec{k}, \vec{k}_2, \vec{k}_1) := (2\pi)^3 \, \delta_{\mathrm{D}}(\vec{k} + \vec{k}_1 + \vec{k}_2) \, \frac{-\vec{k} \cdot \vec{k}_2}{2 \, k_2^2} \,, \tag{4.73}$$

$$\gamma_{222}(\vec{k}, \vec{k}_1, \vec{k}_2) := (2\pi)^3 \, \delta_{\mathrm{D}}(\vec{k} + \vec{k}_1 + \vec{k}_2) \, \frac{k^2 \, (\vec{k}_1 \cdot \vec{k}_2)}{k_1^2 \, k_2^2} \,. \tag{4.74}$$

By means of a Laplace transform it is possible to obtain an implicit integral solution of the equations of motion,

$$\Psi_a(\vec{k}, \eta) = g_{ab}(\eta)\,\Psi_b^{(i)}(\vec{k}) + \int_0^\eta d\eta'\, g_{ab}(\eta - \eta')\,\gamma_{bcd}(\vec{k}, -\vec{k}_1, -\vec{k}_2)\,\Psi_b(\vec{k}_1, \eta')\,\Psi_c(\vec{k}_2, \eta')\,, \quad (4.75)$$

where g is the retarded Green's function of the linearised equations of motion,

$$g(\eta_1, \eta_2) := \left(\frac{e^{\eta_1 - \eta_2}}{5} \begin{pmatrix} 3 & 2 \\ 3 & 2 \end{pmatrix} + \frac{e^{-\frac{3}{2}(\eta_1 - \eta_2)}}{5} \begin{pmatrix} 2 & -2 \\ -3 & 3 \end{pmatrix} \right) \theta(\eta_1 - \eta_2)\,, \quad (4.76)$$

usually referred to as the linear propagator, and $\Psi^{(i)}$ denotes the initial field configuration. When choosing the same initial conditions as described in subsection 3.1.3, both initial field components are given by the initial density contrast, $\Psi^{(i)} = (\delta^{(i)}, \delta^{(i)})$.[1]

Correlation functions $\langle \Psi_{a_1} \cdots \Psi_{a_n} \rangle$ can now be calculated perturbatively by inserting the implicit solution (4.75), expanding it to some given order in the initial field configuration $\Psi^{(i)}$ and taking the average over the initial conditions in the end. Since we are considering Gaussian initial conditions, this average will always factorise into the 2-point correlators

$$\langle \Psi_a^{(i)}(\vec{k}_1)\,\Psi_b^{(i)}(\vec{k}_2) \rangle =: (2\pi)^3\,\delta_{\mathrm{D}}(\vec{k}_1 + \vec{k}_2)\,P_{ab}^{(i)}(k_1) = (2\pi)^3\,\delta_{\mathrm{D}}(\vec{k}_1 + \vec{k}_2)\,P_\delta^{(i)}(k) \quad \forall a, b\,, \quad (4.77)$$

according to Wick's theorem. Most importantly for us, this means that the perturbative expansion scheme in SPT matches the expansion in orders of the initial density contrast power spectrum that we considered in the previous subsection. Comparing the expressions for the density contrast correlators $\langle \delta \cdots \delta \rangle$ obtained from SPT with those obtained from KFT, both expanded to the same order in $P_\delta^{(i)}$, thus represents the closest possible comparison between both frameworks. In this thesis, we will explicitly compare the expressions found for the first- and second-order results of the 2-point correlator.

The linear result in SPT is given by

$$\langle \delta(\vec{k}_1, \eta_1)\,\delta(\vec{k}_2, \eta_2) \rangle_1^{(\mathrm{SPT})} = (2\pi)^3\,\delta_{\mathrm{D}}(\vec{k}_1 + \vec{k}_2)\,g_{1a}(\eta_1)\,P_{ab}^{(i)}(k_1)\,g_{1b}(\eta_2) \quad (4.78)$$

$$= (2\pi)^3\,\delta_{\mathrm{D}}(\vec{k}_1 + \vec{k}_2)\,P_\delta^{(i)}(k)\,e^{\eta_1 + \eta_2}\,, \quad (4.79)$$

and agrees with the linear KFT result found in (4.39),

$$\langle \delta(\vec{k}_1, \eta_1)\,\delta(\vec{k}_2, \eta_2) \rangle_1^{(\mathrm{KFT})} = (\bar{\rho})^{-2}\,G_{ff,1}(1, 2)\Big|_{\vec{l}_1 = \vec{l}_2 = 0} = (\bar{\rho})^{-2}\,\Delta_{ff}^{(\mathrm{ls})}(1, 2)\Big|_{\vec{l}_1 = \vec{l}_2 = 0}\,, \quad (4.80)$$

as we already pointed out in subsection 4.2.1 specifically for the equal-time correlator. We want to stress that this has to be the case, as all approximations made during the derivation of SPT are actually exact as long as one considers the linear regime of cosmic structure formation.

Let us now compare the results obtained in second order in $P_\delta^{(i)}$, which is the lowest nonlinear correction. In SPT the respective expression reads

$$\langle \delta(\vec{k}_1, \eta_1)\,\delta(\vec{k}_2, \eta_2) \rangle_2^{(\mathrm{SPT})} = P_{13}(\vec{k}_1, \eta_1, \vec{k}_2, \eta_2) + P_{13}(\vec{k}_2, \eta_2, \vec{k}_1, \eta_1) + P_{22}(\vec{k}_1, \eta_1, \vec{k}_2, \eta_2)\,, \quad (4.81)$$

---

[1] In the literature this choice is referred to as growing mode initial conditions.

where

$$P_{13}(\vec{k}_1, \eta_1, \vec{k}_2, \eta_2) = 4 \int\limits_0^{\eta_1} \mathrm{d}\eta_1' \int\limits_0^{\eta_2} \mathrm{d}\eta_2' \int \frac{\mathrm{d}^3 k_1'}{(2\pi)^3} \int \frac{\mathrm{d}^3 k_2'}{(2\pi)^3} \, g_{1a}(\eta_1) \, P_{ab}^{(i)}(k_1) \, g_{cb}(\eta_1') \, \gamma_{cde}(\vec{k}_1, \vec{k}_1', \vec{k}_2')$$
$$\times g_{df}(\eta_1') \, P_{fg}^{(i)}(k_1') \, g_{hg}(\eta_2') \, g_{ei}(\eta_1', \eta_2')$$
$$\times \gamma_{jhi}(\vec{k}_2, -\vec{k}_1', -\vec{k}_2') \, g_{1j}(\eta_2, \eta_2') \,, \tag{4.82}$$

$$P_{22}(\vec{k}_1, \eta_1, \vec{k}_2, \eta_2) = 2 \int\limits_0^{\eta_1} \mathrm{d}\eta_1' \int\limits_0^{\eta_2} \mathrm{d}\eta_2' \int \frac{\mathrm{d}^3 k_1'}{(2\pi)^3} \int \frac{\mathrm{d}^3 k_2'}{(2\pi)^3} \, g_{1a}(\eta_1, \eta_1') \, \gamma_{abc}(\vec{k}_1, \vec{k}_1', \vec{k}_2')$$
$$\times g_{bd}(\eta_1') \, P_{de}^{(i)}(k_1') \, g_{fe}(\eta_2') \, g_{cg}(\eta_1') \, P_{gh}^{(i)}(k_2') \, g_{ih}(\eta_2')$$
$$\times \gamma_{jhi}(\vec{k}_2, -\vec{k}_1', -\vec{k}_2') \, g_{1j}(\eta_2, \eta_2') \,. \tag{4.83}$$

As we can see, P_{13} and P_{22} show the same general structure as the product- and convolution-contributions discussed in our 1-loop calculations, respectively. Performing the remaining time and wavevector integrals and comparing the resulting expression with the KFT result presented in Appendix F reveals that both do not only share the same structure, though, but are in fact *exactly* the same,

$$\langle \delta(\vec{k}_1, \eta_1) \, \delta(\vec{k}_2, \eta_2) \rangle_2^{(\mathrm{SPT})} = \langle \delta(\vec{k}_1, \eta_1) \, \delta(\vec{k}_2, \eta_2) \rangle_2^{(\mathrm{KFT})} = (\bar{\rho})^{-2} \, G_{ff,2}(1,2) \Big|_{\vec{l}_1 = \vec{l}_2 = 0} \,. \tag{4.84}$$

This is a very surprising result that we do not fully understand yet. Our naive expectation was that both expressions should show some differences, as the approximations made in the derivation of SPT are expected to introduce deviations from the full particle dynamics once structure formation becomes nonlinear. And even if the effect of these deviations turned out to be less significant than expected, they should nonetheless leave their mark on our analytical results. There are at least four possible explanations for this observation:

- The approximations made in SPT might only affect higher-order nonlinear corrections. This would be the simplest explanation and it could be tested by comparing the corrections in third or higher order in $P_\delta^{(i)}$. Computing these quickly becomes a very formidable task, though.

- SPT and KFT might only appear to yield the same results in this particular expansion scheme. It is known that the perturbative expansion of SPT does not converge towards the full nonlinear result [56, 57]. Thus even if the results obtained from both frameworks agreed in every single order in $P_\delta^{(i)}$, one could not conclude both frameworks to predict the same full nonlinear result.

- The dynamical effects not captured by SPT might be irrelevant for the highly symmetric initial conditions assumed in cosmic structure formation. For example, it could be that the effect of stream-crossing on the evolution of collective-field correlators precisely vanishes

once we are taking the average over the statistically homogeneous, isotropic, rotation-free and Gaussian initial conditions. A possible hint at this is given by [56] who tested the effects of crossing streams in pure Zel'dovich dynamics. They showed that a resummation of SPT is able to recover the exact nonlinear result for the power spectrum in these simplified dynamics even though the hydrodynamical equations of motion break down at shell-crossing. It is however open if this property is preserved in the full gravitational dynamics.

- Our calculations within KFT might implicitly introduce the same approximations as SPT in a way that we have missed so far. The only approximation we made that we are aware of is to neglect all shot-noise contributions by taking the thermodynamic limit. As argued in section 4.1, though, this is expected to be an excellent approximation on all scales relevant for cosmic structure formation, as the additional terms would be suppressed by powers of the huge mean number density of dark matter particles. Hence, if it turned out that all particle dynamical effects not captured by SPT are indeed pure shot-noise contributions, then this would mean that the approximations made in SPT are better justified than we expected.

We do not know yet which of these explanations, if any, is correct and it is quite possible that the truth actually lies somewhere in between. It is certain, though, that investigating this in more detail will be crucial to fully understand the capabilities but also possible limits of the KFT framework. Beyond that, it might also shed some new light on the transition from a particle to a fluid picture in general. We are thus planning to look into this matter in the future.

As a final remark, we want to stress that the further development of KFT is almost certainly going to provide new insights into the cosmic structure formation in dark matter, even if it should turn out that KFT and SPT are formally equivalent in this setting. The reason for this is that the natural expansion schemes of both frameworks are fundamentally different. SPT is inherently built upon the expansion in orders of the initial power spectrum, while the natural macroscopic perturbative scheme of KFT is a combined expansion in the number of loops and the order of freely evolved n-point phase-space density cumulants taken into account, as discussed in subsection 4.3.2. Therefore, KFT allows to tackle this problem from a completely new angle. In the last two subsections we only expanded KFT in orders of $P_\delta^{(i)}$ to bypass the current numerical limitations we are faced with otherwise. But the fact that this expansion mixed contributions from the tree- and 1-loop-level clearly shows that this is not the natural choice for KFT.

This becomes particularly important when considering the fact that the perturbative series of SPT is known to diverge. While this can be partially fixed by means of various resummation schemes, e. g. [52, 58–61], the fundamentally different approach of KFT might allow to investigate cosmic structure formation in an *inherently* convergent scheme instead. Of course, it still remains to be shown that our macroscopic perturbation theory is indeed convergent. But the properties of the full spatial tree-level propagator $\Delta_{\rho\rho}$, discussed in section 4.2, are already very promising. The crucial next step will now be to overcome the numerical limitations currently preventing us from applying the macroscopic perturbation theory without any approximations.

5. Baryonic effects

In the previous chapter we only considered structure formation in dark matter. However, as described in subsection 2.2.4, there are a number of different baryonic effects that have to be taken into account for an accurate description of the evolution of structures on cosmologically small scales. In this chapter, we focus on one of these: the influence of the baryonic gas dynamics on a gravitationally coupled system of dark and baryonic matter. There have been a few works studying this in Eulerian perturbation theory [62–64], but all of these only modelled the effect of baryonic pressure by introducing a simplified time-independent comoving Jeans length. Instead, we are aiming at a consistent treatment of the full ideal gas dynamics.

It was first shown in [65] how the hydrodynamical equations can be incorporated into KFT by introducing effective mesoscopic particles. After briefly summarising this derivation, we show how the mesoscopic particle model can be implemented into the resummed KFT framework and how it can be coupled to microscopic dark matter particles. Results on the linear structure formation in this coupled system obtained from the macroscopic propagator are presented.

This is done in two steps: First, we consider the case of isothermal baryons, which greatly simplifies the treatment in KFT and allows us to focus on the additional complications introduced by the treatment of two coupled particle species. In a second step, we demonstrate the implementation of adiabatic gas dynamics, which is more involved, as it requires to describe particles with internal degrees of freedom. Results on the linear structure formation in a cosmological setting are thus only presented for the isothermal case, as the full numerical computation of the macroscopic propagator in the adiabatic case is still work in progress.

5.1. Baryon dynamics

5.1.1. Ideal hydrodynamics

On cosmological scales, baryonic matter is well-described by an ideal gas, and hence its dynamics is governed by the three Euler equations. For a general ideal fluid, these read

$$0 = \frac{\mathrm{d}}{\mathrm{d}t}\rho_{\mathrm{m}} + \rho_{\mathrm{m}}\,\vec{\nabla}\cdot\vec{u}\,, \tag{5.1}$$

$$0 = \frac{\mathrm{d}}{\mathrm{d}t}\vec{\pi} + \vec{\pi}\left(\vec{\nabla}\cdot\vec{u}\right) + \vec{\nabla}P\,, \tag{5.2}$$

$$0 = \frac{\mathrm{d}}{\mathrm{d}t}\varepsilon + (\varepsilon + P)\,\vec{\nabla}\cdot\vec{u}\,, \tag{5.3}$$

where ρ_{m} denotes the fluid's mass density, $\vec{u}$ its velocity field, $\vec{\pi} = \vec{u}\rho_{\mathrm{m}}$ its momentum density, P its pressure and ε internal energy density [66]. They represent the conservation of mass, momentum and energy, respectively.

To close this set of equations, we still need to relate ε and P. Following [65], we choose to express both in terms of the enthalpy density $h = \varepsilon + P$ and use the equation of state of an ideal gas,

$$h = \gamma \varepsilon = \frac{\gamma}{\gamma - 1} P \,. \tag{5.4}$$

Here, γ denotes the adiabatic index of the gas defined as the ratio of the gas's heat capacities at constant pressure and volume, C_P and C_V. For an ideal gas it can conveniently be expressed in terms of the number of degrees of freedom f of an individual gas particle,

$$\gamma := \frac{C_P}{C_V} = \frac{f + 2}{f} \,. \tag{5.5}$$

For a monoatomic gas in three dimensions, $f = 3$ and thus $\gamma = 5/3$, for example.

Using (5.4), equations (5.2) and (5.3) can be rewritten in terms of the enthalpy density,

$$0 = \frac{\mathrm{d}}{\mathrm{d}t} \vec{\pi} + \vec{\pi} \left(\vec{\nabla} \cdot \vec{u} \right) + \frac{\gamma - 1}{\gamma} \vec{\nabla} h \,, \tag{5.6}$$

$$0 = \frac{\mathrm{d}}{\mathrm{d}t} h + \gamma \, h \, \vec{\nabla} \cdot \vec{u} \,, \tag{5.7}$$

where the second equation now represents enthalpy conservation.

5.1.2. Mesoscopic particles

The Euler equations describe the dynamics of idealised smooth fluid fields. The framework of KFT, on the contrary, is built upon the dynamics of discrete particles. To bring both together we make use of one of the most fundamental assumptions in fluid dynamics: the existence of a hydrodynamical scale hierarchy. It states that there is a length scale which is much larger than the mean free path of the microscopic gas particles, but at the same time much smaller than all scales of interest. If this assumption holds true, we can formally divide the fluid into individual fluid elements with their size corresponding to this intermediate scale.

To incorporate hydrodynamics into KFT, these fluid elements are treated as effective mesoscopic particles, each being characterised by three properties. The first two are its center of mass position $\vec{q}$ and its center of mass momentum $\vec{p}$, corresponding to the averaged positions and momenta of the microscopic particles contained in the fluid element, respectively. Beyond that, a mesoscopic particle must carry information about the local thermodynamic properties of the the fluid, emerging from the random motion and frequent collisions of the microscopic particles associated with it. In the case of an ideal gas this information is fully captured by assigning each mesoscopic particle an enthalpy $\mathcal{H}$ as a third property.

The equations of motion of these effective particles are then deduced from the Euler equations. The way this is achieved in [65] closely follows the ideas of smoothed-particle hydrodynamics (SPH), an approach used in hydrodynamical simulations [67]. One starts by assigning each particle a smooth density contribution specified by a kernel function w. Then the fluid's mass density, momentum density and enthalpy density can be approximated by a sum over the respective

smoothed individual particle contributions,

$$\rho_{\mathrm{m}}(\vec{q}, t) = \sum_{j=1}^{N} m\, w\big(|\vec{q} - \vec{q}_j(t)|\big) , \tag{5.8}$$

$$\vec{\pi}(\vec{q}, t) = \sum_{j=1}^{N} \vec{p}_j(t)\, w\big(|\vec{q} - \vec{q}_j(t)|\big) , \tag{5.9}$$

$$h(\vec{q}, t) = \sum_{j=1}^{N} \mathcal{H}_j(t)\, w\big(|\vec{q} - \vec{q}_j(t)|\big) . \tag{5.10}$$

Here, we already assumed that all mesoscopic particles have the same mass m, i. e. they contain the same number of microscopic fluid particles. In this thesis, we further choose w to be a Gaussian function of width σ_w normalised to unity, i. e.

$$w(q) := \big(2\pi\, \sigma_w^2\big)^{-3/2}\, \mathrm{e}^{-\frac{q^2}{2\sigma_w^2}} , \tag{5.11}$$

$$w(k) = \mathrm{e}^{-\frac{\sigma_w^2}{2} k^2} \tag{5.12}$$

in real and Fourier space, respectively. The length scale σ_w can be identified with the size of the fluid elements and hence has to be chosen to fit into the hydrodynamical scale hierarchy.

The values of the mesoscopic particle momenta and enthalpies are obtained by evaluating the corresponding continuous fluid fields at the positions of the respective particles,

$$\vec{p}_j(t) := m\, \vec{u}\big(\vec{q}_j(t), t\big) , \tag{5.13}$$

$$\mathcal{H}_j(t) := m\, \tilde{\mathcal{H}}\big(\vec{q}_j(t), t\big) , \tag{5.14}$$

where $\tilde{\mathcal{H}}$ denotes the specific enthalpy, i. e. the enthalpy per mass. Note that we do not directly use a momentum and an enthalpy field here since those quantities are not uniquely defined for a continuous fluid, but require to specify some additional coarse graining scale.

Given (5.8), the mass conservation equation (5.1) is automatically satisfied if we let the particles move according to

$$\dot{\vec{q}}_j(t) = \vec{u}\big(\vec{q}_j(t), t\big) = \frac{\vec{p}_j(t)}{m} . \tag{5.15}$$

To obtain the equations of motion for the particle momenta and enthalpies, we insert $\vec{\pi} = \vec{u}\rho_{\mathrm{m}}$ and $h = \tilde{\mathcal{H}}\rho_{\mathrm{m}}$ into the momentum and enthalpy conservation equations (5.6) and (5.7), and use (5.1) to find

$$\dot{\vec{p}}_j(t) = m\, \frac{\mathrm{d}}{\mathrm{d}t}\vec{u}\big(\vec{q}_j(t), t\big) = -\frac{m}{\rho_{\mathrm{m}}(\vec{q}, t)}\, \frac{\gamma - 1}{\gamma}\, \vec{\nabla}_q h(\vec{q}, t)\Big|_{\vec{q} = \vec{q}_j(t)} , \tag{5.16}$$

$$\dot{\mathcal{H}}_j(t) = m\, \frac{\mathrm{d}}{\mathrm{d}t}\tilde{\mathcal{H}}\big(\vec{q}_j(t), t\big) = -\frac{m}{\rho_{\mathrm{m}}(\vec{q}, t)}\, (\gamma - 1)\, h(\vec{q}, t)\, \vec{\nabla}_q \cdot \vec{u}(\vec{q}, t)\Big|_{\vec{q} = \vec{q}_j(t)} \tag{5.17}$$

$$= -\frac{m}{\rho_{\mathrm{m}}(\vec{q}, t)}\, (\gamma - 1) \left[\vec{\nabla}_q \cdot (\vec{u}h)(\vec{q}, t) - \vec{u}(\vec{q}, t) \cdot \vec{\nabla}_q h(\vec{q}, t) \right]\Big|_{\vec{q} = \vec{q}_j(t)} . \tag{5.18}$$

In the last line we re-expressed the velocity divergence in such a way that the derivative always acts on a smoothed density field and hence on w. Inserting (5.10), the analogous relation for the composite field $\vec{u}h$,

$$(\vec{u}h)(\vec{q}, t) = \sum_{j=1}^{N} \frac{\vec{p}_j(t)}{m} \mathcal{H}_j(t) \, w(|\vec{q} - \vec{q}_j(t)|) \,, \tag{5.19}$$

as well as (5.13) into these equations yields

$$\dot{\vec{p}}_j(t) = -\frac{m}{\rho_{\mathrm{m}}(\vec{q}_j, t)} \frac{\gamma - 1}{\gamma} \sum_{k=1}^{N} \mathcal{H}_k(t) \, \vec{\nabla}_{q_j} w(|\vec{q}_j(t) - \vec{q}_k(t)|) \,, \tag{5.20}$$

$$\dot{\vec{\mathcal{H}}}_j(t) = -\frac{m}{\rho_{\mathrm{m}}(\vec{q}_j, t)} (\gamma - 1) \sum_{k=1}^{N} \mathcal{H}_k(t) \frac{\vec{p}_k(t) - \vec{p}_j(t)}{m} \vec{\nabla}_{q_j} w(|\vec{q}_j(t) - \vec{q}_k(t)|) \,. \tag{5.21}$$

It turns out that the mass density appearing in the denominator of both equations of motion poses a problem for the treatment in KFT. This is because KFT exploits that all nonlinear contributions to the dynamics can be factorised into sums over single-particle quantities, i. e. they can be expressed as products of collective fields for which there is a well-defined functional derivative operator. To deal with the inverse mass density, we thus expand it into a Taylor series around the mean mass density $\bar{\rho}_{\mathrm{m}}$. Since we are only investigating the linear effects of fluid dynamics in this thesis, we restrict ourselves to the 0th order term

$$\frac{1}{\rho_{\mathrm{m}}(\vec{q}_j, t)} \approx \frac{1}{\bar{\rho}_{\mathrm{m}}} \,. \tag{5.22}$$

Higher order terms amount to nonlinear corrections and should only become relevant when density fluctuations are large.

5.2. Isothermal case

Rather than directly trying to incorporate the complete mesoscopic dynamics into the resummed KFT framework, we first consider the case of an isothermal fluid, which allows to simplify the mesoscopic dynamics significantly. Large parts of this research have been carried out together with Master students Daniel Geiß and Ivan Kostyuk under our direct supervision.

Together with Daniel Geiß we investigated the implementation of the isothermal mesoscopic model into the resummed KFT framework and the application of this to a purely baryonic system in an expanding space-time. We further implemented the treatment of a coupled system of dark and isothermal baryonic matter in a static space-time. Many of the results of this work discussed here can thus also be found in his Master's thesis [68].

Together with Ivan Kostyuk we extended the numerical implementation of the computation of the macroscopic propagator to the case of two particle species, which allowed us to investigate the linear evolution of coupled dark and isothermal baryonic matter also in an expanding space-time. We then used this to investigate the formation of BAO and the effects of the baryonic pressure on cosmic small-scale structures. The results of this work presented here will therefore also be part of his Master's thesis.

5.2.1. KFT path integral

An isothermal ideal gas at temperature T is described by the equation of state

$$P = \frac{k_{\mathrm{B}} T}{m_{\mathrm{mic}}} \rho_{\mathrm{m}} = c_T^2 \, \rho_{\mathrm{m}} \,, \tag{5.23}$$

where m_{mic} is the mass of a microscopic gas particle and c_T denotes the isothermal speed of sound. Using (5.4), (5.8) and (5.10), this implies a constant enthalpy per mesoscopic particle,

$$\mathcal{H}_j = \frac{\gamma}{\gamma - 1} \, m \, c_T^2 \,, \tag{5.24}$$

effectively reducing its dynamical degrees of freedom to just $\vec{q}$ and $\vec{p}$, satisfying

$$\dot{\vec{q}}_j(t) = \frac{\vec{p}_j(t)}{m} \,, \tag{5.25}$$

$$\dot{\vec{p}}_j(t) = -\frac{m \, c_T^2}{\bar{\rho}} \sum_{k=1}^{N} \vec{\nabla}_{q_j} w\big(|\vec{q}_j(t) - \vec{q}_k(t)| \big) \,. \tag{5.26}$$

When comparing these equations of motion with (3.84) and (3.85) we see that they are formally equivalent to those of a microscopic Hamiltonian system with an effective repulsive interaction potential

$$v_P(q) := \frac{m \, c_T^2}{\bar{\rho}} \, w(q) \,, \tag{5.27}$$

modelling the effects of pressure.

To describe a self-gravitating isothermal gas, we have to add the gravitational potential v_G acting between the mesoscopic particles to this pressure potential. As discussed in detail in [68], the expression for v_G technically has to take the finite size of the fluid elements into account that the mesoscopic particles are supposed to represent. When two fluid elements get close to each other, the gravitational interaction between them does not scale with their inverse distance any more, but is smoothed by their internal distribution of microscopic particles. However, since the smoothing scale σ_w is by construction small compared to all scales of interest, we can safely neglect this effect and approximate v_G by the gravitational point-particle potential, given by

$$v_G(q) := -\frac{G \, m^2}{q} \,, \tag{5.28}$$

$$v_G(k) \;= -\frac{4\pi \, G \, m^2}{k^2} \tag{5.29}$$

in real and Fourier space, respectively.

This now allows us to apply the whole KFT formalism, as laid out in chapter 3 without any modifications to a system of self-gravitating isothermal baryons. Before we use this in a cosmological setting, though, let us first consider our test case of static space-time with initial density auto-correlations but vanishing initial momenta, introduced in subsection 3.2.3. This way, we can use the analytic expression (3.95) for the statistical macroscopic propagator Δ_{ff} to qualitatively

study the effects we expect to see in the numerical treatment of the cosmological case. Inserting $v = v_P + v_G$, we find the function c defined in (3.94) to be given by

$$c(k) = \sqrt{\bar{\rho} \, \frac{v_P(k) + v_G(k)}{m}} \tag{5.30}$$

$$\approx \sqrt{c_T^2 - \frac{4\pi G \, \bar{\rho}_{\mathrm{m}}}{k^2}} \; . \tag{5.31}$$

In the second line we used that $w(k) \approx 1$ as long as we restrict ourselves to the validity range of our mesoscopic model, $k \ll \sigma_w^{-2}$.

We find that for large wavenumbers the value of $c(k)$ is real, whereas it is imaginary for small wavenumbers. From our discussion in subsection 3.2.3 we know that this implies growing modes on large scales, and oscillating modes on small scales, which is exactly what we would expect from a self-gravitating gas. On large scales the long-ranged gravitational interaction dominates, building up structures, while small scales are dominated by the gas's pressure, preventing the gravitational collapse of structures and creating wave-like perturbations. The propagation velocity of these waves is given by the value of $c(k)$ on the pressure-dominated scales and matches the expected isothermal speed of sound c_T. We can also correctly reproduce the value of the Jeans wavenumber k_{J}, describing the transition scale between both regimes [39, 66], by setting $c(k)$ to zero,

$$k_{\mathrm{J}} = k \big|_{c(k)=0} = \frac{\sqrt{4\pi G \, \bar{\rho}_{\mathrm{m}}}}{c_T} \; . \tag{5.32}$$

To illustrate this behaviour, Figure 5.1 shows the density and momentum-density power spectra obtained from Δ_{ff} normalised to the initial density power spectrum $P_\delta^{(\mathrm{i})}$,

$$\bar{P}_\delta^{(\Delta)}(k_1, t_1) := \frac{P_\delta^{(\Delta)}(k_1, t_1)}{P_\delta^{(\mathrm{i})}(k_1)} = \frac{\Delta_{ff}(1,2)}{(2\pi)^3 \, \delta_{\mathrm{D}}(\vec{k}_1 + \vec{k}_2) \, \bar{\rho}^2 \, P_\delta^{(\mathrm{i})}(k_1)} \bigg|_{\substack{\vec{k}_2 = -\vec{k}_1 \\ \vec{l}_1 = \vec{l}_2 = 0 \\ t_2 = t_1}} = \cos^2\!\big(k_1 t_1 \, c(k_1)\big) \, , \tag{5.33}$$

$$\bar{P}_\pi^{(\Delta)}(k_1, t_1) := \frac{P_\pi^{(\Delta)}(k_1, t_1)}{P_\delta^{(\mathrm{i})}(k_1)} = \frac{\mathrm{i}\frac{\partial}{\partial \vec{l}_1} \cdot \mathrm{i}\frac{\partial}{\partial \vec{l}_2} \, \Delta_{ff}(1,2)}{(2\pi)^3 \, \delta_{\mathrm{D}}(\vec{k}_1 + \vec{k}_2) \, \bar{\rho}^2 \, P_\delta^{(\mathrm{i})}(k_1)} \bigg|_{\substack{\vec{k}_2 = -\vec{k}_1 \\ \vec{l}_1 = \vec{l}_2 = 0 \\ t_2 = t_1}} = m^2 c^2(k_1) \sin^2\!\big(k_1 t_1 \, c(k_1)\big) \, . $$

$$\tag{5.34}$$

In both of them we can clearly see the transition from the growing to the oscillating regime at $k = k_{\mathrm{J}}$. We also note that $\bar{P}_\delta^{(\Delta)}$ and $\bar{P}_\pi^{(\Delta)}$ oscillate with a phase shift of 180°. Again, this matches the expected behaviour, as the momenta should be lowest at the peaks and valleys of the density field, and highest in between where the density gradient is largest.

Altogether, these findings nicely demonstrate the physical consistency of the mesoscopic particle approach in resummed KFT when applied to an isothermal gas. In contrast, it was found in [69] that an expansion to some finite order in the interaction operator $\hat{S}_{\mathrm{I}}$ quickly develops unphysical features like negative densities. This can now be understood as a consequence of truncating the Taylor expansions of the trigonometric functions appearing in the macroscopic
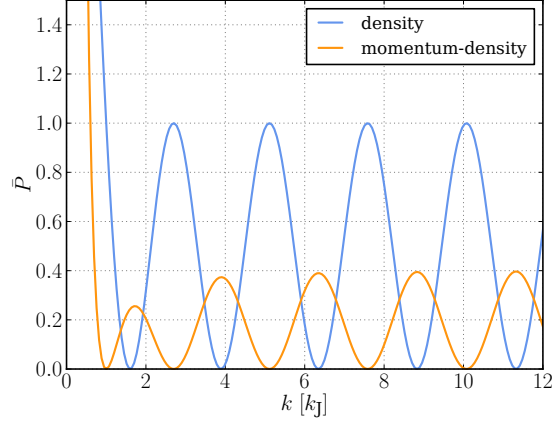
Figure 5.1.: Normalised density contrast and momentum-density contrast power spectra for a self-gravitating isothermal gas. Below the Jeans wavenumber k_{J} gravitational collapse leads to structure growth, above it pressure prevents this and creates sound waves.

propagator. Hence, the partial resummation of particle interactions described in subsection 3.2.2 is crucial for the treatment of hydrodynamical effects, and thus the macroscopic perturbation theory should be better suited to describe those than the microscopic perturbation theory.

5.2.2. Coupling micro- and mesoscopic particles

To study the joint dynamics of gravitationally coupled dark and baryonic matter, we have to extend the KFT formalism to systems of two separate species of particles – one microscopic, the other mesoscopic. For this purpose, let us introduce a particle species label α and denote the phase-space trajectories of the two species by $\vec{x}_j^{\alpha}(t) = \left(\vec{q}_j^{\alpha}(t), \vec{p}_j^{\alpha}(t)\right)$ with $j = 1, \ldots, N^{\alpha}$, where $\alpha = \mathrm{d}$ for dark and $\alpha = \mathrm{b}$ for baryonic particles. In analogy to the single-particle case, we bundle these into N^{α}-particle tensors $\boldsymbol{x}^{\alpha}$ and introduce the auxiliary fields $\boldsymbol{\chi}^{\alpha}$ conjugate to $\boldsymbol{x}^{\alpha}$.

If we further replace the original unlabelled tensor fields $\boldsymbol{x}$ and $\boldsymbol{\chi}$ by the tensor-field vectors $x := \left(\boldsymbol{x}^{\mathrm{d}}, \boldsymbol{x}^{\mathrm{b}}\right)$ and $\chi := \left(\boldsymbol{\chi}^{\mathrm{d}}, \boldsymbol{\chi}^{\mathrm{b}}\right)$, respectively, and accordingly redefine $\psi := (x, \chi)$, then the partition function of the full two-particle-species system retains the form (3.8). The free and interacting parts of the action now read

$$S_{\psi,0}[\psi] = \chi \cdot \left(\dot{x} + E_0[x]\right) = \sum_{\alpha=\mathrm{d,b}} \boldsymbol{\chi}^{\alpha} \cdot \left(\dot{\boldsymbol{x}}^{\alpha} + E_0^{\alpha}\left[\boldsymbol{x}^{\alpha}\right]\right), \tag{5.35}$$

$$S_{\psi,\mathrm{I}}[\psi] = \chi \cdot E_{\mathrm{I}}[x] \qquad = \sum_{\alpha=\mathrm{d,b}} \boldsymbol{\chi}^{\alpha} \cdot E_{\mathrm{I}}^{\alpha}[x], \tag{5.36}$$

where $E_0 := \left(E_0^{\mathrm{d}}, E_0^{\mathrm{b}}\right)$ and $E_{\mathrm{I}} := \left(E_{\mathrm{I}}^{\mathrm{d}}, E_{\mathrm{I}}^{\mathrm{b}}\right)$ denote the free and interacting parts of the two particle species' equations of motion, respectively. Note that E_{I}^{α} depends on the phase-space trajectories of both particle species as they interact gravitationally.

To find the equations of motion of an individual dark or baryonic matter particle in this coupled system, there are three aspects we have to take into account:

- The two species will generally have different particle masses m^α, mean mass densities $\bar{\rho}_m^\alpha$ and mean number densities $\bar{\rho}^\alpha$.

- Both contribute to the total gravitational potential energy

$$\mathcal{H}_{\mathrm{I},G}\left[q^{\mathrm{d}}(t), q^{\mathrm{b}}(t)\right] := \frac{1}{2} \sum_{\alpha,\gamma=\mathrm{d},\mathrm{b}} \sum_{j=1}^{N^\alpha} \sum_{\substack{k=1 \\ k\neq j \text{ if } \alpha=\gamma}}^{N^\gamma} v_G^{\alpha\gamma}\left(|\vec{q}_j^\alpha(t) - \vec{q}_k^\gamma(t)|\right), \tag{5.37}$$

with

$$v_G^{\alpha\gamma}(q) := -\frac{G\,m^\alpha m^\gamma}{q}. \tag{5.38}$$

- Only the mesoscopic baryonic particles interact via the effective pressure potential, which we can conveniently represent by the additional potential energy contribution

$$\mathcal{H}_{\mathrm{I},P}\left[q^{\mathrm{b}}(t)\right] := \frac{1}{2} \sum_{\substack{j,k=1 \\ j\neq k}}^{N^{\mathrm{b}}} v_P^{\mathrm{b}}\left(|\vec{q}_j^{\mathrm{b}}(t) - \vec{q}_k^{\mathrm{b}}(t)|\right), \tag{5.39}$$

with

$$v_P^{\mathrm{b}}(q) := \frac{m^{\mathrm{b}}\,c_T^2}{\bar{\rho}^{\mathrm{b}}}\,w(q). \tag{5.40}$$

We thus find

$$\dot{\vec{q}}_j^\alpha(t) = \frac{\vec{p}_j^\alpha(t)}{m^\alpha}, \tag{5.41}$$

$$\dot{\vec{p}}_j^\alpha(t) = -\vec{\nabla}_{q_j^\alpha}\left(\mathcal{H}_{\mathrm{I},G}\left[q^{\mathrm{d}}(t), q^{\mathrm{b}}(t)\right] + \mathcal{H}_{\mathrm{I},P}\left[q^{\mathrm{b}}(t)\right]\right). \tag{5.42}$$

This implies that the expressions (3.33) and (3.43) for $S_{\psi,\mathrm{I}}$, remain unchanged if we redefine the collective fields as 2-dimensional particle-species vectors $\Phi_f := \left(\Phi_f^{\mathrm{d}}, \Phi_f^{\mathrm{b}}\right)$, $\Phi_B := \left(\Phi_B^{\mathrm{d}}, \Phi_B^{\mathrm{b}}\right)$ and $\Phi_{\mathcal{F}} := \left(\Phi_{\mathcal{F}}^{\mathrm{d}}, \Phi_{\mathcal{F}}^{\mathrm{b}}\right)$ with components

$$\Phi_f^\alpha(1) := \sum_{j=1}^{N^\alpha} \mathrm{e}^{-\mathrm{i}\vec{k}_1\cdot\vec{q}_j^\alpha(t_1)-\mathrm{i}\vec{l}_1\cdot\vec{p}_j^\alpha(t_1)}, \tag{5.43}$$

$$\Phi_B^\alpha(1) := \sum_{j=1}^{N} \vec{\chi}_{pj}^\alpha(t_1)\cdot\mathrm{i}\vec{k}_1\,\mathrm{e}^{-\mathrm{i}\vec{k}\cdot\vec{q}_j^\alpha(t_1)-\mathrm{i}\vec{l}_1\cdot\vec{p}_j^\alpha(t_1)}, \tag{5.44}$$

$$\Phi_{\mathcal{F}}^\alpha(1) := \sum_{\gamma=\mathrm{d},\mathrm{b}} \left(\sigma_{fB}^{\alpha\gamma}\cdot\Phi_B^\gamma\right)(1), \tag{5.45}$$

and σ_{fB} as a 2×2 matrix with components

$$\sigma_{fB}^{\alpha\gamma}(1,2) = \sigma_{Bf}^{\gamma\alpha}(2,1) := -\left(v_G^{\alpha\gamma}(k_1) + \delta_{\alpha\mathrm{b}}\,\delta_{\gamma\mathrm{b}}\,v_P^{\mathrm{b}}(k_1)\right)(2\pi)^9\,\delta_{\mathrm{D}}\left(\vec{k}_1+\vec{k}_2\right)\delta_{\mathrm{D}}\left(\vec{l}_1\right)\delta_{\mathrm{D}}\left(\vec{l}_2\right)\delta_{\mathrm{D}}(t_1-t_2). \tag{5.46}$$

Similarly, the expressions (3.34), (3.39) and (3.44) for the different generating functionals $Z_\Phi[H]$, $Z_{\Phi,0}[H]$ and $Z_{\tilde\Phi,0}[\tilde H]$ also retain their form if we additionally redefine the respective source fields as $H_f := \left(H_f^d, H_f^b\right)$, $H_B := \left(H_B^d, H_B^b\right)$ and $H_{\mathcal{F}} := \left(H_{\mathcal{F}}^d, H_{\mathcal{F}}^b\right)$. The particle species components of the collective-field cumulants are then given by

$$G_{f\cdots f B\cdots B}^{\alpha_1\cdots\alpha_{n_f}\gamma_1\cdots\gamma_{n_B}}(1,\ldots,n_f,1',\cdots,n_B') := \prod_{u=1}^{n_f}\left(\frac{\delta}{\mathrm{i}\delta H_f^{\alpha_u}(u)}\right)\prod_{r=1}^{n_{\mathcal{F}}}\left(\frac{\delta}{\mathrm{i}\delta H_B^{\gamma_r}(r')}\right)W_\Phi[H]\bigg|_{H=0}, \quad (5.47)$$

with analogous definitions for the components of the bare and dressed free cumulants. In [68] it was further shown that the properties 1 to 3 of the free collective-field cumulants for a system of a single particle species discussed in subsection 3.1.3 generalise to the case of two species.

Crucially, this means that the complete reformulation of KFT in terms of macroscopic fields presented in section 3.2 for a single particle-species can be applied in exactly the same fashion to a system of two particle species if the macroscopic fields, propagators and vertices acquire the same particle species substructure as the collective fields and cumulants thereof. In particular, the overall structure of the macroscopic perturbation theory will remain unchanged and one would just have to extend the diagrammatic language introduced in subsection 3.2.4 by adding a second line type representing the macroscopic fields of baryons.[1]

However, some additional remarks regarding the computation of the macroscopic propagator have to be made since the definition (3.79) of the causal propagators Δ_R and Δ_A now involves an additional matrix inversion, due to $G_{f\mathcal{F}}^{(0)}$ becoming a 2×2 matrix. To deal with this numerically, it is useful to perform the matrix inversion in (3.79) first, yielding

$$\Delta_R^{dd} = \left(\mathcal{I} - \mathrm{i}G_{f\mathcal{F}}^{dd(0)} - \mathrm{i}G_{f\mathcal{F}}^{db(0)}\cdot I^{bb}\cdot\mathrm{i}G_{f\mathcal{F}}^{bd(0)}\right)^{-1}, \quad (5.48)$$

$$\Delta_R^{bb} = \left(\mathcal{I} - \mathrm{i}G_{f\mathcal{F}}^{bb(0)} - \mathrm{i}G_{f\mathcal{F}}^{bd(0)}\cdot I^{dd}\cdot\mathrm{i}G_{f\mathcal{F}}^{db(0)}\right)^{-1}, \quad (5.49)$$

$$\Delta_R^{bd} = I^{bb}\cdot\mathrm{i}G_{f\mathcal{F}}^{bd(0)}\cdot\Delta_R^{dd}, \quad (5.50)$$

$$\Delta_R^{db} = I^{dd}\cdot\mathrm{i}G_{f\mathcal{F}}^{db(0)}\cdot\Delta_R^{bb}, \quad (5.51)$$

with

$$I^{\alpha\alpha} := \left(\mathcal{I} - \mathrm{i}G_{f\mathcal{F}}^{(0)\,\alpha\alpha}\right)^{-1}. \quad (5.52)$$

This set of equations can then be solved iteratively by first computing I^{dd} and I^{bb}, then Δ_R^{dd} and Δ_R^{dd}, and lastly Δ_R^{db} and Δ_R^{bd}, where the individual functional inversions in the first and second step can be performed completely analogously to the one discussed in Appendix C.

We further want to point out that Δ_R and Δ_A can still be computed fully analytically if $G_{f\mathcal{F}}^{(0)}(1,2)$ evaluated at $\vec{l}_1 = \vec{l}_2 = 0$ is time-translation invariant, i. e. if it depends on t_1 and t_2 only in terms of their difference. In that case, all calculations performed in Appendix C proceed in the same way

---

[1]We will not discuss the extension of the diagrammatic language here in detail, as this would only become relevant when computing higher-order perturbative results for a two-particle-species system, which is beyond the scope of this thesis.

as for a single particle species as long as one takes into account that every occurring macroscopic 2-point function acquires a 2×2 matrix structure. That is, every product of 2-point functions becomes a matrix product and the reciprocal of the 2-point function appearing in (C.9) becomes a matrix inverse.

Our test scenario of a static space-time with initial density-correlations and vanishing initial momenta allows such an analytical calculation. The necessary expressions for the dressed free collective-field cumulants of gravitationally coupled micro- and isothermal mesoscopic particles can be obtained by generalising their expressions for a single particle species, (3.89) to (3.91), in the following way:

- The number density $\bar{\rho}$ and particle mass m have to be replaced by the values $\bar{\rho}^{\alpha}$ and m^{α} of the respective particle species.

- The interaction potential v appearing in $G_{f\mathcal{F}}^{(0)}$ has to be replaced by a matrix with components $v^{\alpha\gamma} = v_G^{\alpha\gamma} + \delta_{\alpha b} \, \delta_{\gamma b} \, v_P^{b}$.

- The density contrast power spectrum $P_{\delta}^{(i)}$ appearing in $G_{ff}^{(0)}$ has to be replaced by a matrix with components $P_{\delta}^{(i)\,\alpha\gamma}$, describing the initial auto- and cross-correlations between the densities of the different particle species.

To keep things simple, though, we assume all auto- and cross-spectra to be the same, $P_{\delta}^{(i)\,\alpha\gamma} = P_{\delta}^{(i)}$. We then find

$$G_f^{(0)\,\alpha}(1) = (2\pi)^3 \, \delta_{\mathrm{D}}\big(\vec{k}_1\big) \, \bar{\rho}^{\alpha} \, , \tag{5.53}$$

$$G_{f\mathcal{F}}^{(0)\,\alpha\gamma}(1,2) = (2\pi)^3 \, \delta_{\mathrm{D}}\big(\vec{k}_1 + \vec{k}_2\big) \, (2\pi)^3 \, \delta_{\mathrm{D}}\big(\vec{l}_2\big) \, \theta(t_1 - t_2)$$
$$\times \mathrm{i}k_1^2 \left(v_G^{\alpha\gamma}(k_1) + \delta_{\alpha b} \, \delta_{\gamma b} \, v_P^{b}(k_1) \right) \left(\frac{t_1 - t_2}{m^{\alpha}} + \frac{\vec{k}_1 \cdot \vec{l}_1}{k_1^2} \right) , \tag{5.54}$$

$$G_{ff}^{(0)\,\alpha\gamma}(1,2) = (2\pi)^3 \, \delta_{\mathrm{D}}\big(\vec{k}_1 + \vec{k}_2\big) \, \bar{\rho}^{\alpha} \bar{\rho}^{\gamma} \, P_{\delta}^{(i)}(k_1) \, . \tag{5.55}$$

Even though the Laplace transforms and matrix algebra involved in the computation of the macroscopic propagator for this system can be performed analytically, the expressions quickly become rather unwieldy. Therefore, we used the computer algebra software Wolfram Mathematica for these calculations. The resulting expression for the statistical propagator Δ_{ff} is found to be

$$\Delta_{ff}^{\alpha\gamma}(1,2) = (2\pi)^3 \, \delta_{\mathrm{D}}\big(\vec{k}_1 + \vec{k}_2\big) \, \bar{\rho}^{\alpha} \bar{\rho}^{\gamma} \, P_{\delta}^{(i)}(k_1) \, D^{\alpha}(1) \, D^{\gamma}(2) \tag{5.56}$$

with the functions D^{α} splitting into several contributions with different time-dependencies,

$$D^{\alpha}(1) = \sum_{\ell=\pm} \left[D_{\mathrm{c},\ell}^{\alpha}\big(\vec{s}_1\big) \, \cos\big(k_1 t_1 \, c_{\ell}(k_1)\big) + D_{\mathrm{s},\ell}^{\alpha}\big(\vec{s}_1\big) \, \sin\big(k_1 t_1 \, c_{\ell}(k_1)\big) \right] . \tag{5.57}$$

The coefficients $D^\alpha_{c,\pm}$ and $D^\alpha_{s,\pm}$ are given by

$$D^d_{c,\pm}(\vec{s}) = \frac{1}{2}\left(1 \pm \frac{\bar{v}(k) - 2\bar{v}^b_P(k)}{\sqrt{\bar{v}^2_T(k) - 4\bar{v}^d_G(k)\,\bar{v}^b_P(k)}}\right), \tag{5.58}$$

$$D^b_{c,\pm}(\vec{s}) = \frac{1}{2}\left(1 \pm \frac{\bar{v}(k)}{\sqrt{\bar{v}^2(k) - 4\bar{v}^d_G(k)\,\bar{v}^b_P(k)}}\right), \tag{5.59}$$

$$D^\alpha_{s,\pm}(\vec{s}) = \frac{\vec{k} \cdot \vec{l}}{k}\, m^\alpha c_\pm(k)\, D^\alpha_{c,\pm}(\vec{s}), \tag{5.60}$$

and the functions $c_\pm$ read

$$c_\pm(k) := \frac{1}{\sqrt{2}}\sqrt{\bar{v}(k) \pm \sqrt{\bar{v}^2(k) - 4\bar{v}^d_G(k)\,\bar{v}^b_P(k)}}, \tag{5.61}$$

where we defined the mass- and density-weighted potentials

$$\bar{v}^\alpha_G(k) := \frac{\bar{\rho}^\alpha}{m^\alpha}\, v^{\alpha\alpha}_G(k) = -\frac{4\pi\, G\, \bar{\rho}^\alpha_m}{k^2}, \tag{5.62}$$

$$\bar{v}^b_P(k) := \frac{\bar{\rho}^b}{m^b}\, v^b_P(k) \;\;= c^2_T\, w(k), \tag{5.63}$$

$$\bar{v}(k) := \bar{v}^d_G(k) + \bar{v}^b_G(k) + \bar{v}^b_P(k). \tag{5.64}$$

Since $\bar{v}^d_G < 0$ and $\bar{v}^b_P > 0$ for all wavenumbers, we can immediately conclude that c_+ is always real, whereas c_- is always imaginary. Thus regardless of the scale we are looking at, D^α will always be given by a superposition of growing and oscillating modes. This is very different from the pure self-gravitating isothermal gas discussed in the previous subsection, for which the regimes of growing and oscillating modes are strictly separated by the Jeans wavenumber k_J. However, a closer inspection of the coefficients in front of the different modes reveals that for baryons there is still an *effective* scale-separation of these modes. To see this, we focus on the density contrast fluctuations, described by $D(1)$ at $\vec{l}_1 = 0$. Then $D^\alpha_{s,\pm} = 0$ and

$$|D^b_{c,+}(\vec{s})| < |D^b_{c,-}(\vec{s})| \quad \text{if } k < k_J, \tag{5.65}$$

$$|D^b_{c,+}(\vec{s})| > |D^b_{c,-}(\vec{s})| \quad \text{if } k > k_J, \tag{5.66}$$

$$|D^d_{c,+}(\vec{s})| < |D^d_{c,-}(\vec{s})| \quad \text{for any } k. \tag{5.67}$$

At early times, when $\cos(ktc_+)$ and $\cos(ktc_-)$ are still comparable in magnitude, we thus expect the growing modes of the baryons to dominate on wavenumbers smaller than the k_J, while the oscillating modes should dominate on larger wavenumbers. At late enough times, the growing mode should dominate even on large wavenumbers, though. For the dark matter, on the other hand, the growing mode is expected to dominate at all times and on all scales. Figure 5.2, which
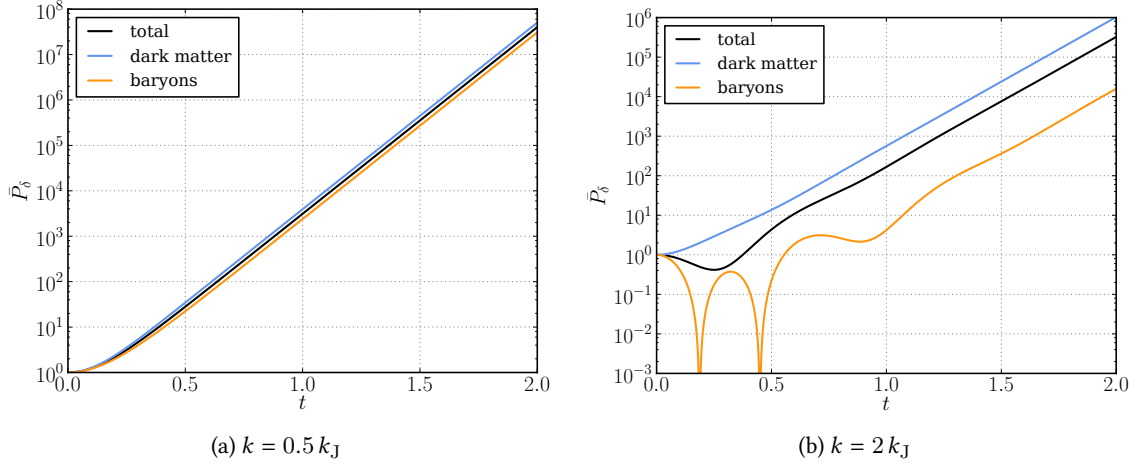
(a) $k = 0.5\,k_J$

(b) $k = 2\,k_J$

Figure 5.2.: Time-evolution of the normalised density contrast power spectra of the different matter components in a system of gravitationally coupled dark and isothermal baryonic matter, shown at two different wavenumbers. Below the Jeans wavenumber k_J (a) gravitational collapse leads at all times to structure growth in all matter components. Above it (b) the baryonic structure growth is suppressed at early times, but sets in once the combined dark and baryonic gravitational attraction overcomes the baryon pressure.

plots the time-evolution of the normalised density contrast power spectra of the dark, baryonic and total matter,

$$\bar{P}_\delta^{(\Delta)\,\alpha\gamma}(k_1, t_1) := \frac{P_\delta^{(\Delta)\,\alpha\gamma}(k_1, t_1)}{P_\delta^{(i)}(k_1)} = \left. \frac{\mathrm{i}\frac{\partial}{\partial \vec{l}_1} \cdot \mathrm{i}\frac{\partial}{\partial \vec{l}_2} \Delta_{ff}^{\alpha\gamma}(1,2)}{(2\pi)^3\,\delta_{\mathrm{D}}(\vec{k}_1 + \vec{k}_2)\,\bar{\rho}^\alpha\,\bar{\rho}^\gamma\,P_\delta^{(i)}(k_1)} \right|_{\substack{\vec{k}_2 = -\vec{k}_1 \\ \vec{l}_1 = \vec{l}_2 = 0 \\ t_2 = t_1}}, \tag{5.68}$$

$$\bar{P}_\delta^{(\Delta)\,\mathrm{tot}}(k_1, t_1) := \left(\bar{\rho}_{\mathrm{m}}^{\mathrm{d}} + \bar{\rho}_{\mathrm{m}}^{\mathrm{b}}\right)^{-2} \sum_{\alpha, \gamma = \mathrm{d, b}} \bar{\rho}_{\mathrm{m}}^\alpha\,\bar{\rho}_{\mathrm{m}}^\gamma\,\bar{P}_\delta^{(\Delta)\,\alpha\gamma}(k_1, t_1). \tag{5.69}$$

for the two wavenumbers $0.5\,k_J$ and $2\,k_J$, confirms these expectations. Physically, this behaviour can be explained by the pressureless dark matter forming deeper and deeper gravitational wells during its gravitational collapse to the point where the combined gravitational attraction of dark and baryonic matter is strong enough to overcome the baryon pressure.

In Figure 5.3 we further show the k-dependence of the normalised density contrast and momentum-density contrast power spectra, where the latter are defined as

$$\bar{P}_\pi^{(\Delta)\,\alpha\gamma}(k_1, t_1) := \frac{P_\pi^{(\Delta)\,\alpha\gamma}(k_1, t_1)}{P_\delta^{(i)}(k_1)} = \left. \frac{\Delta_{ff}^{\alpha\gamma}(1,2)}{(2\pi)^3\,\delta_{\mathrm{D}}(\vec{k}_1 + \vec{k}_2)\,\bar{\rho}^\alpha\,\bar{\rho}^\gamma\,P_\delta^{(i)}(k_1)} \right|_{\substack{\vec{k}_2 = -\vec{k}_1 \\ \vec{l}_1 = \vec{l}_2 = 0 \\ t_2 = t_1}}, \tag{5.70}$$

$$\bar{P}_\pi^{(\Delta)\,\mathrm{tot}}(k_1, t_1) := \left(\bar{\rho}_{\mathrm{m}}^{\mathrm{d}} + \bar{\rho}_{\mathrm{m}}^{\mathrm{b}}\right)^{-2} \sum_{\alpha, \gamma = \mathrm{d, b}} \bar{\rho}_{\mathrm{m}}^\alpha\,\bar{\rho}_{\mathrm{m}}^\gamma\,\bar{P}_\pi^{(\Delta)\,\alpha\gamma}(k_1, t_1). \tag{5.71}$$

First of all, we note that the scale-separation just described can be clearly seen for the baryonic component in both types of spectra. Beyond that, Figure 5.3a shows the structure growth of dark

(a) Density contrast
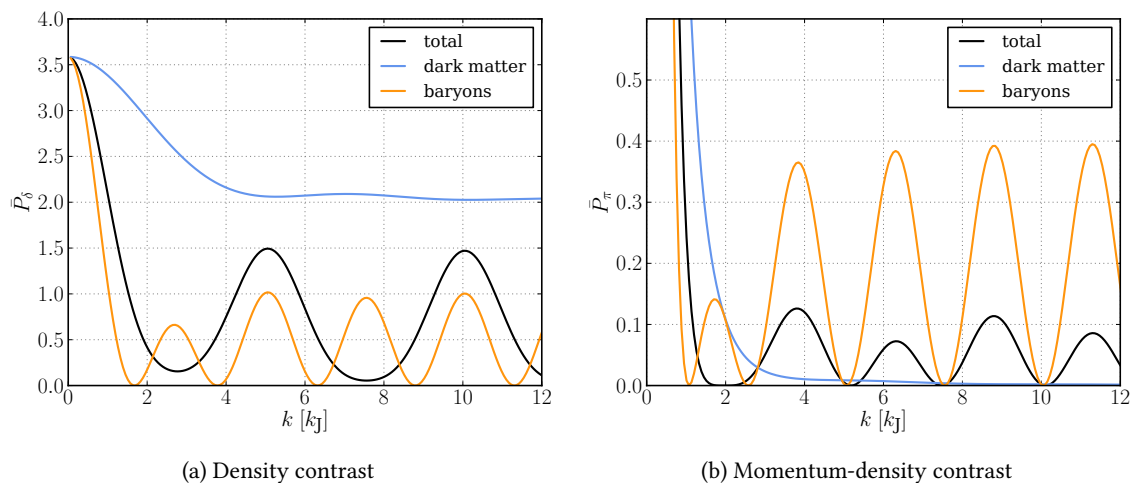
(b) Momentum-density contrast

Figure 5.3.: Normalised density contrast (a) and momentum-density contrast (b) power spectra of the different matter components in a system of gravitationally coupled dark and isothermal baryonic matter. On small scales, where baryons are pressure dominated, the structure growth of the dark and total matter components is partially suppressed and acquires oscillatory features.

matter to be partially suppressed and to acquire small oscillatory features on those scales where the baryon pressure is relevant. This demonstrates that the dark matter is indeed affected by the baryon pressure even though it only couples to the baryons gravitationally. In a cosmological setting we expect this effect to be less pronounced, though, as baryons only account for approximately 16% of the total cosmic matter density rather than the 50% used in the computation of Figure 5.3.

Altogether, these findings show that the macroscopic propagator of a gravitationally coupled system of dark and baryonic matter is able to capture several non-trivial dynamical effects that are absent in systems of a single dark or baryonic particle species. The partial resummation of particle interactions described in subsection 3.2.2 seems to be crucial for this since it was found in [70] that the strong interplay between both species observed here is not grasped by an expansion in the interaction operator $\hat{S}_I$ to finite order. This implies that a system of two coupled particle species is better described within the macroscopic than the microscopic perturbation theory.

Finally, we want to point out that the procedure described in this subsection can be extended straightforwardly to more than two different species of particles if needed.

5.2.3. Expanding space-time

To investigate the influence of baryons on the structure growth in a cosmological setting, the only thing left is to adopt the mesoscopic particle model to an expanding space-time and the coordinate choice made in section 4.1. Since the only difference between the microscopic and the isothermal mesoscopic particle dynamics is the effective pressure potential v_P^b, it suffices to consider how it is modified by this.

We first note that our interpretation of the mesoscopic particles as fluid elements containing a fixed number of microscopic particles requires the size of the fluid element and thus the smoothing

length σ_w to become time-dependent and scale with the cosmic expansion, $\sigma_w \to a\sigma_w$. However, this rescaling is cancelled exactly by re-expressing (5.11) in comoving coordinates, $\vec{q} \to a\vec{q}$, and the number density in (5.40) in terms of the comoving number density, $\bar{\rho}^{\mathrm{b}} \to \bar{\rho}^{\mathrm{b}}/a^3$. Overall, v_P^{b} thus remains unchanged by this and the derivation of the equations of motion of a microscopic particle in expanding space-time in Appendix E can be equally applied to a mesoscopic particle if we add the total pressure potential experienced by a single mesoscopic particle,

$$V_P(\vec{q}, t) := \frac{1}{m^{\mathrm{b}}} \sum_{j=1}^{N^{\mathrm{b}}} v_P^{\mathrm{b}}\left(|\vec{q} - \vec{q}_j^{\mathrm{b}}(t)|\right) \tag{5.72}$$

to the total gravitational potential V_G in (E.1). Going through this derivation yields the following equations of motion for the two particle species,

$$\frac{\mathrm{d}\vec{q}_j^\alpha}{\mathrm{d}\eta} = \vec{p}_j^\alpha \,, \tag{5.73}$$

$$\frac{\mathrm{d}\vec{p}_j^\alpha}{\mathrm{d}\eta} = -\left(\frac{3}{2}\frac{\Omega_{\mathrm{m}}}{f_+^2} - 1\right)\vec{p}_j^\alpha - \vec{\nabla}_{q_j^\alpha}\left(\tilde{V}_G + \tilde{V}_P\right) \approx -\frac{1}{2}\vec{p}_j^\alpha - \vec{\nabla}_{q_j^\alpha}\left(\tilde{V}_G + \tilde{V}_P\right) \,, \tag{5.74}$$

with the effective total gravitational and pressure potentials $\tilde{V}_G$ and $\tilde{V}_P$ resulting from our choice of the time variable $\eta(t) = \ln(D_+(t)/D_+(t_{\mathrm{i}}))$ and the momentum variable $\vec{p} = \mathrm{d}\vec{q}/\mathrm{d}\eta$.

The potential $\tilde{V}_G$ satisfies the Poisson equation

$$\nabla_q^2 \tilde{V}_G = \frac{3}{2} \sum_{\alpha=\mathrm{d,b}} \frac{\Omega_{\mathrm{m}}^\alpha}{f_+^2} \frac{\Phi_\rho^\alpha - \bar{\rho}^\alpha}{\bar{\rho}^\alpha} \approx \frac{3}{2} \sum_{\alpha=\mathrm{d,b}} \frac{\Omega_{\mathrm{m}}^\alpha}{\Omega_{\mathrm{m}}} \frac{\Phi_\rho^\alpha - \bar{\rho}^\alpha}{\bar{\rho}^\alpha} \,, \tag{5.75}$$

where we again used the approximation $\Omega_{\mathrm{m}}/f_+^2 \approx 1$ for ΛCDM cosmologies during the matter- and Λ-dominated epochs. It is solved by

$$\tilde{V}_G(\vec{q}, t) = \sum_{\alpha=\mathrm{d,b}} \sum_{j=1}^{N^\alpha} \tilde{v}_G^\alpha\left(|\vec{q} - \vec{q}_j^\alpha(t)|\right) \tag{5.76}$$

with the effective single-particle gravitational potential $\tilde{v}_G^\alpha$ reading

$$\tilde{v}_G^\alpha(k) := -\frac{3}{2}\frac{\Omega_{\mathrm{m}}^\alpha}{\Omega_{\mathrm{m}}}\frac{1}{\bar{\rho}^\alpha \, k^2} = -\frac{3}{2}\frac{\Omega_{\mathrm{m},0}^\alpha}{\Omega_{\mathrm{m},0}}\frac{1}{\bar{\rho}^\alpha \, k^2} \tag{5.77}$$

in Fourier space. In the second step we conveniently expressed the ratio of the two dimensionless matter density parameters by their values today, exploiting that this ratio is constant in time since dark and baryonic matter do not transform into each other.[2]

---

[2]While many dark matter models predict interactions between dark matter and known standard model particles, none would lead to a significant exchange between dark matter and non-relativistic baryonic matter during the epochs of matter- and Λ-domination.

The potential $\tilde{V}_P$ can be written as

$$\tilde{V}_P(\vec{q}, t) := \sum_{j=1}^{N^{\mathrm{b}}} \tilde{v}_P^{\mathrm{b}}\big(|\vec{q} - \vec{q}_j^{\mathrm{b}}(t)|\big) \,, \tag{5.78}$$

where the effective single-particle pressure potential $\tilde{v}_P^{\mathrm{b}}$ turns out to read

$$\tilde{v}_P^{\mathrm{b}}(k, \eta) := \frac{v_P^{\mathrm{b}}(k)}{m^{\mathrm{b}} a^2 H^2 f_+^2} = \frac{\Omega_{\mathrm{m}}}{f_+^2} \frac{a(\eta)\, c_T^2}{\Omega_{\mathrm{m},0} H_0^2 \bar{\rho}^{\mathrm{b}}} \, w(k) \approx \frac{a(\eta)\, c_T^2}{\Omega_{\mathrm{m},0} H_0^2 \bar{\rho}^{\mathrm{b}}} \, w(k) \tag{5.79}$$

in Fourier space. Here, we inserted the Fourier transform of (5.40) and additionally used that $\Omega_{\mathrm{m}} H^2 / a^3$ is constant in time to express the total matter density parameter and the Hubble function by their values today.

By construction, the free equations of motion for the two individual particle species are precisely the same as those of the pure cosmic dark matter system discussed in chapter 4. Consequently, they are both solved by the same Green's function $\mathcal{G}$ with components (4.5) to (4.8). Therefore, there are only three aspects that have to be taken into account to generalise the expressions for the free collective-field cumulants of pure dark matter in expanding space-time, (4.11) to (4.13), to the case of the coupled system of dark matter and isothermal baryons:

- The number density $\bar{\rho}$ has to be replaced by the value $\bar{\rho}^\alpha$ of the respective particle species.

- The interaction potential $\tilde{v}$ appearing in $G_{f\mathcal{F}}^{(0)}$ has to be replaced by a matrix with components $\tilde{v}^{\alpha\gamma} = \tilde{v}_G^\alpha + \delta_{\alpha\mathrm{b}}\, \delta_{\gamma\mathrm{b}}\, \tilde{v}_P^{\mathrm{b}}$.

- The function C_2 appearing in $G_{ff}^{(0)}$, describing the initial correlations of densities and momenta, has to be generalised such that it allows to choose the initial auto- and cross-correlations between particles of the different species independently.

We can simplify this even further, though. First, we note that the mean number density of the mesoscopic baryonic particles $\bar{\rho}^{\mathrm{b}}$ as well as the mass of a single mesoscopic baryonic particle m^{b} do not have any physical reality on their own. Only their product, i. e. the mean baryonic mass density $\bar{\rho}_{\mathrm{m}}^{\mathrm{b}}$, is an actual observable. So as long as we make sure not to apply the mesoscopic model in a situation where the assumptions of the hydrodynamical scale hierarchy break down – which is of no concern for any cosmologically relevant scale – we are free to choose the values of $\bar{\rho}^{\mathrm{b}}$ and m^{b} in any way that keeps $\bar{\rho}_{\mathrm{m}}^{\mathrm{b}}$ fixed. We exploit this freedom by matching the masses of dark and baryonic particles, $m^{\mathrm{b}} = m^{\mathrm{d}}$. Then their number densities satisfy

$$\frac{\bar{\rho}^\alpha}{\bar{\rho}^\gamma} = \frac{\bar{\rho}_{\mathrm{m}}^\alpha}{\bar{\rho}_{\mathrm{m}}^\gamma} \frac{m^\gamma}{m^\alpha} = \frac{\bar{\rho}_{\mathrm{m}}^\alpha}{\bar{\rho}_{\mathrm{m}}^\gamma} = \frac{\Omega_{\mathrm{m}}^\alpha}{\Omega_{\mathrm{m}}^\gamma} \,. \tag{5.80}$$

Similar to the test system discussed in the previous subsection, we further assume the initial auto- and cross-correlations between dark and baryonic matter to be exactly the same, i. e. characterised by the same initial density contrast power spectrum $P_\delta^{(\mathrm{i})}$. This corresponds to a scenario where before our chosen initial instance in time all cosmic matter acts like dark matter, and the difference

between baryonic and dark matter only becomes relevant after that. In reality, this is not true since baryons, unlike dark matter, couple to photons and thus evolve very differently during the epoch of radiation domination, as described in subsection 2.2.4. For our considerations here, however, we neglect this difference, as we are primarily interested in studying the effect of the different *dynamics* of dark and baryonic matter rather than the influence of their different initial conditions.

With these two simplifications, the free collective 1- and 2-point cumulants for the coupled system of cosmic dark and isothermal baryonic matter are given by

$$G_f^{(0)\,\alpha}(1) = (2\pi)^3\,\delta_{\mathrm{D}}\big(\vec{k}_1\big)\,\bar{\rho}^\alpha\,\mathrm{e}^{-\frac{\sigma_p^2}{2}\tilde{T}_1^2 l_1^2}\,,\tag{5.81}$$

$$G_{f\mathcal{F}}^{(0)\,\alpha\gamma}(1,2) = (2\pi)^3\,\delta_{\mathrm{D}}\big(\vec{k}_1+\vec{k}_2\big)\,(2\pi)^3\,\delta_{\mathrm{D}}\big(\vec{l}_2\big)\,\mathrm{i}\left(-\frac{3}{2}\frac{\Omega_{\mathrm{m},0}^\alpha}{\Omega_{\mathrm{m},0}} + \delta_{\alpha\mathrm{b}}\,\delta_{\gamma\mathrm{b}}\,\frac{a(\eta_2)c_T^2}{\Omega_{\mathrm{m},0}H_0^2}\,k_1^2\right)$$

$$\times\,\theta(\eta_1-\eta_2)\left(T_{12}+\tilde{T}_{12}\,\frac{\vec{k}_1\cdot\vec{l}_1}{k_1^2}\right)\mathrm{e}^{-\frac{\sigma_p^2}{2}\left((T_1-T_2)\vec{k}_1+\tilde{T}_1\vec{l}_1\right)^2}\,,\tag{5.82}$$

$$G_{ff}^{(0)\,\alpha\gamma}(1,2) = (2\pi)^3\,\delta_{\mathrm{D}}\big(\vec{k}_1+\vec{k}_2\big)\,\bar{\rho}^\alpha\bar{\rho}^\gamma\,C_2(1,2)\,\mathrm{e}^{-\frac{\sigma_p^2}{2}\left[\left(T_1\vec{k}_1+\tilde{T}_1\vec{l}_1\right)^2+\left(-T_2\vec{k}_1+\tilde{T}_2\vec{l}_2\right)^2\right]}\,.\tag{5.83}$$

5.2.4. Baryon acoustic oscillations

To test our formalism in a realistic cosmological setting, we will first use it to describe the formation of baryon acoustic oscillations (BAO), described in subsection 2.2.4. This should provide a good benchmark for our model, as it presents a physical situation where pressure effects are crucial on scales and times that are well described by linear structure formation.

An accurate treatment of the BAO formation actually requires to describe the adiabatic evolution of a tightly coupled baryon-photon fluid. However, CMB observations show that the relative temperature fluctuations are tiny, $\delta T/T \lesssim 10^{-5}$. Hence, our isothermal mode, which assumes a spatially constant temperature, should be a plausible first approximation if we allow this global temperature to follow a given time-evolution. Furthermore, since our approach can only describe non-relativistic particles, an explicit description of the photon dynamics is not possible. But we can exploit the tight coupling between photons and baryons via Compton scattering to model the influence of photons as an additional effective pressure component felt by the baryons.

We start with the equation of state of a thermal photon gas of temperature T^{p},

$$P^{\mathrm{p}} = \frac{\zeta(4)}{\zeta(3)}\,k_{\mathrm{B}}T^{\mathrm{p}}\,\rho^{\mathrm{p}}\,,\tag{5.84}$$

that relates the photon pressure P^{p} to the photon number density ρ^{p} [71]. Here, ζ denotes the Riemann-Zeta function. In the tight-coupling regime, the number densities of the photons and the microscopic baryonic particles are approximately proportional, $\rho_{\mathrm{mic}}^{\mathrm{b}} = \eta_{\mathrm{b/p}}\,\rho^{\mathrm{p}}$ with $\eta_{\mathrm{b/p}} = 1.01\cdot 10^{-9}$. The tiny value of $\eta_{\mathrm{b/p}}$ further implies that the pressure felt by the baryons is completely dominated by the pressure of the photons, $P^{\mathrm{b}}\approx P^{\mathrm{p}}$. We can thus turn (5.84) into an effective equation of state for the mesoscopic baryons,

$$P^{\mathrm{b}} = \frac{\zeta(4)}{\zeta(3)}\,\frac{k_{\mathrm{B}}T^{\mathrm{p}}}{\eta_{\mathrm{b/p}}}\,\rho_{\mathrm{mic}}^{\mathrm{b}} = \frac{\zeta(4)}{\zeta(3)}\,\frac{k_{\mathrm{B}}T_0^{\mathrm{p}}}{a\,\eta_{\mathrm{b/p}}m_{\mathrm{mic}}^{\mathrm{b}}}\,\rho_{\mathrm{m}}^{\mathrm{b}}\,,\tag{5.85}$$
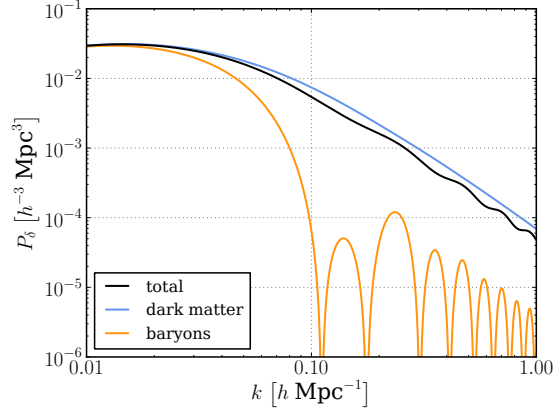
Figure 5.4.: Density contrast power spectra of the different matter components in a system of gravitationally coupled dark and isothermal baryonic matter, including an effective photon pressure, evolved from the time of matter-radiation equality to the time of CMB decoupling. The total matter spectrum shows the formation of wiggles qualitatively comparable to the observed BAOs.

where T_0^{p} is the temperature of the photon gas today. In the second step we expressed $\rho_{\mathrm{mic}}^{\mathrm{b}}$ in terms of the baryon mass density $\rho_{\mathrm{m}}^{\mathrm{b}}$ and the microscopic baryon particle mass $m_{\mathrm{mic}}^{\mathrm{b}}$, and used that the photon temperature is inversely proportional to the scale factor a. Comparing (5.85) with the isothermal gas equation of state (5.23) then allows us to identify an effective time-dependent isothermal speed of sound,

$$\tilde{c}_T(\eta) = \frac{\zeta(4)}{\zeta(3)} \frac{k_{\mathrm{B}} T_0}{a(\eta)\, \eta_{\mathrm{b/p}} m_{\mathrm{mic}}^{\mathrm{b}}} \,, \tag{5.86}$$

that we can insert into the expression (5.82) for $G_{f\mathcal{F}}^{(0)}$.

For our calculations we choose to set the initial conditions at the time of matter-radiation equality at a redshift of $z = 3600$ since this allows us to approximate the initial density contrast power spectrum by a BBKS spectrum rather than having to consider the details of the power spectrum evolution during the epoch of radiation domination. Furthermore, our choice of coordinates is only valid during the epochs of matter and Λ domination. The microscopic baryon mass is set to the mass of a proton, $m_{\mathrm{mic}}^{\mathrm{b}} = 1.67 \cdot 10^{-27}\,\mathrm{kg}$, and today's temperature of the photon gas is given by the CMB temperature today, $T_0^{\mathrm{p}} = 2.726\,\mathrm{K}$. We evolve the macroscopic propagator numerically until the time of CMB decoupling at a redshift of $z = 1090$ and plot the resulting density contrast power spectra of the dark, baryonic and total matter in Figure 5.4.

We see that the baryon power spectrum is getting suppressed and shows strong oscillations on wavenumbers $k \gtrsim 0.1h\,\mathrm{Mpc}$. While the dark matter power spectrum appears to be largely unaffected by this, the oscillations do leave a clear imprint in the form of wiggles on the total matter power spectrum. Qualitatively, these wiggles seem comparable with the observed BAOs. For a more quantitative comparison, we plot the computed total matter power spectrum in Figure 5.5a next to the Eisenstein-Hu spectrum [38] described in subsection 2.2.4. Additionally, to separate the BAO feature from the underlying purely gravitational structure growth, we show their relative deviation from a BBKS power spectrum [12] in Figure 5.5b. We observe three main differences:

(a) Density contrast power spectrum

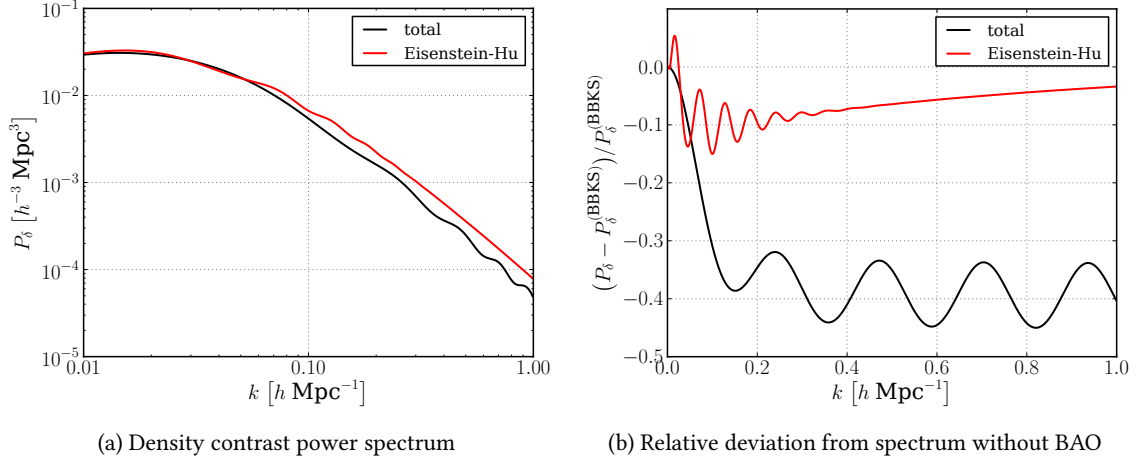(b) Relative deviation from spectrum without BAO

Figure 5.5.: Total matter density contrast power spectrum (a) and its relative deviation from a BBKS spectrum [12] (b) in a system of gravitationally coupled dark and isothermal baryonic matter, including an effective photon pressure, evolved from the time of matter-radiation equality to the time of CMB decoupling. For comparison, the Eisenstein-Hu spectrum [38] is shown. Positions and amplitudes of the BAO in both spectra agree within a factor of approximately 4. Note in (b) that the positive peak of the Eisenstein-Hu spectrum at very low k and its rising slope at large k are not related to the BAO, but are a result of the slight mismatch of the Eisenstein-Hu and BBKS fitting formulas at the peak and tail of the power spectrum, respectively.

The positions of the wiggles in our result are stretched by a factor of roughly 3.5 compared to those in the Eisenstein-Hu spectrum. The wiggle amplitude in Eisenstein-Hu decreases with larger k while it remains constant in our result. And our result shows a mean suppression of the power spectrum that is by a factor of approximately 4 too large compared to Eisenstein-Hu. Overall, we thus find that our results for the position and amplitude of the BAO agree within a factor of 4 with the fit by Eisenstein & Hu. We expect this agreement to improve if some of the approximations we made are dropped, as we will explain in the following.

The missing decay of the wiggle amplitude, for example, is easily explained by the fact that we did not include the effects of Silk damping in our analysis, i. e. we did not take into account that small-scale density fluctuations were damped away by photon diffusion during the time of recombination [38, 72]. The rescaled wiggle positions are most likely a result of assuming that the formation of the BAO started only after matter-radiation equality, which is not correct. We are thus missing the earlier phases of BAO formation when the photon temperature and thus also the effective speed of sound (5.86) were higher. A higher speed of sound would then lead to a larger BAO wavelength, corresponding to smaller wavenumbers of the BAO peaks in the power spectrum. The precise reason for the suppression of power being too strong, on the other hand, is less obvious to us. We mostly suspect that this is caused by the fact that we ignored the non-negligible gravitational pull of the photons in the early stages of the matter-dominated epoch. But it might also be related to our isothermal approximation or our approximation of equal initial auto- and cross-correlations of dark and baryonic matter. Further analyses which drop these approximations one at a time would be necessary to pinpoint the responsible effect.

Since most of these approximations are due to the effects of photon rather than baryon dynamics, though, we nonetheless consider this a successful first test of our mesoscopic model. We further want to point out that the one approximation which mostly concerns the baryon dynamics itself was the isothermal assumption, whose influence will be investigated in section 5.3.

5.2.5. Baryonic small-scale effects

Let us now apply our coupled dark and baryonic matter approach to study the late-time baryonic effects on small-scale structure formation. For this application, the isothermal model is in fact just a very crude approximation since baryons heat up significantly during their gravitational collapse, creating significant temperature fluctuations. Nevertheless, this should still allow us to infer if we are generally able to capture the correct qualitative behaviour of the coupled dark and baryonic matter on these scales.

Like in the description of the BAO formation, it is important to take the global time-evolution of the mean baryon temperature into account if we want to approximate the actual adiabatic dynamics as closely as possible. It turns out that even after recombination the baryon temperature still follows the photon gas temperature for some time [73]. After that the baryons are cooling adiabatically, i. e. $T^b \propto V^{1-\gamma} \propto a^{3(1-\gamma)}$. Approximating all baryons as atomic hydrogen gas, with an adiabatic index $\gamma = 5/3$, we thus use

$$T^b(a) = T_0^p \times \begin{cases} \frac{1}{a} & \text{if } a \leq \tilde{a}, \\ \frac{\tilde{a}}{a^2} & \text{if } a > \tilde{a} \end{cases} \tag{5.87}$$

as a simple model for the time-dependent baryon temperature. Here, $\tilde{a}$ denotes the scale factor from which on we consider the baryon temperature to decouple from the photon temperature. We will test three different values: the limiting cases $\tilde{a} = 1/(z_i + 1)$ and $\tilde{a} = 1$, corresponding to a baryon temperature that decouples immediately or follows the photon temperature until today, respectively, and the intermediate value $\tilde{a} = 1/200$, which had been suggested in [73].

We fix the initial time of our analysis to the time of CMB decoupling, $z_i = 1090$, using a BBKS spectrum [12] as the initial density contrast power spectrum, and evolve the macroscopic propagator numerically until today at redshift zero to obtain the resulting density contrast power spectra of the dark, baryonic and total matter. Their relative differences to the spectrum of a system of pure dark matter are plotted in Figure 5.6.

They all show a relative suppression of power on wavenumbers $k \gtrsim 1\,h/\mathrm{Mpc}$, with the suppression being strongest for $\tilde{a} = 1$, and weakest for $\tilde{a} = 1/z_i$. This is to be expected, as these two cases correspond to the slowest and fastest decrease of the baryon temperature and thus of the effective speed of sound $\tilde{c}_T$, respectively. At $k = 1\,h/\mathrm{Mpc}$ the relative suppression of the baryon spectrum ranges between values of 0.5% and 2%. At $k = 10\,h/\mathrm{Mpc}$ this increases to a range of 50% to 80%.

We compare these findings with the results from [74], plotted in Figure 5.7, who ran two different hydrodynamical simulations of coupled dark and baryonic matter. The red curves correspond to a run with adiabatic gas dynamics, the green ones to a run including radiative cooling and star formation. Let us first focus on the adiabatic run, as it is closer to the system considered here. In this run they find a suppression of the different spectra on small k that looks qualitatively similar

(a) $\tilde{a} = 1$

(b) $\tilde{a} = \frac{1}{200}$

(c) $\tilde{a} = \frac{1}{z_i + 1}$
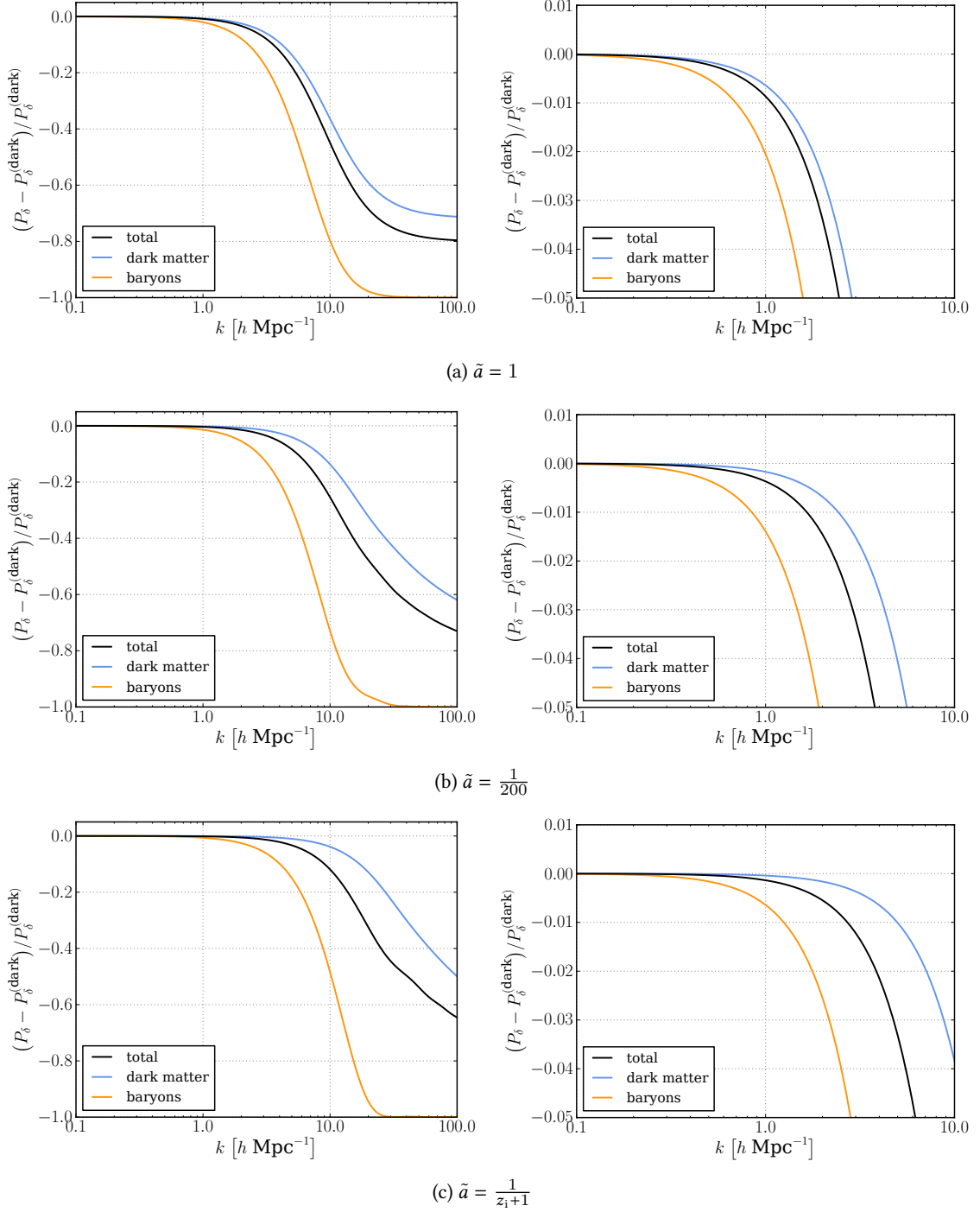
Figure 5.6.: Relative deviation of the density contrast power spectra of the different matter components in a system of gravitationally coupled dark and isothermal baryonic matter from the spectrum of a pure dark matter system, evolved from the time of CMB decoupling to today. Different models for the time-evolution of the mean baryon temperature have been used: following the photon temperature (a), adiabatic cooling (c), and a model that switches between both at a scale factor of $\tilde{a} = 1/200$ (b). The plots on the right show a close-up view of the behaviour around $k = 1\,h/\mathrm{Mpc}$.

Figure 5.7.: Plot taken from [74], showing the deviation of the density contrast power spectra of the dark (dotted lines), baryonic (dashed lines) and total matter (solid lines) obtained from hydrodynamical simulations relative to the spectrum from a pure dark matter simulation. Two hydrodynamical simulation runs were performed: an adiabatic non-radiative one (red) and one that additionally includes radiative cooling and the effects of star formation (green).

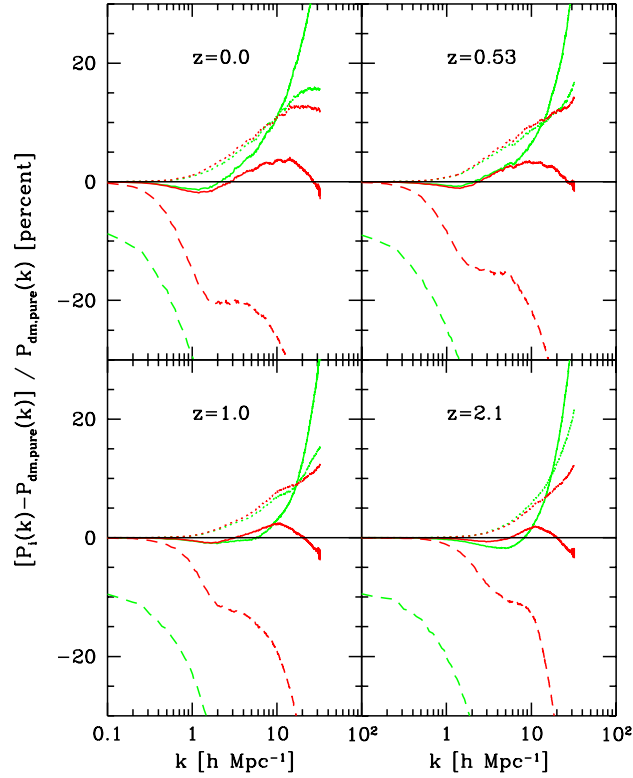to our results, but is significantly stronger. The relative suppression of the baryon spectrum at redshift zero, for example, already reaches a value of roughly 15% at $k = 1\,h/\mathrm{Mpc}$, which is nearly 8 times larger than the maximal suppression we find at this wavenumber. A possible explanation for this deviation could be that our calculation underestimates the speed of sound in the baryonic gas, similarly to what we have seen in the computation of the BAO in the previous subsection. Unlike in the case of the BAO, though, we do not expect this to be caused by an underestimation of the *mean* baryon temperature since even our results with $\tilde{a} = 1$, which overestimate the mean baryon temperature significantly, are nearly an order of magnitude below the simulation results. Instead, this suggests that the local temperature *fluctuations* during gravitational collapse are crucial to achieve the strong power suppressions found in the simulation. If that is the case, an adiabatic description of the baryons will be necessary to reproduce this.

For larger wavenumbers, $k \gtrsim 1\,h/\mathrm{Mpc}$, even the qualitative behaviour of their spectra starts to differ significantly from those we computed. On those wavenumbers, the simulation results show a sudden increase in power such that the dark and total matter power spectra are actually

enhanced rather than suppressed compared to the pure dark matter simulation. Considering that the baryon pressure is expected to counteract the gravitational collapse, this result seems very unintuitive. A possible interpretation of this behaviour has been suggested in [75]. They suspect that during the gravitational collapse the dark matter is able to transfer energy to the gas by heating it up, which then allows the dark matter to fall more quickly into the gravitational well. If this is indeed the underlying physical process, then it is no surprise that our calculations do not capture it. In our isothermal approximation the gas can not absorb any energy of the dark matter by heating up. Beyond that, however, it is very likely that this energy transfer is a nonlinear dynamical process. In that case it could not be captured by our tree-level results even if we drop the isothermal approximation. We will return to this point after discussing the coupling between dark matter and adiabatic baryons in subsection 5.3.3.

The results of the radiative simulation run in Figure 5.7 further show that radiative cooling and star formation strongly affect the baryon spectrum even on wavenumbers $k < 0.1\,h/\mathrm{Mpc}$. If we want to be able to fully describe the baryonic structures on those scales, we will thus have to find a way to model at least some of these effects. Their influence on the dark and total matter power spectrum, though, only becomes relevant on wavenumbers $k \gtrsim 1\,h/\mathrm{Mpc}$. Results from a different suite of simulations run by [76] confirm this.

Altogether, the qualitatively correct results of our isothermal tree-level calculations on mildly non-linear scales are promising, but clearly demonstrate that the incorporation of the adiabatic gas dynamics as well as the inclusion of loop-corrections and eventually even radiative processes will be essential for the description of the small-scale baryonic effects on cosmic structure formation.

5.3. Adiabatic case

5.3.1. KFT path integral

Incorporating the adiabatic mesoscopic particle model into KFT requires to extend the phase-space of microscopic particles, introduced in subsection 3.1.1, by the enthalpy. We thus redefine the microscopic fields as $\vec{x}_j = \left(\vec{q}_j, \vec{p}_j, \mathcal{H}_j\right)$ and $\vec{\chi}_j = \left(\vec{\chi}_{q_j}, \vec{\chi}_{p_j}, \chi_{\mathcal{H}_j}\right)$, satisfying the equations of motion (5.15), (5.20) and (5.21). Inserting these into (3.14) further shows that the corresponding functional Jacobian determinant still equals unity, even though the dynamics is not Hamiltonian any more. Crucially, the partition function Z thus retains the form (3.8).

The free equations of motion are now solved by the extended Green's function

$$\mathcal{G}(t, t') \coloneqq \begin{pmatrix} g_{qq}(t, t')\,\mathcal{I}_3 & g_{qp}(t, t')\,\mathcal{I}_3 & \vec{0} \\ g_{pq}(t, t')\,\mathcal{I}_3 & g_{pp}(t, t')\,\mathcal{I}_3 & \vec{0} \\ \vec{0}^\top & \vec{0}^\top & g_{\mathcal{H}\mathcal{H}}(t, t') \end{pmatrix} \propto \theta(t - t'), \tag{5.88}$$

where $\vec{0}$ denotes a three-dimensional vector whose entries are all zero. For a static space-time

one finds

$$g_{qq}(t,t') = g_{pp}(t,t') = g_{\mathcal{H}\mathcal{H}}(t,t') = \theta(t-t'),\tag{5.89}$$

$$g_{qp}(t,t') = \frac{t-t'}{m}\,\theta(t-t'),\tag{5.90}$$

$$g_{pq}(t,t') = 0,\tag{5.91}$$

as shown in Appendix A.4.

To find a macroscopic reformulation of the partition function, we would like to express the interacting part of the action in terms of collective fields again, similarly to what we had done in subsection 3.1.2 in the case of Hamiltonian dynamics. There is one notable difference between the Hamiltonian and the adiabatic mesoscopic interactions, though: while the former only depend on the spatial particle distances, the latter are additionally dependent on the particle momenta and enthalpies. One possible way to deal with this, would be to introduce collective enthalpy-density and momentum-enthalpy-density fields which absorb these explicit momentum- and enthalpy-dependencies. However, if we did that, the macroscopic reformulation as laid out in subsection 3.2.1 would require to replace all of these by individual macroscopic fields and introduce a conjugate auxiliary field for each of them, too. The resulting macroscopic perturbation theory would thus become rather unwieldy.

Instead, we will exploit the fact that every conceivable collective density field can be expressed as a moment of the extended phase-space density field

$$\Phi_f(\vec{x},t) := \sum_{j=1}^{N} \delta_{\mathrm{D}}(\vec{q}-\vec{q}_j(t))\;\delta_{\mathrm{D}}(\vec{p}-\vec{p}_j(t))\;\delta_{\mathrm{D}}(\mathcal{H}-\mathcal{H}_j(t))\,,\tag{5.92}$$

which we conveniently denote by the same symbol as the original phase-space density field (3.22). This way, we will end up with a macroscopic perturbation theory structurally equivalent to the one for Hamiltonian dynamics.

Since both the particle momenta and enthalpies are affected by the mesoscopic interactions, we further have to introduce two separate respective response fields,

$$\Phi_{B_p}(\vec{x},t) := \sum_{j=1}^{N} \vec{\chi}_{p_j}(t)\cdot\vec{\nabla}_q\,\delta_{\mathrm{D}}(\vec{q}-\vec{q}_j(t))\;\delta_{\mathrm{D}}(\vec{p}-\vec{p}_j(t))\;\delta_{\mathrm{D}}(\mathcal{H}-\mathcal{H}_j(t))\,,\tag{5.93}$$

$$\vec{\Phi}_{B_{\mathcal{H}}}(\vec{x},t) := \sum_{j=1}^{N} \chi_{\mathcal{H}_j}(t)\cdot\vec{\nabla}_q\,\delta_{\mathrm{D}}(\vec{q}-\vec{q}_j(t))\;\delta_{\mathrm{D}}(\vec{p}-\vec{p}_j(t))\;\delta_{\mathrm{D}}(\mathcal{H}-\mathcal{H}_j(t))\,.\tag{5.94}$$

The interacting part of the action can then be expressed as

$$S_{\psi,\mathrm{I}}[\psi] = \int\mathrm{d}^7x\int_{t_i}^{\infty}\mathrm{d}t\int\mathrm{d}^7x'\int_{t_i}^{\infty}\mathrm{d}t'\left(\Phi_f(\vec{x},t)\,\sigma_{fB_p}(\vec{x},t,\vec{x}',t')\,\Phi_{B_p}(\vec{x}',t')\right.$$
$$\left. + \Phi_f(\vec{x},t)\,\vec{\sigma}_{fB_{\mathcal{H}}}(\vec{x},t,\vec{x}',t')\cdot\vec{\Phi}_{B_H}(\vec{x}',t')\right),\tag{5.95}$$

where we defined the two interaction matrix elements

$$\sigma_{fB_p}(x, t, x', t') = \sigma_{B_pf}(x', t', x, t) := -\frac{m}{\bar{\rho}_m}\frac{\gamma - 1}{\gamma}\mathcal{H}\,w(\vec{q} - \vec{q}')\,,\tag{5.96}$$

$$\vec{\sigma}_{fB_{\mathcal{H}}}(x, t, x', t') = \vec{\sigma}_{B_{\mathcal{H}}f}(x', t', x, t) := -\frac{m}{\bar{\rho}_m}(\gamma - 1)\mathcal{H}\frac{\vec{p} - \vec{p}'}{m}\,w(\vec{q} - \vec{q}')\,,\tag{5.97}$$

which absorb the explicit momentum and enthalpy dependencies.

In analogy to the Hamiltonian case, it will be more convenient to work in the Fourier space conjugate to the extended phase-space. Let us thus redefine the Fourier vector as $\vec{s} := (\vec{k}, \vec{l}, y)$, where y denotes the Fourier variable conjugate to the enthalpy $\mathcal{H}$. The corresponding Fourier transforms of the three collective fields read

$$\Phi_f(1) = \sum_{j=1}^{N} e^{-i\vec{k}_1\cdot\vec{q}_j(t_1) - i\vec{l}_1\cdot\vec{p}_j(t_1) - iy_1\mathcal{H}_j(t_1)}\,,\tag{5.98}$$

$$\Phi_{B_p}(1) = \sum_{j=1}^{N} \vec{\chi}_{p_j}(t)\cdot i\vec{k}_1\,e^{-i\vec{k}_1\cdot\vec{q}_j(t_1) - i\vec{l}_1\cdot\vec{p}_j(t_1) - iy_1\mathcal{H}_j(t_1)}\,,\tag{5.99}$$

$$\vec{\Phi}_{B_{\mathcal{H}}}(1) = \sum_{j=1}^{N} \chi_{\mathcal{H}_j}(t)\,i\vec{k}_1\,e^{-i\vec{k}_1\cdot\vec{q}_j(t_1) - i\vec{l}_1\cdot\vec{p}_j(t_1) - iy_1\mathcal{H}_j(t_1)}\,,\tag{5.100}$$

and $S_{\psi,\mathrm{I}}$ becomes

$$S_{\psi,\mathrm{I}}[\psi] = \int\mathrm{d}1\int\mathrm{d}2\left(\Phi_f(-1)\,\sigma_{fB_p}(1, -2)\,\Phi_{B_p}(2) + \Phi_f(-1)\,\vec{\sigma}_{fB_{\mathcal{H}}}(1, -2)\,\vec{\Phi}_{B_{\mathcal{H}}}(2)\right)\tag{5.101}$$

$$= \Phi_f\cdot\sigma_{fB_p}\cdot\Phi_{B_p} + \Phi_f\cdot\vec{\sigma}_{fB_{\mathcal{H}}}\cdot\vec{\Phi}_{B_{\mathcal{H}}}\tag{5.102}$$

with

$$\sigma_{fB_p}(1, 2) = \sigma_{B_pf}(2, 1) = -\frac{m}{\bar{\rho}_m}\frac{\gamma - 1}{\gamma}\,w(k_1)\,i\partial_{y_1}\,(2\pi)^{11}\,\delta_{\mathrm{D}}(\vec{k}_1 + \vec{k}_2)\,\delta_{\mathrm{D}}(\vec{l}_1)\,\delta_{\mathrm{D}}(\vec{l}_2)$$
$$\times\delta_{\mathrm{D}}(y_1)\,\delta_{\mathrm{D}}(y_2)\,\delta_{\mathrm{D}}(t_1 - t_2)\,,\tag{5.103}$$

$$\vec{\sigma}_{fB_{\mathcal{H}}}(1, 2) = \vec{\sigma}_{B_{\mathcal{H}}f}(2, 1) = -\frac{1}{\bar{\rho}_m}(\gamma - 1)\,w(k_1)\,i\partial_{y_1}\,(i\vec{\partial}_{l_1} - \vec{\partial}_{l_2})\,(2\pi)^{11}\,\delta_{\mathrm{D}}(\vec{k}_1 + \vec{k}_2)$$
$$\times\delta_{\mathrm{D}}(\vec{l}_1)\,\delta_{\mathrm{D}}(\vec{l}_2)\,\delta_{\mathrm{D}}(y_1)\,\delta_{\mathrm{D}}(y_2)\,\delta_{\mathrm{D}}(t_1 - t_2)\,,\tag{5.104}$$

where we reused the short-hand notations introduced for the Hamiltonian systems. The most notable difference to the interaction matrix element σ_{fB} of the microscopic and the isothermal mesoscopic model is the appearance of derivative operators in σ_{fB_p} and $\vec{\sigma}_{fB_{\mathcal{H}}}$, which implement the aforementioned moments of the phase-space density.

Finally, we choose to absorb both response fields into the definition of a *single* dressed response field,

$$\Phi_{\mathcal{F}} = \sigma_{fB_p}\cdot\Phi_{B_p} + \vec{\sigma}_{fB_{\mathcal{H}}}\cdot\vec{\Phi}_{B_{\mathcal{H}}}\,,\tag{5.105}$$

as this brings the interacting part of the action into a form that exactly matches the expression (3.43) for Hamiltonian systems. Consequently, the reformulation of the partition function solely in terms of macroscopic fields as well as the structure of the resulting macroscopic perturbation theory discussed in section 3.2 remain completely unchanged. All the additional effects of adiabatic gas dynamics are instead absorbed into a more complex internal structure of the dressed free collective-field cumulants, which are still defined via (3.45). This demonstrates the advantage of introducing a dressed response field in the first place.

5.3.2. Macroscopic propagator

The derivatives with respect to the Fourier conjugate variables of momentum and enthalpy appearing in $G_{f\mathcal{F}}^{(0)}$ force us to rethink the way we compute the macroscopic propagator, as the equation (C.1) defining the functional inverse expressions (3.79) for the causal propagators Δ_{R} and Δ_{A} now becomes an integro-differential equation rather than a pure integral equation. To get around this complication, we first note that $G_{f\mathcal{F}}^{(0)}$ can generally be split into three contributions with different numbers of derivatives appearing,

$$G_{f\mathcal{F}}^{(0)}(1,2) = \sum_{n=0}^{2} \tilde{G}_{f\mathcal{F},n}^{(0)}\big(\vec{k}_1, \vec{l}_1, y_1; t_1, t_2\big)\, \delta_n(1,2)\,, \tag{5.106}$$

where

$$\delta_0(1,2) := (2\pi)^7\, \delta_{\mathrm{D}}\big(\vec{k}_1 + \vec{k}_2\big)\; \delta_{\mathrm{D}}\big(\vec{l}_2\big)\; \delta_{\mathrm{D}}(y_2)\,, \tag{5.107}$$

$$\delta_1(1,2) := (2\pi)^7\, \delta_{\mathrm{D}}\big(\vec{k}_1 + \vec{k}_2\big)\; \delta_{\mathrm{D}}\big(\vec{l}_2\big)\, \mathrm{i}\partial_{y_2}\, \delta_{\mathrm{D}}(y_2)\,, \tag{5.108}$$

$$\delta_2(1,2) := (2\pi)^7\, \delta_{\mathrm{D}}\big(\vec{k}_1 + \vec{k}_2\big)\; \vec{k}_2 \cdot \mathrm{i}\vec{\partial}_{l_2}\, \delta_{\mathrm{D}}\big(\vec{l}_2\big)\, \mathrm{i}\partial_{y_2}\, \delta_{\mathrm{D}}(y_2)\,. \tag{5.109}$$

The functions $\tilde{G}_{f\mathcal{F},n}^{(0)}$, which do not contain any derivatives or delta distributions any more, can be projected out of $G_{f\mathcal{F}}^{(0)}$ in the following way,

$$\tilde{G}_{f\mathcal{F},0}^{(0)}\big(\vec{k}_1, \vec{l}_1, y_1; t_1, t_2\big) := \int \frac{\mathrm{d}^7 s_2}{(2\pi)^7}\, G_{f\mathcal{F}}^{(0)}(1,2)\,, \tag{5.110}$$

$$\tilde{G}_{f\mathcal{F},1}^{(0)}\big(\vec{k}_1, \vec{l}_1, y_1; t_1, t_2\big) := \int \frac{\mathrm{d}^7 s_2}{(2\pi)^7}\, G_{f\mathcal{F}}^{(0)}(1,2)\, \mathrm{i}y_2\,, \tag{5.111}$$

$$\tilde{G}_{f\mathcal{F},2}^{(0)}\big(\vec{k}_1, \vec{l}_1, y_1; t_1, t_2\big) := \int \frac{\mathrm{d}^7 s_2}{(2\pi)^7}\, G_{f\mathcal{F}}^{(0)}(1,2)\, \frac{\vec{k}_2 \cdot \mathrm{i}\vec{l}_2}{k_2^2}\, \mathrm{i}y_2\,, \tag{5.112}$$

using the relation $r\,\partial_r\, \delta_{\mathrm{D}}(r) = -\,\delta_{\mathrm{D}}(r)$.

Inserting (5.106) into the Neumann series expansion (3.81) of the causal propagators then suggests the following ansatz for Δ_{R},

$$\Delta_{\mathrm{R}}(1,2) = \mathcal{I}(1,2) + \sum_{n=0}^{2} \tilde{\Delta}_{\mathrm{R},n}\big(\vec{k}_1, \vec{l}_1, y_1; t_1, t_2\big)\, \delta_n(1,2)\,. \tag{5.113}$$

Using this ansatz as well as the expression (5.106) of $G_{f\mathcal{F}}^{(0)}$ in (C.1) then allows us to reduce the complicated integro-differential equation into a system of three coupled integral equations in time only,

$$\tilde{\Delta}_{\mathrm{R},n}(\vec{k}_1, \vec{l}_1, y_1; t_1, t_2) = \left(\Delta_{\mathrm{R}} \cdot \tilde{G}_{f\mathcal{F},n}^{(0)}\right)(\vec{k}_1, \vec{l}_1, y_1; t_1, t_2) \tag{5.114}$$

$$= \tilde{G}_{f\mathcal{F},n}^{(0)}(\vec{k}_1, \vec{l}_1, y_1; t_1, t_2)$$

$$+ \int_{t_2}^{t_1} dt_1' \sum_{m=0}^{2} \tilde{\Delta}_{\mathrm{R},m}(\vec{k}_1, \vec{l}_1, y_1; t_1, t_1') \, \Omega_{mn}(\vec{k}_1, \vec{l}_1, y_1; t_1', t_2) \,. \tag{5.115}$$

Here, we defined

$$\Omega_{mn}(\vec{k}_1, \vec{l}_1, y_1; t_1', t_2) := \int \frac{d^7 s_1'}{(2\pi)^7} \, \delta_m(1, -1') \, \tilde{G}_{f\mathcal{F},n}^{(0)}(\vec{k}_1', \vec{l}_1', r_1'; t_1', t_2) \,, \tag{5.116}$$

collecting all the different possible combinations of operators δ_m acting on the free cumulants $\tilde{G}_{f\mathcal{F},n}^{(0)}$.

To solve this system of integral equations numerically, it is useful to reformulate it as a set of nested equations. After some algebra we find

$$\tilde{\Delta}_{\mathrm{R},2} = \Big[\tilde{G}_{f\mathcal{F},2}^{(0)} + \tilde{G}_{f\mathcal{F},0}^{(0)} \cdot \mathrm{I}_{00} \cdot \Omega_{02}$$
$$+ \left(\tilde{G}_{f\mathcal{F},1}^{(0)} + \tilde{G}_{f\mathcal{F},0}^{(0)} \cdot \mathrm{I}_{00} \cdot \Omega_{01} \right) \cdot \mathrm{I}_{11} \cdot \left(\Omega_{12} + \Omega_{10} \cdot \mathrm{I}_{00} \cdot \Omega_{02} \right) \Big] \cdot \mathrm{I}_{22} \,, \tag{5.117}$$

$$\tilde{\Delta}_{\mathrm{R},1} = \Big[\tilde{G}_{f\mathcal{F},1}^{(0)} + \tilde{G}_{f\mathcal{F},0}^{(0)} \cdot \mathrm{I}_{00} \cdot \Omega_{01} + \tilde{\Delta}_{\mathrm{R},2} \cdot \left(\Omega_{21} + \Omega_{20} \cdot \mathrm{I}_{00} \cdot \Omega_{01} \right) \Big] \cdot \mathrm{I}_{11} \,, \tag{5.118}$$

$$\tilde{\Delta}_{\mathrm{R},0} = \Big[\tilde{G}_{f\mathcal{F},0}^{(0)} + \tilde{\Delta}_{\mathrm{R},1} \cdot \Omega_{10} + \tilde{\Delta}_{\mathrm{R},2} \cdot \Omega_{20} \Big] \cdot \mathrm{I}_{00} \,, \tag{5.119}$$

where we defined the functional inverses

$$\mathrm{I}_{00} = \left(\mathcal{I} - \Omega_{00} \right)^{-1} \,, \tag{5.120}$$

$$\mathrm{I}_{11} = \left(\mathcal{I} - \Omega_{11} - \Omega_{10} \cdot \mathrm{I}_{00} \cdot \Omega_{01} \right)^{-1} \,, \tag{5.121}$$

$$\mathrm{I}_{22} = \left[\mathcal{I} - \Omega_{22} - \Omega_{20} \cdot \mathrm{I}_{00} \cdot \Omega_{02} - \left(\Omega_{21} + \Omega_{20} \cdot \mathrm{I}_{00} \cdot \Omega_{01} \right) \cdot \mathrm{I}_{11} \cdot \left(\Omega_{12} + \Omega_{10} \cdot \mathrm{I}_{00} \cdot \Omega_{02} \right) \right]^{-1} \,. \tag{5.122}$$

Similarly to the equations (5.48) to (5.52) in the case of two different species of particles, one can solve these equations iteratively. First, one has to perform the functional inverses I_{00}, I_{11} and I_{22}, in that order, analogously to the one in Appendix C. Afterwards one can use these results to compute the different contributions to $\tilde{\Delta}_{\mathrm{R}}$ in the order $\tilde{\Delta}_{\mathrm{R},2}$, $\tilde{\Delta}_{\mathrm{R},1}$ and $\tilde{\Delta}_{\mathrm{R},0}$, which only requires to perform time integrals. A full numerical implementation of this is still work in progress, though.

In some situations, however, the coupled integral equations (5.115) can also be solved analytically. To see this, we define the vectors $\tilde{\Delta}_{\mathrm{R}}$ and $\tilde{G}_{f\mathcal{F}}^{(0)}$ with components $\tilde{\Delta}_{\mathrm{R},n}$ and $\tilde{G}_{f\mathcal{F},n}^{(0)}$,

respectively, as well as the matrix Ω with components Ω_{mn}. The system of integral equations then condenses to a single matrix integral equation,

$$\tilde{\Delta}_{\mathrm{R}}(\vec{k}_1, \vec{l}_1, y_1; t_1, t_2) = \tilde{G}^{(0)}_{f\mathcal{F}}(\vec{k}_1, \vec{l}_1, y_1; t_1, t_2) + \int\limits_{t_2}^{t_1} \mathrm{d}t_1' \, \tilde{\Delta}_{\mathrm{R}}(\vec{k}_1, \vec{l}_1, y_1; t_1, t_1') \, \Omega(\vec{k}_1, \vec{l}_1, y_1; t_1', t_2) \,,$$

$$(5.123)$$

resembling the equation (C.5) found in the case of Hamiltonian dynamics more closely. This allows us to generalise the argumentation used in Appendix C to conclude that the computation of $\tilde{\Delta}_{\mathrm{R}}$ and thus Δ_{R} can be performed fully analytically if Ω depends on its two time arguments only in terms of their difference. Similarly to the case of two particle species discussed in subsection 5.2.2, the computation of the macroscopic propagator then proceeds analogously to the steps detailed in Appendix C as long as one takes the additional matrix algebra into account.

Once more we demonstrate this for our usual test system in static space-time with initial density correlations and vanishing initial momenta. To extend this to the case of an adiabatic gas, we also have to specify initial conditions for the particles' enthalpies. A simple choice that preserves the time translation invariance of Ω is to give every mesoscopic particle the same initial enthalpy $\mathcal{H}_{\mathrm{i}}$. In Appendix B.2 we show how the corresponding general expressions for the free collective-field cumulants can be obtained. Inserting the Green's function components (5.89) to (5.91) as well as the interaction matrix elements (5.103) and (5.104) into these expression then yields

$$G^{(0)}_f(1) = (2\pi)^3 \, \delta_{\mathrm{D}}(\vec{k}_1) \, \bar{\rho} \, \mathrm{e}^{-\mathrm{i}y_1 \mathcal{H}_{\mathrm{i}}} \,, \tag{5.124}$$

$$G^{(0)}_{f\mathcal{F}}(1,2) = (2\pi)^7 \, \delta_{\mathrm{D}}(\vec{k}_1 + \vec{k}_2) \, \bar{\rho} \, \mathrm{i} \left[\left(v_G(k_1) + v_{P_p}(k_1) \, \mathrm{i}\partial_{y_2} \right) \left(k_1^2 \, \frac{t_1 - t_2}{m} + \vec{k}_1 \cdot \vec{l}_1 \right) \right.$$
$$\left. + v_{P_{\mathcal{H}}}(k_1) \, y_1 \, \vec{k}_1 \cdot \mathrm{i}\vec{\partial}_{l_2} \, \mathrm{i}\partial_{y_2} \right] \delta_{\mathrm{D}}(\vec{l}_2) \, \delta_{\mathrm{D}}(y_2) \, \mathrm{e}^{-\mathrm{i}y_1 \mathcal{H}_{\mathrm{i}}} \, \theta(t_1 - t_2) \,, \tag{5.125}$$

$$G^{(0)}_{ff}(1,2) = (2\pi)^3 \, \delta_{\mathrm{D}}(\vec{k}_1 + \vec{k}_2) \, \bar{\rho}^2 \, P^{(\mathrm{i})}_\delta(k_1) \, \mathrm{e}^{-\mathrm{i}(y_1 + y_2)\mathcal{H}_{\mathrm{i}}} \,. \tag{5.126}$$

Here, we defined the two potentials

$$v_{P_p}(k) := \frac{\gamma - 1}{\gamma \, \bar{\rho}} \, w(k) \,, \tag{5.127}$$

$$v_{P_{\mathcal{H}}}(k) := \frac{\gamma - 1}{\bar{\rho}_{\mathrm{m}}} \, w(k) \,, \tag{5.128}$$

associated with the effects of pressure gradients and pressure-volume work, respectively. Since we want to describe a self-gravitating adiabatic gas, we also added the gravitational potential v_G defined in (5.29) to the momentum part of the interaction.

We compute the resulting statistical propagator Δ_{ff}, using Wolfram Mathematica to perform the involved matrix algebra and Laplace transforms. The final result is given by

$$\Delta_{ff}(1,2) = (2\pi)^3 \, \delta_{\mathrm{D}}(\vec{k}_1 + \vec{k}_2) \, \bar{\rho}^2 \, P^{(\mathrm{i})}_\delta(k_1) \, D'(1) \, D'(2) \tag{5.129}$$

with

$$D'(1) := \left(1 - \bar{\rho}\, \frac{\mathcal{H}_i\, v_{P_p}(k_1) + v_G(k_1)}{mc^2(k_1)} \left[\left(1 - iy_1\, \mathcal{H}_i\, \bar{\rho}_m\, v_{P_{\mathcal{H}}}(k_1)\right)\left(1 - \cos\left(k_1 t_1\, c(k_1)\right)\right) \right.\right.$$
$$\left.\left. + mc(k_1)\frac{\vec{k}_1 \cdot \vec{l}_1}{k_1^2}\, \sin\left(k_1 t_1\, c(k_1)\right)\right]\right) e^{-i\mathcal{H}_i s_1} \,. \tag{5.130}$$

and

$$c'(k) := \sqrt{\bar{\rho}\, \frac{\mathcal{H}_i\, v_{P_p}(k)\left(1 + \bar{\rho}_m\, v_{P_{\mathcal{H}}}(k)\right) + v_G(k)}{m}} \tag{5.131}$$

$$\approx \sqrt{(\gamma - 1)\frac{\mathcal{H}_i}{m} - \frac{4\pi\, G\, \bar{\rho}_m}{k^2}} \,. \tag{5.132}$$

In the second line we used that $w(k) \approx 1$ as long as we restrict ourselves to the validity range of our mesoscopic model, $k \ll \sigma_w^{-2}$. Note that we introduced the prime here to distinguish them from the analogous quantities in the isothermal case.

From the expression for c' we infer that the self-gravitating adiabatic gas shares the same characteristic transition from growing modes on large scales to oscillating modes on small scales as the self-gravitating isothermal gas described in subsection 5.2.1. There are a few notable differences, though, that we would like to point out. First of all, the wave propagation speed in the pressure dominated regime, given by the value of $c'(k)$ on those small scales, matches the expected adiabatic speed of sound c_S rather than the isothermal one c_T,

$$c'(k)\Big|_{v_G \ll \mathcal{H}_i v_{P_p}} = \sqrt{(\gamma - 1)\frac{\mathcal{H}_i}{m}} = \sqrt{(\gamma - 1)\frac{\bar{\mathcal{H}}}{m}} = \sqrt{\gamma\, \frac{k_B \bar{T}}{m_{mic}}} = c_S \,. \tag{5.133}$$

Here we used that the initial enthalpy per particle has to equal the mean enthalpy per particle at all times, due to the global enthalpy conservation, and inserted the equation of state of an ideal gas. The Jeans wavenumber k_J changes accordingly,

$$k_J = k\Big|_{c'(k)=0} = \frac{\sqrt{4\pi G\, \bar{\rho}_m}}{c_S} \,. \tag{5.134}$$

In Figure 5.8 we further plot the tree-level results for normalised density contrast, momentum-density contrast and enthalpy-density contrast power spectra of the self-gravitating adiabatic

gas,

$$\bar{P}_\delta^{(\Delta)}(k_1, t_1) := \frac{P_\delta^{(\Delta)}(k_1, t_1)}{P_\delta^{(i)}(k_1)} = \frac{\Delta_{ff}(1,2)}{(2\pi)^3\,\delta_{\mathrm{D}}(\vec{k}_1 + \vec{k}_2)\,\bar{\rho}^2\,P_\delta^{(i)}(k_1)}\Bigg|_{\substack{\vec{k}_2=-\vec{k}_1 \\ \vec{l}_1=\vec{l}_2=0 \\ y_1=y_2=0 \\ t_2=t_1}} , \qquad (5.135)$$

$$\bar{P}_\pi^{(\Delta)}(k_1, t_1) := \frac{P_\pi^{(\Delta)}(k_1, t_1)}{P_\delta^{(i)}(k_1)} = \frac{\mathrm{i}\frac{\partial}{\partial\vec{l}_1}\cdot\mathrm{i}\frac{\partial}{\partial\vec{l}_2}\,\Delta_{ff}(1,2)}{(2\pi)^3\,\delta_{\mathrm{D}}(\vec{k}_1 + \vec{k}_2)\,\bar{\rho}^2\,P_\delta^{(i)}(k_1)}\Bigg|_{\substack{\vec{k}_2=-\vec{k}_1 \\ \vec{l}_1=\vec{l}_2=0 \\ y_1=y_2=0 \\ t_2=t_1}} , \qquad (5.136)$$

$$\bar{P}_h^{(\Delta)}(k_1, t_1) := \frac{P_{\mathcal{H}}^{(\Delta)}(k_1, t_1)}{P_\delta^{(i)}(k_1)} = \frac{\mathrm{i}\frac{\partial}{\partial y_1}\mathrm{i}\frac{\partial}{\partial y_2}\,\Delta_{ff}(1,2)}{(2\pi)^3\,\delta_{\mathrm{D}}(\vec{k}_1 + \vec{k}_2)\,\bar{\rho}^2\,P_\delta^{(i)}(k_1)}\Bigg|_{\substack{\vec{k}_2=-\vec{k}_1 \\ \vec{l}_1=\vec{l}_2=0 \\ y_1=y_2=0 \\ t_2=t_1}} , \qquad (5.137)$$

next to the corresponding isothermal results. Thereby, the enthalpy-density constrast spectrum $\bar{P}_h^{(\Delta)}$ of the isothermal gas is obtained by multiplying its density contrast spectrum $\bar{P}_\delta^{(\Delta)}$ with the constant squared value of the enthalpy per isothermal mesoscopic particle (5.24). To make the results comparable, we chose to identify the initial temperature of the adiabatic gas with the constant temperature of the isothermal gas.

The first thing we note is that the oscillation frequency of the adiabatic spectra is larger then that of the isothermal spectra, resulting from the adiabatic speed of sound being higher than the isothermal one by a factor of $\sqrt{\gamma}$. Second, we see that the oscillation amplitude of the momentum-density spectra is smaller for the adiabatic gas. The most notable difference, though, can be observed in the density contrast spectra. While the isothermal oscillation peaks all have the same amplitude, the adiabatic peaks are strongly alternating in height – an effect that is most likely caused by the pressure-volume work. Lastly, we want to point out that the density contrast and enthalpy-density contrast spectra of the adiabatic gas are clearly not proportional to each other. Hence, our results are able to describe the local fluctuations of the enthalpy and thus the temperature themselves.

Altogether, these findings demonstrate that our resummed mesoscopic model is not only able to describe the dynamics of an isothermal gas in a physically consistent manner, but also the significantly richer dynamics of an adiabatic gas. From the perspective of the planned cosmological application of this model, the fact that local temperature fluctuations are captured is probably the most important aspect, as these were suspected in subsection 5.2.5 to be essential for an accurate treatment of the baryonic effects on small scales.

5.3.3. Coupling to dark matter in static space-time

To couple adiabatic baryons to dark matter we formally would have to start by introducing separate extended phase-space trajectories for both particle species, construct their joint partition function and reformulate this in terms of macroscopic fields. Instead of going through this laborious process, though, we can take a shortcut by combining the results of the preceding two subsections with the insights into how to couple micro- and mesoscopic particles gained in subsection 5.2.2.

(a) Density contrast

(b) Momentum-density contrast

(c) Enthalpy-density contrast
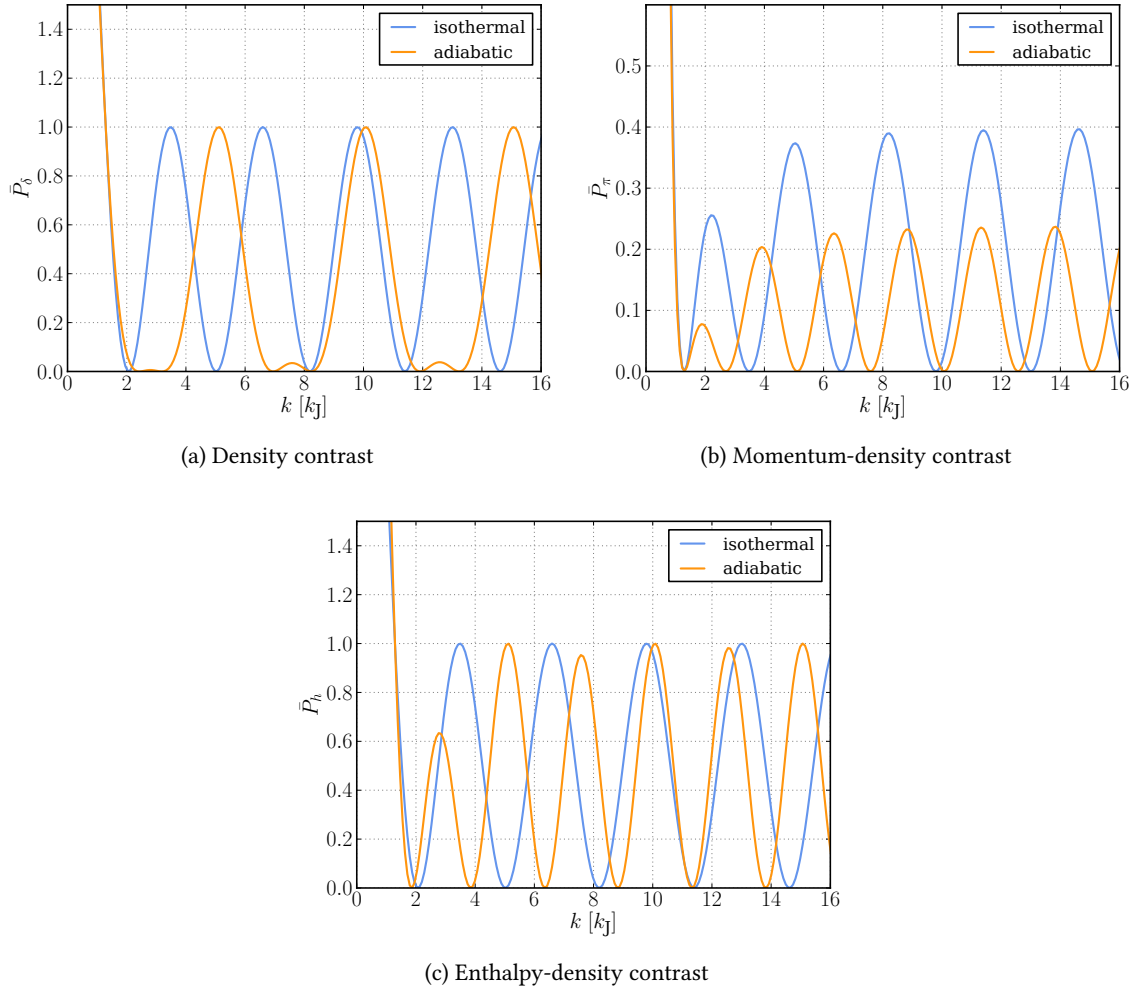
Figure 5.8.: Comparison between the normalised density contrast (a), momentum-density contrast (b) and enthalpy-density contrast (c) power spectra of a self-gravitating isothermal and a self-gravitating adiabatic gas with equal initial temperature. Most notable are the generally higher oscillation frequency of the adiabatic spectra, the alternating peak heights of the adiabatic density contrast spectrum and the higher amplitudes of the adiabatic momentum-density spectrum.

In both cases, we inferred that the macroscopic reformulation proceeds exactly as laid down in section 3.2 if one allows the macroscopic fields, propagators and vertices to acquire some substructure – either different components for the individual particle species coupled by gravity or a more complex internal structure of the dressed free collective-field cumulants involving derivative operators.

A joint system of adiabatic baryons and dark matter can hence be described within the macroscopic perturbation theory if we introduce separate particle-species components Φ_f^α and $\Phi_{\mathcal{F}}^\alpha$ of the extended phase-space density field (5.92) as well as the extended dressed response field (5.105), respectively, where the latter is given by

$$\Phi_{\mathcal{F}}^\alpha = \sum_{\gamma=\mathrm{d,b}} \left[\sigma_{fB_P}^{\alpha\gamma} \cdot \Phi_{B_P}^{\gamma} + \vec{\sigma}_{fB_{\mathcal{H}}}^{\alpha\gamma} \cdot \Phi_{B_{\mathcal{H}}}^{\gamma} \right], \tag{5.138}$$

with

$$\sigma_{fB_P}^{\alpha\gamma}(1,2) := \sigma_{B_Pf}^{\gamma\alpha}(2,1) = -\left(v_G^{\alpha\gamma}(k_1,t_1) + \delta_{\alpha\mathrm{b}}\,\delta_{\gamma\mathrm{b}}\,v_{P_P}^{\mathrm{b}}(k_1,t_1)\,\mathrm{i}\partial_{y_1} \right)$$
$$\times (2\pi)^{11}\,\delta_{\mathrm{D}}(\vec{k}_1+\vec{k}_2)\,\delta_{\mathrm{D}}(\vec{l}_1)\,\delta_{\mathrm{D}}(\vec{l}_2)\,\delta_{\mathrm{D}}(y_1)\,\delta_{\mathrm{D}}(y_2)\,\delta_{\mathrm{D}}(t_1-t_2), \tag{5.139}$$

$$\vec{\sigma}_{fB_{\mathcal{H}}}^{\alpha\gamma}(1,2) := \vec{\sigma}_{B_{\mathcal{H}}f}^{\gamma\alpha}(2,1) = -\delta_{\alpha\mathrm{b}}\,\delta_{\gamma\mathrm{b}}\,v_{P_{\mathcal{H}}}^{\mathrm{b}}(k_1,t_1)\,\mathrm{i}\partial_{y_1}\left(\mathrm{i}\vec{\partial}_{l_1}-\vec{\partial}_{l_2}\right)$$
$$\times \delta_{\mathrm{D}}(\vec{k}_1+\vec{k}_2)\,\delta_{\mathrm{D}}(\vec{l}_1)\,\delta_{\mathrm{D}}(\vec{l}_2)\,\delta_{\mathrm{D}}(y_1)\,\delta_{\mathrm{D}}(y_2)\,\delta_{\mathrm{D}}(t_1-t_2). \tag{5.140}$$

Here, $v_G^{\alpha\gamma}$ is the gravitational potential defined in (5.38), and

$$v_{P_P}^{\mathrm{b}}(k) := \frac{\gamma-1}{\gamma\,\bar{\rho}^{\mathrm{b}}}\,w(k), \tag{5.141}$$

$$v_{P_H}^{\mathrm{b}}(k) := \frac{\gamma-1}{\bar{\rho}_{\mathrm{m}}^{\mathrm{b}}}\,w(k), \tag{5.142}$$

are the baryonic potentials associated with the effects pressure gradients and pressure-volume work, respectively.

Generalising the the expressions for the dressed free collective field cumulants of a single adiabatic particle species, (5.124) to (5.126), to the two-particle system proceeds analogously to the case of an isothermal gas discussed in subsection 5.2.2. The only difference is that we also have to make sure that only the baryons obtain a non-vanishing initial enthalpy. We thus find

$$G_f^{(0)\,\alpha}(1) = (2\pi)^3\,\delta_{\mathrm{D}}(\vec{k}_1)\,\bar{\rho}^\alpha\,\mathrm{e}^{-\mathrm{i}\,\delta_{\alpha\mathrm{b}}\,y_1\,\mathcal{H}_{\mathrm{i}}}, \tag{5.143}$$

$$G_{f\mathcal{F}}^{(0)\,\alpha\gamma}(1,2) = (2\pi)^7\,\delta_{\mathrm{D}}(\vec{k}_1+\vec{k}_2)\,\bar{\rho}^\alpha\,\mathrm{i}\left[\left(v_G^{\alpha\gamma}(k_1) + \delta_{\alpha\mathrm{b}}\,\delta_{\gamma\mathrm{b}}\,v_{P_P}^{\mathrm{b}}(k_1)\,\mathrm{i}\partial_{y_2} \right)\left(k_1^2\,\frac{t_1-t_2}{m} + \vec{k}_1\cdot\vec{l}_1 \right) \right.$$
$$\left. + \delta_{\alpha\mathrm{b}}\,\delta_{\gamma\mathrm{b}}\,v_{P_{\mathcal{H}}}^{\mathrm{b}}(k_1)\,y_1\,\vec{k}_1\cdot\mathrm{i}\vec{\partial}_{l_2}\,\mathrm{i}\partial_{y_2} \right]\,\delta_{\mathrm{D}}(\vec{l}_2)\,\delta_{\mathrm{D}}(y_2)\,\mathrm{e}^{-\mathrm{i}y_1\,\mathcal{H}_{\mathrm{i}}\,\delta_{\alpha\mathrm{b}}}\,\theta(t_1-t_2), \tag{5.144}$$

$$G_{ff}^{(0)\,\alpha\gamma}(1,2) = (2\pi)^3\,\delta_{\mathrm{D}}(\vec{k}_1+\vec{k}_2)\,\bar{\rho}^\alpha\,\bar{\rho}^\gamma\,P_\delta^{(\mathrm{i})}(k_1)\,\mathrm{e}^{-\mathrm{i}(\delta_{\alpha\mathrm{b}}\,y_1+\delta_{\gamma\mathrm{b}}\,y_2)\mathcal{H}_{\mathrm{i}}}. \tag{5.145}$$

The resulting expression for the statistical propagator, calculated using Wolfram Mathematica, can be written in a form very closely to the result (5.56) in the isothermal case,

$$\Delta_{ff}^{\alpha\gamma}(1,2) = (2\pi)^3 \, \delta_{\mathrm{D}}\big(\vec{k}_1 + \vec{k}_2\big) \, \bar{\rho}^\alpha \, \bar{\rho}^\gamma \, P_\delta^{(\mathrm{i})}(k_1) \, D'^\alpha(1) \, D'^\gamma(2) \tag{5.146}$$

with

$$D'^\alpha(1) = D_0'^\alpha(\vec{s}_1) + \sum_{\ell=\pm} \Big[D_{\mathrm{c},\ell}'^\alpha(\vec{s}_1) \, \cos\big(k_1 t_1 \, c_\ell'(k_1)\big) + D_{\mathrm{s},\ell}'^\alpha(\vec{s}_1) \, \sin\big(k_1 t_1 \, c_\ell'(k_1)\big) \Big] \, . \tag{5.147}$$

The explicit expressions for the coefficients $D_0'^\alpha$, $D_{\mathrm{c},\pm}'^\alpha$ and $D_{\mathrm{s},\pm}'^\alpha$ as well as the functions $c_\pm'$ are rather lengthy and can be found in Appendix G.

Structurally, the only difference between the statistical propagators in the isothermal and the adiabatic case is the appearance of an additional constant mode $D_0'^\alpha$ in the adiabatic result. The general scale-dependent behaviour of structure formation found in the isothermal case is not affected by this, though, as we can see from the time-evolution of the normalised density contrast spectra,

$$\bar{P}_\pi^{(\Delta)\,\alpha\gamma}(k_1, t_1) = \frac{P_\pi^{(\Delta)\,\alpha\gamma}(k_1, t_1)}{P_\delta^{(\mathrm{i})}(k_1)} = \left. \frac{\Delta_{ff}^{\alpha\gamma}(1,2)}{(2\pi)^3 \, \delta_{\mathrm{D}}\big(\vec{k}_1 + \vec{k}_2\big) \, \bar{\rho}^\alpha \, \bar{\rho}^\gamma \, P_\delta^{(\mathrm{i})}(k_1)} \right|_{\substack{\vec{k}_2 = -\vec{k}_1 \\ \vec{l}_1 = \vec{l}_2 = 0 \\ y_1 = y_2 = 0 \\ t_2 = t_1}} , \tag{5.148}$$

$$\bar{P}_\pi^{(\Delta)\,\mathrm{tot}}(k_1, t_1) = \big(\bar{\rho}_{\mathrm{m}}^{\mathrm{d}} + \bar{\rho}_{\mathrm{m}}^{\mathrm{b}}\big)^{-2} \sum_{\alpha,\gamma=\mathrm{d},\mathrm{b}} \bar{\rho}_{\mathrm{m}}^\alpha \, \bar{\rho}_{\mathrm{m}}^\gamma \, \bar{P}_\pi^{(\Delta)\,\alpha\gamma}(k_1, t_1) \, , \tag{5.149}$$

shown in Figure 5.9. It still holds that the dark matter evolution is always dominated by the growing modes, while the baryons show an effective time-dependent transition scale between a dominantly growing regime on large scales and a dominantly oscillating regime on small scales.

To compare the effects of the different gas dynamics more quantitatively, we plot their results for the normalised density contrast power spectra of the dark, baryonic and total matter in Figure 5.10 next to each other. There are two important differences that we want to point out. First, the adiabatic baryon spectrum shows the same characteristic pattern of strongly alternating peak heights seen in Figure 5.8a for a self-gravitating adiabatic gas on its own. The isothermal baryon spectrum, on the other hand shows only a negligible variation in peak height caused by the coupling to the dark matter. Second, the suppression of the dark and total matter spectra on the pressure dominated scales caused by the adiabatic baryons is substantially weaker than the suppression caused by the isothermal baryons. However, an enhancement of the dark matter spectrum, as found in the simulations [74–76] discussed in subsection 5.3.3, can not be seen.

Overall, these results show that the macroscopic propagator is capable of capturing the differences in structure formation between a system that couples dark matter to adiabatic baryons and a system that couples it to isothermal baryons. Furthermore, we have seen that these differences do not only affect the baryonic structures but also the dark and total matter structures. This supports our suspicions that an accurate treatment of the baryonic effects in cosmic structure formation requires to take the adiabatic gas dynamics into account. The crucial next step will thus be to implement the full numerical computation of the macroscopic propagator in the adiabatic

(a) $k = 0.5\,k_{\mathrm{J}}$
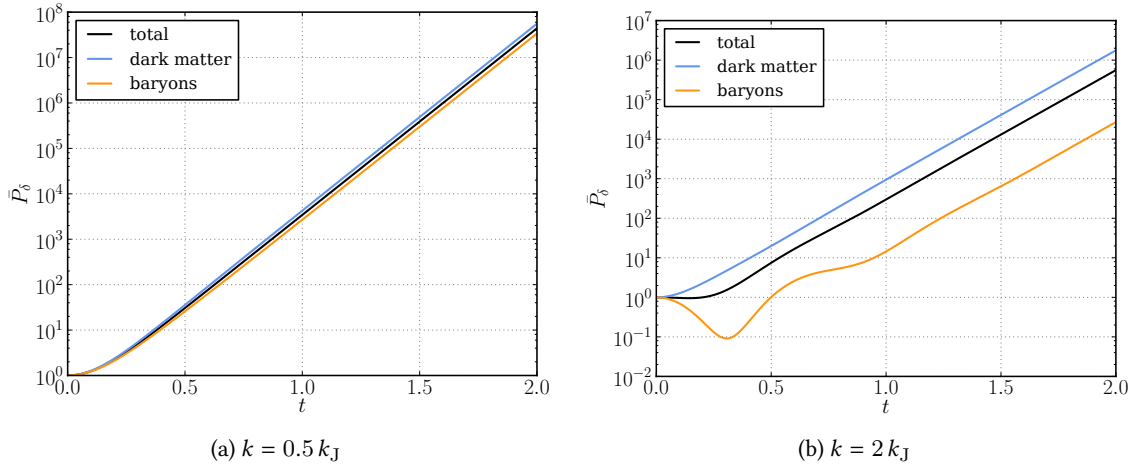
(b) $k = 2\,k_{\mathrm{J}}$

Figure 5.9.: Time-evolution of normalised density contrast power spectra of the different matter components in a system of gravitationally coupled dark and adiabatic baryonic matter, shown at two different wavenumbers. Below the Jeans wavenumber k_{J} (a) gravitational collapse leads at all times to structure growth in all matter components. Above it (b) the baryonic structure growth is suppressed at early times, but sets in once the combined dark and baryonic gravitational attraction overcomes the baryon pressure.

case needed for the application in an expanding space-time. After that we will extend our analysis to the computation of loop corrections, to investigate if these are able to describe the enhancement of the dark matter power spectrum absent in our tree-level results.

(a) Dark matter

(b) Baryonic matter
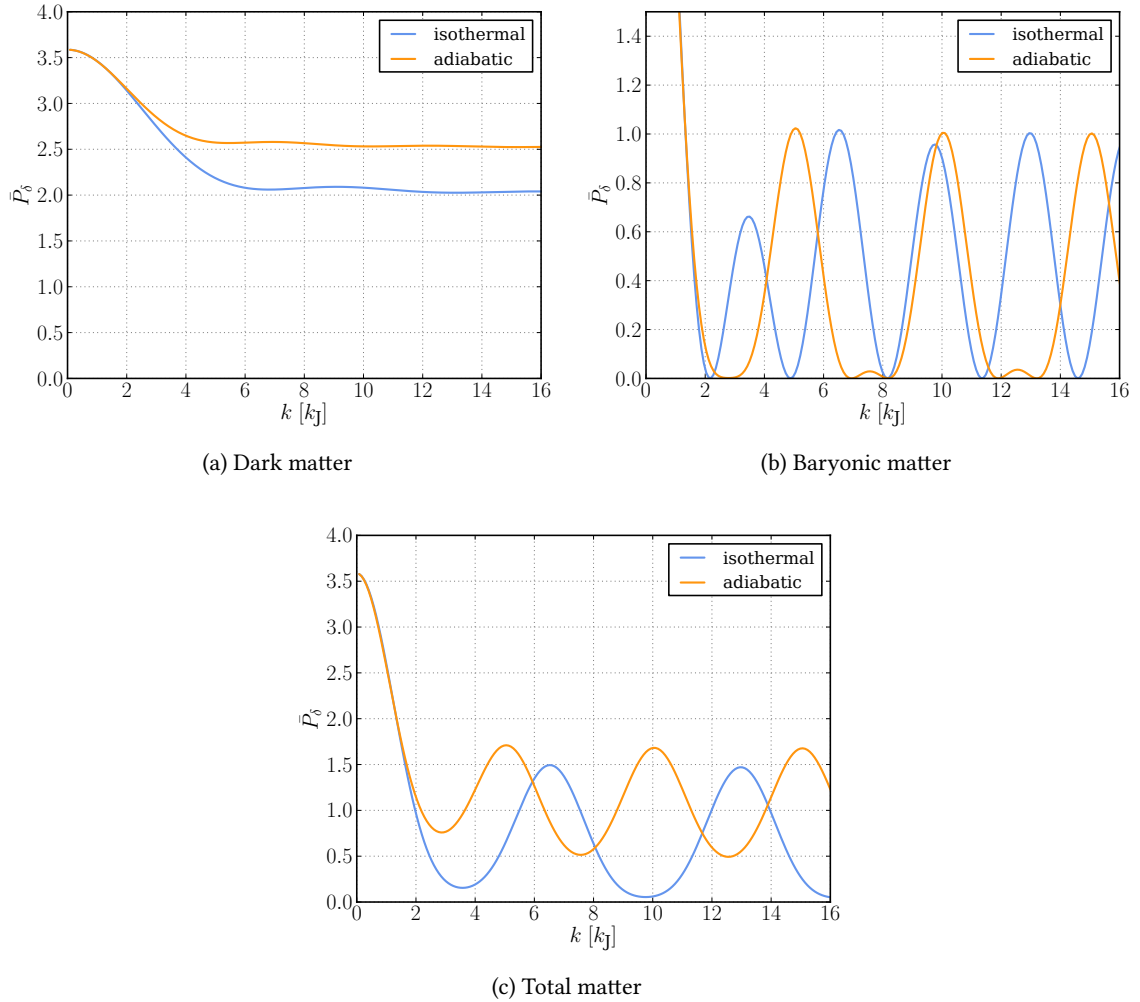
(c) Total matter

Figure 5.10.: Comparison between the normalised dark (a), baryonic (b) and total matter (c) power spectra of a system that couples dark matter to isothermal baryons and a system that couples dark matter to adiabatic baryons. The initial baryon temperatures are the same for both systems. Most notable are the alternating peak heights of the baryon spectrum and the weaker suppression of the dark and total matter spectra in the system with adiabatic baryons.

6. Conclusions

In this thesis, we used the framework of resummed KFT to investigate the structure formation in dark as well as baryonic matter, eventually aiming at an accurate analytic description of the evolution of cosmic structures on scales below $1\,\mathrm{Mpc}/h$. We specifically focussed on two different aspects: the nonlinear evolution of pure dark matter structures and the influence of baryonic gas dynamics on their coupled linear evolution. In this chapter, we will summarise our results and conclusions.

In our study of the dark matter structure formation we first computed the tree-level contribution to the density contrast power spectrum. This reproduced the well-known linear growth of structures on large scales while it showed power on small scales to be suppressed by the momentum dispersion of dark matter particles. However, unlike the Zel'dovich approximation, which overpredicts the dissolution of small-scale structure, our result never drops below the power spectrum resulting from the full nonlinear free-streaming of particles expected from Hamiltonian dynamics.

In a second step we computed the first nonlinear corrections to the power spectrum by using the same expansion scheme as standard Eulerian perturbation theory (SPT), i. e. in orders of the linear power spectrum. Surprisingly, this yielded exactly the same result as the 1-loop correction in SPT, despite the fact that our approach, unlike SPT, is capable of describing crossing streams of particles. The reason for this is not understood yet, but we suggested several possible explanations that we are planning to investigate in future research. This will be crucial to fully understand the capabilities but also possible limits of the KFT framework. Beyond that, it might also provide new insights into the transition from a particle to a fluid picture in general.

However, our investigations also showed that the natural expansion scheme in resummed KFT is actually in the order of the full nonlinear, freely evolved n-point phase-space density cumulants that are taken into account. This is fundamentally different from the SPT scheme and thus has the potential of overcoming the difficulties SPT is faced with when trying to describe scales beyond the mildly nonlinear regime. So far, we could not investigate this in more detail since we are limited by the numerically challenging evaluation of the free n-point phase-space density cumulants. An important next step will thus be to improve our numerical implementations to the point where they allow us to exploit the full potential of resummed KFT.

In our study of the baryonic effects on structure formation we demonstrated how isothermal as well as adiabatic gas dynamics can be incorporated into resummed KFT by treating baryons as effective mesoscopic particles corresponding to small fluid elements. The results found for the linear evolution of these purely baryonic systems are consistent with the behaviour expected from a self-gravitating isothermal and adiabatic gas, respectively. This is an improvement over the microscopic KFT expansion in orders of the interaction which tends to develop unphysical features like negative densities. We thus expect systems with hydrodynamic interactions to be generally better described within the framework of resummed KFT.

We further demonstrated how the mesoscopic baryons can be gravitationally coupled to microscopic dark matter particles. The results obtained for the linear evolution of this coupled system showed a behaviour that could not be obtained from a single dark or baryonic component. Most notably, we found that an effective time-dependent Jeans length for the baryons emerges. From this we conclude that any approach trying to model the joint structure formation in dark and baryonic matter in terms of a single effective type of matter is most likely inherently limited. Instead, a true 2-species description appears to be essential.

In the case of isothermal gas dynamics, we also investigated the formation of structures in the coupled system in two cosmological settings. As a benchmark of our approach, we first considered a situation where nonlinear effects should play a minor role: the formation of baryon acoustic oscillations in the early matter-dominated epoch. Our results for their position and amplitude agreed within a factor of 4 with a fit obtained from numerical Boltzmann solvers. As most of the deviations could be explained in terms of approximations due to our effective treatment of the photon gas, we consider this a successful first test.

Afterwards we investigated the effect of isothermal baryon dynamics on the small-scale structures observed today. Our results showed a suppression of the baryonic power spectrum that is qualitatively comparable with the results found in numerical simulations. Quantitatively, however, we underpredicted this suppression by nearly an order of magnitude. Furthermore, the simulations show an enhancement of the dark matter power spectrum that is completely absent in our results. We could conclude that this is most likely explained by our simplified isothermal treatment and the fact that we are only considering the linear evolution of our coupled system of dark and baryonic matter. In the future, we thus plan to extend our analysis of the small-scale structure formation in an expanding space-time to the case of adiabatic gas dynamics. Once this will be achieved we will investigate the effect of loop-corrections.

Altogether, our results found in this thesis show that the resummed KFT approach is a promising candidate for an analytic framework capable of accurately describing the cosmic small-scale structure formation. But they also show that we are still quite far away from actually reaching this goal. The focus of our future research will thus lie on overcoming the current limitations preventing us from using the full potential of resummed KFT.

A. Computation of the retarded Green's function

A.1. General form

The free equations of motion of a single particle are assumed to be linear in its phase-space-coordinate $\vec{x}$. They can thus be written as

$$\left(\partial_t + \mathcal{E}_0(t)\right)\vec{x}(t) = 0\,, \tag{A.1}$$

with some possibly time-dependent matrix $\mathcal{E}_0$. The general solution to this differential equation, given the phase-space coordinate is known at some time t', reads

$$\vec{x}(t) = \vec{x}(t')\exp\left\{-\int_{t'}^t \mathrm{d}\bar{t}\,\mathcal{E}_0(\bar{t})\right\}\,. \tag{A.2}$$

Since we are investigating the evolution of systems given some initial state and not a final one, we are only interested in the situation $t \geq t'$. We can thus directly read off the corresponding retarded Green's function

$$\mathcal{G}(t,t') = \exp\left\{-\int_{t'}^t \mathrm{d}\bar{t}\,\mathcal{E}_0(\bar{t})\right\}\theta(t-t')\,. \tag{A.3}$$

A.2. Hamiltonian test system in static space-time

In the case of the Hamiltonian test system in static space-time introduced in subsection 3.2.3, we can infer from (3.84) and (3.84) that

$$\mathcal{E}_0(t) = \begin{pmatrix} 0_3 & -\frac{1}{m}\mathcal{I}_3 \\ 0_3 & 0_3 \end{pmatrix}\,, \tag{A.4}$$

where 0_d denotes a d-dimensional matrix with all entries being zero. Using $\mathcal{E}_0^2 = 0$, the respective Green's function is found to be

$$\mathcal{G}(t,t') = \sum_{n=0}^{1}\frac{1}{n!}\begin{pmatrix} 0_3 & \frac{t-t'}{m}\mathcal{I}_3 \\ 0_3 & 0_3 \end{pmatrix}^n\theta(t-t') = \begin{pmatrix} \mathcal{I}_3 & \frac{t-t'}{m}\mathcal{I}_3 \\ 0_3 & \mathcal{I}_3 \end{pmatrix}\theta(t-t')\,. \tag{A.5}$$

A.3. Cosmic structure formation

In the case of cosmic structure formation we can infer from (4.2) and (4.3) that

$$\mathcal{E}_0(\eta) = \begin{pmatrix} 0_3 & -\mathcal{I}_3 \\ 0_3 & \frac{1}{2}\,\mathcal{I}_3 \end{pmatrix}. \tag{A.6}$$

The respective Green's function is then found to be

$$\mathcal{G}(\eta, \eta') = \sum_{n=0}^{\infty} \frac{1}{n!} \begin{pmatrix} 0_3 & -(\eta - \eta')\,\mathcal{I}_3 \\ 0_3 & \frac{1}{2}\,(\eta - \eta')\,\mathcal{I}_3 \end{pmatrix}^n \theta(\eta - \eta') \tag{A.7}$$

$$= \mathcal{I}_6\,\theta(\eta - \eta') + \sum_{n=1}^{\infty} \frac{1}{n!} \begin{pmatrix} 0_3 & -2\left(-\frac{1}{2}\,(\eta - \eta')\right)^n \mathcal{I}_3 \\ 0_3 & \left(-\frac{1}{2}\,(\eta - \eta')\right)^n \mathcal{I}_3 \end{pmatrix} \theta(\eta - \eta') \tag{A.8}$$

$$= \begin{pmatrix} \mathcal{I}_3 & 2\left(1 - e^{-\frac{1}{2}(\eta - \eta')}\right) \mathcal{I}_3 \\ 0_3 & e^{-\frac{1}{2}(\eta - \eta')}\,\mathcal{I}_3 \end{pmatrix} \theta(\eta - \eta'). \tag{A.9}$$

A.4. Adiabatic mesoscopic test system in static space-time

In the case of the adiabatic mesoscopic test system in static space-time introduced in section 5.3, we can infer from (5.15), (5.20) and (5.21) that

$$\mathcal{E}_0(t) = \begin{pmatrix} 0_3 & -\frac{1}{m}\,\mathcal{I}_3 & \vec{0} \\ 0_3 & 0_3 & \vec{0} \\ \vec{0}^{\mathsf{T}} & \vec{0}^{\mathsf{T}} & 0 \end{pmatrix}, \tag{A.10}$$

where $\vec{0}$ denotes a 3-dimensional vector with all entries being zero. Like in the Hamiltonian case we can use $\mathcal{E}_0^2 = 0$ to find the respective Green's function,

$$\mathcal{G}(t, t') = \sum_{n=0}^{1} \frac{1}{n!} \begin{pmatrix} 0_3 & \frac{t - t'}{m}\,\mathcal{I}_3 & \vec{0} \\ 0_3 & 0_3 & \vec{0} \\ \vec{0}^{\mathsf{T}} & \vec{0}^{\mathsf{T}} & 0 \end{pmatrix}^n \theta(t - t') = \begin{pmatrix} \mathcal{I}_3 & \frac{t - t'}{m}\,\mathcal{I}_3 & \vec{0} \\ 0_3 & \mathcal{I}_3 & \vec{0} \\ \vec{0}^{\mathsf{T}} & \vec{0}^{\mathsf{T}} & 1 \end{pmatrix} \theta(t - t'). \tag{A.11}$$

B. General expressions for the free collective-field cumulants

B.1. Hamiltonian systems

In [48] general expressions for the free collective-field cumulants in statistically homogeneous and isotropic Hamiltonian systems with Gaussian initial conditions have been derived. For the non-vanishing 1- to 4-point cumulants used in this thesis these expressions read

$$
G_f^{(0)}(1) = (2\pi)^3 \, \delta_{\mathrm{D}}\big(\vec{L}_{q\{1\}}\big) \, \bar{\rho} \, \mathrm{e}^{-\frac{\sigma_p^2}{2} \vec{L}_{p\{1\}}^2} \, ,
\tag{B.1}
$$

$$
G_{fB\cdots B}^{(0)}(1, 1', \ldots, n_B') = (2\pi)^3 \, \delta_{\mathrm{D}}\big(\vec{L}_{q\{1,1',\ldots,n_B'\}}\big) \, \bar{\rho} \prod_{r=1}^{n_B}\Big(\mathrm{i}\vec{k}_r' \cdot \vec{L}_{p\{1,1',\ldots,n_B'\}}(t_r')\Big) \, \mathrm{e}^{-\frac{\sigma_p^2}{2} \vec{L}_{p\{1,1',\ldots,n_B'\}}^2} \, ,
\tag{B.2}
$$

$$
G_{ff}^{(0)}(1, 2) = (2\pi)^3 \, \delta_{\mathrm{D}}\big(\vec{L}_{q\{1,2\}}\big) \, \bar{\rho}^2 \, C_2\big(\vec{L}_{\{1\}}, \vec{L}_{\{2\}}\big) \, \mathrm{e}^{-\frac{\sigma_p^2}{2}\big(\vec{L}_{p\{1\}}^2 + \vec{L}_{p\{2\}}^2\big)} \, ,
\tag{B.3}
$$

$$
\begin{aligned}
G_{ffB}^{(0)}(1, 2, 1') = {} & (2\pi)^3 \, \delta_{\mathrm{D}}\big(\vec{L}_{q\{1,2,1'\}}\big) \, \bar{\rho}^2 \, \mathrm{i}\vec{k}_1' \cdot \vec{L}_{p\{1,1'\}}(t_1') \\
& \times C_2\big(\vec{L}_{\{1,1'\}}, \vec{L}_{\{2\}}\big) \, \mathrm{e}^{-\frac{\sigma_p^2}{2}\big(\vec{L}_{p\{1,1'\}}^2 + \vec{L}_{p\{2\}}^2\big)} \\
& + (1 \leftrightarrow 2) \, ,
\end{aligned}
\tag{B.4}
$$

$$
\begin{aligned}
G_{ffBB}^{(0)}(1, 2, 1', 2') = {} & (2\pi)^3 \, \delta_{\mathrm{D}}\big(\vec{L}_{q\{1,2,1',2'\}}\big) \, \bar{\rho}^2 \\
& \times \Bigg[\Big(\mathrm{i}\vec{k}_1' \cdot \vec{L}_{p\{1,1',2'\}}(t_1')\Big) \Big(\mathrm{i}\vec{k}_2' \cdot \vec{L}_{p\{1,1',2'\}}(t_2')\Big) \\
& \quad \times C_2\big(\vec{L}_{\{1,1',2'\}}, \vec{L}_{\{2\}}\big) \, \mathrm{e}^{-\frac{\sigma_p^2}{2}\big(\vec{L}_{p\{1,1',2'\}}^2 + \vec{L}_{p\{2\}}^2\big)} \\
& \quad + \Big(\mathrm{i}\vec{k}_1' \cdot \vec{L}_{p\{1,1'\}}(t_1')\Big) \Big(\mathrm{i}\vec{k}_2' \cdot \vec{L}_{p\{2,2'\}}(t_2')\Big) \\
& \quad \times C_2\big(\vec{L}_{\{1,1'\}}, \vec{L}_{\{2,2'\}}\big) \, \mathrm{e}^{-\frac{\sigma_p^2}{2}\big(\vec{L}_{p\{1,1'\}}^2 + \vec{L}_{p\{2,2'\}}^2\big)} \Bigg] \\
& + (1 \leftrightarrow 2) \, ,
\end{aligned}
\tag{B.5}
$$

$$
G_{fff}^{(0)}(1, 2, 3) = (2\pi)^3 \, \delta_{\mathrm{D}}\big(\vec{L}_{q\{1,2,3\}}\big) \, \bar{\rho}^3 \, C_3\big(\vec{L}_{\{1\}}, \vec{L}_{\{2\}}, \vec{L}_{\{3\}}\big) \, \mathrm{e}^{-\frac{\sigma_p^2}{2}\big(\vec{L}_{p\{1\}}^2 + \vec{L}_{p\{2\}}^2 + \vec{L}_{p\{3\}}^2\big)} \, ,
\tag{B.6}
$$

$$G^{(0)}_{fffB}(1, 2, 3, 1') = (2\pi)^3\, \delta_{\mathrm{D}}\big(\vec{L}_{q\{1,2,3\}}\big)\, \bar{\rho}^3\, \mathrm{i}\vec{k}'_1 \cdot \vec{L}_{p\{1,1'\}}(t'_1)$$

$$\times C_3\big(\vec{L}_{\{1,1'\}}, \vec{L}_{\{2\}}, \vec{L}_{\{3\}}\big)\, \mathrm{e}^{-\frac{\sigma_p^2}{2}\big(\vec{L}^2_{p\{1\}} + \vec{L}^2_{p\{2\}} + \vec{L}^2_{p\{3\}}\big)} \tag{B.7}$$

$$+ (1 \leftrightarrow 2 \leftrightarrow 3)\,,$$

where we neglected the contributions due to shot noise, as these are negligible for all systems considered in this thesis. Furthermore, several new quantities and notations have been introduced which we will explain and define in the following.

The vector $\vec{L}_I(t) := \big(\vec{L}_{q\,I}(t), \vec{L}_{p\,I}(t)\big)$ encodes the phase shift of the Fourier transformed phase-space density caused by the free particle motion from time t to a later time t_r with $r \in I$. Its components are defined as

$$\vec{L}_{q\,I}(t) := \sum_{r \in I} \vec{k}_r\, g_{qq}(t_r, t) + \vec{l}_r\, g_{pq}(t_r, t)\,, \qquad \vec{L}_{q\,I} := \vec{L}_{q\,I}(t_{\mathrm{i}})\,, \tag{B.8}$$

$$\vec{L}_{p\,I}(t) := \sum_{r \in I} \vec{k}_r\, g_{qp}(t_r, t) + \vec{l}_r\, g_{pp}(t_r, t)\,, \qquad \vec{L}_{p\,I} := \vec{L}_{p\,I}(t_{\mathrm{i}})\,, \tag{B.9}$$

where g_{qq}, g_{qp}, g_{pq} and g_{pp} are the components of the single-particle Green's function (3.21). If $t = t_{\mathrm{i}}$, we omit writing the time-dependence.

The functions C_2 and C_3 describe the contribution to the 2- and 3-point phase-space density cumulant emerging from the correlations between 2 and 3 freely evolving particles, respectively. The most general expression for C_2 is given by

$$C_2\big(\vec{L}_{I_1}, \vec{L}_{I_2}\big) := \int \mathrm{d}^3 q_{12}\, \mathrm{e}^{-\mathrm{i}\vec{L}_{q\,I_1} \cdot \vec{q}_{12}}\Bigg[\bigg(1 + C_{\delta_1\delta_2} - \mathrm{i}\vec{L}_{p\,I_1} \cdot \vec{C}_{p_1\delta_2} - \mathrm{i}\vec{C}_{\delta_1 p_2} \cdot \vec{L}_{p\,I_2}$$

$$+ \big(-\mathrm{i}\vec{L}_{p\,I_1} \cdot \vec{C}_{p_1\delta_2}\big)\big(-\mathrm{i}\vec{C}_{\delta_1 p_2} \cdot \vec{L}_{p\,I_2}\big)\bigg)\, \mathrm{e}^{-\vec{L}^{\top}_{p\,I_1} C_{p_1 p_2} \vec{L}_{p\,I_2}} - 1\Bigg]\,, \tag{B.10}$$

where $C_{\delta_1\delta_2}$, $\vec{C}_{p_1\delta_2}$, $\vec{C}_{\delta_1 p_2}$ and $C_{p_1 p_2}$ denote the different components of the initial covariance matrix (3.47). For C_3 we refrain from presenting its lengthy general expression here, as we do not need it in its complete form in this thesis. Instead, we are only considering different specialisations or approximations of C_3 which will be presented further below.

The quantity σ_p^2 is the initial 1-point momentum variance,

$$\sigma_p^2 := \frac{1}{3} \operatorname{tr} C_{p_j p_j}\,, \tag{B.11}$$

and $(X_1 \leftrightarrow \cdots \leftrightarrow X_n)$ is to be understood as a short-hand notation for summing over all possible permutations of the labels $X_1, \ldots, X_n$.

For a system with initial density correlations but initially vanishing momenta, which we frequently use as a test scenario, $\vec{C}_{p_1\delta_2}$, $\vec{C}_{\delta_1 p_2}$ and $C_{p_1 p_2}$ vanish identically, leaving us with $C_{\delta_1\delta_2}$ which is conveniently expressed in terms of the initial density contrast power spectrum $P_\delta^{(\mathrm{i})}$, as defined in (3.50). In that case, σ_p^2 and C_3 vanish identically,

$$\sigma_p^2\Big|_{p^{(\mathrm{i})}=0} = 0\,, \tag{B.12}$$

$$C_3\big(\vec{L}_{I_1}, \vec{L}_{I_2}, \vec{L}_{I_3}\big)\Big|_{p^{(\mathrm{i})}=0} = 0\,, \tag{B.13}$$

and C_2 simplifies to

$$C_2(\vec{L}_{I_1}, \vec{L}_{I_2})\Big|_{\boldsymbol{p}^{(i)}=0} = P_\delta^{(i)}(|\vec{L}_{q\,I_1}|) \,. \tag{B.14}$$

In the case of cosmic structure formation, on the other hand, $\vec{C}_{p_1\delta_2}$, $\vec{C}_{\delta_1 p_2}$ and $C_{p_1 p_2}$ are non-vanishing and can also be related to $P_\delta^{(i)}$, as shown in (3.51) and (3.52). Then, σ_p^2, C_2 and C_3 become

$$\sigma_p^2\Big|_{\text{cosmo}} = \frac{1}{3}\int \frac{\mathrm{d}^3 k}{(2\pi)^3}\, \frac{P_\delta^{(i)}(k)}{k^2}\,, \tag{B.15}$$

$$\begin{aligned}
C_2(\vec{L}_{I_1}, \vec{L}_{I_2})\Big|_{\text{cosmo}} &= P_\delta^{(i)}(|\vec{L}_{q\,I_1}|)\left(1 + \frac{\vec{L}_{q\,I_1}\cdot\vec{L}_{p\,I_1}}{\vec{L}_{q\,I_1}^2}\right)\left(1 - \frac{\vec{L}_{q\,I_1}\cdot\vec{L}_{p\,I_2}}{\vec{L}_{q\,I_1}^2}\right) \\
&\quad + \int \frac{\mathrm{d}^3 k}{(2\pi)^3}\, P_\delta^{(i)}(k)\, P_\delta^{(i)}(|\vec{L}_{q\,I_1}+\vec{k}|)\left[\frac{(\vec{k}\cdot\vec{L}_{p\,I_1})\,(\vec{k}\cdot\vec{L}_{p\,I_2})}{k^4}\right. \\
&\quad \times \left(1 + \frac{(\vec{L}_{q\,I_1}+\vec{k})\cdot(\vec{L}_{p\,I_1}+\vec{L}_{p\,I_2})}{|\vec{L}_{q\,I_1}+\vec{k}|^2} + \frac{1}{2}\frac{\left((\vec{L}_{q\,I_1}+\vec{k})\cdot\vec{L}_{p\,I_1}\right)\left((\vec{L}_{q\,I_1}+\vec{k})\cdot\vec{L}_{p\,I_2}\right)}{|\vec{L}_{q\,I_1}+\vec{k}|^4}\right) \\
&\quad \left. - \frac{(\vec{k}\cdot\vec{L}_{p\,I_1})\left((\vec{L}_{q\,I_1}+\vec{k})\cdot\vec{L}_{p\,I_2}\right)}{k^2\,|\vec{L}_{q\,I_1}+\vec{k}|^2}\right] + O\left((P_\delta^{(i)})^3\right),
\end{aligned} \tag{B.16}$$

$$\begin{aligned}
C_3(\vec{L}_{I_1}, \vec{L}_{I_2}, \vec{L}_{I_3})\Big|_{\text{cosmo}} &= P_\delta^{(i)}(|\vec{L}_{q\,I_1}|)\, P_\delta^{(i)}(|\vec{L}_{q\,I_2}|)\left(1 + \frac{\vec{L}_{q\,I_1}\cdot\vec{L}_{p\,I_1}}{\vec{L}_{q\,I_1}^2}\right)\left(1 + \frac{\vec{L}_{q\,I_2}\cdot\vec{L}_{p\,I_2}}{\vec{L}_{q\,I_2}^2}\right) \\
&\quad \times \left(-\frac{\vec{L}_{q\,I_1}\cdot\vec{L}_{p\,I_3}}{\vec{L}_{q\,I_1}^2} - \frac{\vec{L}_{q\,I_2}\cdot\vec{L}_{p\,I_3}}{\vec{L}_{q\,I_2}^2} + \frac{(\vec{L}_{q\,I_1}\cdot\vec{L}_{p\,I_3})\,(\vec{L}_{q\,I_2}\cdot\vec{L}_{p\,I_3})}{\vec{L}_{q\,I_1}^2\,\vec{L}_{q\,I_2}^2}\right) \\
&\quad + \left(I_1 \leftrightarrow I_2 \leftrightarrow I_3\right) + O\left((P_\delta^{(i)})^3\right),
\end{aligned} \tag{B.17}$$

Here, we expanded C_2 and C_3 only to second order in $P_\delta^{(i)}$, as we are not explicitly using the expressions for the higher-order terms in this thesis.

B.2. Adiabatic mesoscopic systems

For the description of adiabatic mesoscopic systems, discussed in section 5.3, we have to extend the results of [48] to particles that have an enthalpy as an additional property. In this thesis, we will restrict ourselves to the case where all particles have the same initial enthalpy $\mathcal{H}_\mathrm{i}$. In that case the initial extended phase-space probability distribution factorises into

$$\mathcal{P}_\mathrm{i}(\boldsymbol{q}^{(i)}, \boldsymbol{p}^{(i)}, \mathcal{H}^{(i)}) = \mathcal{P}_\mathrm{i}^{q,p}(\boldsymbol{q}^{(i)}, \boldsymbol{p}^{(i)})\ \delta_\mathrm{D}(\mathcal{H}^{(i)} - \mathcal{H}_\mathrm{i})\,, \tag{B.18}$$

where $\mathcal{P}_\mathrm{i}^{q,p}$ takes the same form as the full initial phase-space probability distribution of a Hamiltonian system.

If we further assume the free evolution of the extended phase-space trajectories to be described by the Green's function (5.88), then the free evolution of the particle enthalpies is given by

$$\mathcal{H}_j^{(0)}(t) = g_{\mathcal{H}\mathcal{H}}(t, t_\mathrm{i})\,\mathcal{H}_\mathrm{i}\,, \tag{B.19}$$

i. e. it is completely decoupled from the free evolution of the particle positions and momenta. Retracing the steps in [48] then shows that the resulting general expressions for the free collective-field cumulants $G^{(0)}_{f\cdots fB_p\cdots B_p}$ just acquire an additional phase factor $\mathrm{e}^{-\mathrm{i}y_r\,\mathcal{H}^{(0)}(t_r)}$ for each collective field $\Phi(r)$ compared to their expressions for a Hamiltonian system. The resulting expressions for the free 1- and 2-point phase-space density cumulants thus read

$$G_f^{(0)}(1) = (2\pi)^3\,\delta_\mathrm{D}\big(\vec{L}_{q\{1\}}\big)\,\bar{\rho}\,\mathrm{e}^{-\frac{\sigma_p^2}{2}\vec{L}_{p\{1\}}^2}\,\mathrm{e}^{-\mathrm{i}L_{\mathcal{H}\{1,1'\}}\mathcal{H}_\mathrm{i}}\,, \tag{B.20}$$

$$G_{fB_p}^{(0)}(1,1') = (2\pi)^3\,\delta_\mathrm{D}\big(\vec{L}_{q\{1,1'\}}\big)\,\bar{\rho}\,\mathrm{i}\vec{k}_1'\cdot\vec{L}_{p\{1,1'\}}(t_1')\,\mathrm{e}^{-\frac{\sigma_p^2}{2}\vec{L}_{p\{1,1'\}}^2}\,\mathrm{e}^{-\mathrm{i}L_{\mathcal{H}\{1,1'\}}\mathcal{H}_\mathrm{i}}\,, \tag{B.21}$$

$$G_{ff}^{(0)}(1,2) = (2\pi)^3\,\delta_\mathrm{D}\big(\vec{L}_{q\{1,1'\}}\big)\,\bar{\rho}^2\,C_2\big(\vec{L}_{\{1\}},\vec{L}_{\{2\}}\big)\,\mathrm{e}^{-\frac{\sigma_p^2}{2}\big(\vec{L}_{p\{1\}}^2+\vec{L}_{p\{2\}}^2\big)}\,\mathrm{e}^{-\mathrm{i}\big(L_{\mathcal{H}\{1\}}+L_{\mathcal{H}\{2\}}\big)\mathcal{H}_\mathrm{i}}\,, \tag{B.22}$$

where we defined the enthalpy phase-shift factor

$$L_{\mathcal{H}I}(t) := \sum_{r\in I} y_r\,g_{\mathcal{H}\mathcal{H}}(t_r, t)\,, \qquad L_{\mathcal{H},r} := L_{\mathcal{H},r}(t_\mathrm{i})\,, \tag{B.23}$$

in analogy to (B.8) and (B.9). The expressions for cumulants involving the enthalpy response field $\vec{\Phi}_{B_{\mathcal{H}}}$ can then be obtained from the cumulants involving the momentum response field Φ_{B_p} by replacing the momentum phase shift vectors $\vec{L}_{pI}(t)$ with the enthalpy phase shift factors $L_{\mathcal{H}I}(t)$, i. e.

$$G_{f\vec{B}_{\mathcal{H}}}^{(0)}(1,2) = (2\pi)^3\,\delta_\mathrm{D}\big(\vec{L}_{q\{1\}}\big)\,\bar{\rho}\,\mathrm{i}\vec{k}_1'\,L_{\mathcal{H}\{1\}}(t_1')\,\mathrm{e}^{-\frac{\sigma_p^2}{2}\vec{L}_{p\{1,1'\}}^2}\,\mathrm{e}^{-\mathrm{i}L_{\mathcal{H}\{1,1'\}}\mathcal{H}_\mathrm{i}}\,. \tag{B.24}$$

C. Computation of the macroscopic propagator

C.1. General procedure

The causal macroscopic propagators Δ_R and Δ_A are given by the functional inverse (3.79) which is defined as the solution of the integral equation

$$\int \mathrm{d}\bar{1} \left(\mathcal{I}(1, \bar{1}) - \mathrm{i} G^{(0)}_{f\mathcal{F}}(1, \bar{1}) \right) \Delta_\mathrm{R}(-\bar{1}, 2) = \mathcal{I}(1, 2), \tag{C.1}$$

with the identity 2-point function $\mathcal{I}$ introduced in (3.76). The physical systems we are most interested in are statistically homogeneous and have a free Hamiltonian that only depends on the particle momenta but not their positions. The latter implies $g_{qq}(t, t') = \theta(t - t')$ and $g_{pq}(t, t') = 0$, as shown in [1]. In this case we can conclude from (3.46) and (B.2) that $G^{(0)}_{f\mathcal{F}}$ can be written as

$$G^{(0)}_{f\mathcal{F}}(1, 2) = (2\pi)^3\, \delta_\mathrm{D}\big(\vec{k}_1 + \vec{k}_2\big)\, (2\pi)^3\, \delta_\mathrm{D}\big(\vec{l}_2\big)\, \tilde{G}^{(0)}_{f\mathcal{F}}\big(\vec{k}_1, \vec{l}_1; t_1, t_2\big) \propto \theta(t_1 - t_2), \tag{C.2}$$

where we introduced the reduced cumulant $\tilde{G}^{(0)}_{f\mathcal{F}}$ which exploits the constraints set by the delta functions,

$$\tilde{G}^{(0)}_{f\mathcal{F}}\big(\vec{k}_1, \vec{l}_1; t_1, t_2\big) := \int \frac{\mathrm{d}^6 s_2}{(2\pi)^6}\, G^{(0)}_{f\mathcal{F}}(1, 2)\,. \tag{C.3}$$

Inserting (C.2) into the Neumann series (3.81) then suggests the following ansatz for Δ_R,

$$\Delta_\mathrm{R}(1, 2) = \mathcal{I}(1, 2) + (2\pi)^3\, \delta_\mathrm{D}\big(\vec{k}_1 + \vec{k}_2\big)\, (2\pi)^3\, \delta_\mathrm{D}\big(\vec{l}_2\big)\, \tilde{\Delta}_\mathrm{R}\big(\vec{k}_1, \vec{l}_1; t_1, t_2\big)\,, \tag{C.4}$$

where $\tilde{\Delta}_\mathrm{R}\big(\vec{k}_1, \vec{l}_1; t_1 t_2\big) \propto \theta(t_1 - t_2)$. This reduces (C.1) to the following integral equation for $\tilde{\Delta}_\mathrm{R}$,

$$\tilde{\Delta}_\mathrm{R}\big(\vec{k}_1, \vec{l}_1; t_1, t_2\big) = \mathrm{i}\tilde{G}^{(0)}_{f\mathcal{F}}\big(\vec{k}_1, \vec{l}_1; t_1, t_2\big) + \int_{t_2}^{t_1} \mathrm{d}t_{\bar{1}}\ \mathrm{i}\tilde{G}^{(0)}_{f\mathcal{F}}\big(\vec{k}_1, \vec{l}_1; t_1, t_{\bar{1}}\big)\, \tilde{\Delta}_\mathrm{R}\big(\vec{k}_1, 0; t_{\bar{1}}, t_2\big)\,, \tag{C.5}$$

which can be solved in two steps. First, we solve it in the case $\vec{l}_1 = 0$,

$$\tilde{\Delta}_\mathrm{R}\big(\vec{k}_1, 0; t_1, t_2\big) = \mathrm{i}\tilde{G}^{(0)}_{f\mathcal{F}}\big(\vec{k}_1, 0; t_1, t_2\big) + \int_{t_2}^{t_1} \mathrm{d}t_{\bar{1}}\ \mathrm{i}\tilde{G}^{(0)}_{f\mathcal{F}}\big(\vec{k}_1, 0; t_1, t_{\bar{1}}\big)\, \tilde{\Delta}_\mathrm{R}\big(\vec{k}_1, 0; t_{\bar{1}}, t_2\big)\,, \tag{C.6}$$

which can be done independently for all possible values of $\vec{k}_1$. Afterwards we insert the result $\tilde{\Delta}_R(\vec{k}_1, 0; t_1, t_2)$ of this into the right-hand side of (C.5) and perform the time integral to obtain the full $\vec{l}_1$-dependent solution $\tilde{\Delta}_R(\vec{k}_1, \vec{l}_1; t_1, t_2)$.

If $\tilde{G}_{f\mathcal{F}}^{(0)}(\vec{k}_1, 0; t_1, t_2)$ depends on t_1 and t_2 only in terms of their difference $t_{12} := t_1 - t_2$, then according to (3.81) the same should hold for $\tilde{\Delta}_R(\vec{k}_1, 0; t_1, t_2)$, and the time integral in (C.6) becomes a convolution,

$$\tilde{\Delta}_R(\vec{k}_1, 0; t_{12}, 0) = \mathrm{i}\tilde{G}_{f\mathcal{F}}^{(0)}(\vec{k}_1, 0; t_{12}, 0) + \int_0^{t_{12}} \mathrm{d}t_{\bar{1}2} \; \mathrm{i}\tilde{G}_{f\mathcal{F}}^{(0)}(\vec{k}_1, 0; t_{12} - t_{\bar{1}2}, 0) \, \tilde{\Delta}_R(\vec{k}_1, 0; t_{\bar{1}2}, 0) , \quad \text{(C.7)}$$

with $t_{\bar{1}2} := t_{\bar{1}} - t_2$. In this case we can turn the integral equation into an algebraic equation by means of a Laplace transform with respect to t_{12},

$$\begin{aligned}
\mathcal{L}_{t_{12}}\left[\tilde{\Delta}_R(\vec{k}_1, 0; t_{12}, 0)\right](z) &= \mathcal{L}_{t_{12}}\left[\mathrm{i}\tilde{G}_{f\mathcal{F}}^{(0)}(\vec{k}_1, 0; t_{12}, 0)\right](z) \\
&\quad + \mathcal{L}_{t_{12}}\left[\mathrm{i}\tilde{G}_{f\mathcal{F}}^{(0)}(\vec{k}_1, 0; t_{12}, 0)\right](z) \, \mathcal{L}_{t_{12}}\left[\tilde{\Delta}_R(\vec{k}_1, 0; t_{12}, 0)\right](z),
\end{aligned} \quad \text{(C.8)}$$

where z denotes the complex frequency conjugate to t_{12}. Bringing $\tilde{\Delta}_R$ to one side of the equation and performing an inverse Laplace transform then yields the solution of (C.6),

$$\tilde{\Delta}_R(\vec{k}_1, 0; t_{12}, 0) = \mathcal{L}_z^{-1}\left[\left(1 - \mathcal{L}_{t_{12}}\left[\mathrm{i}\tilde{G}_{f\mathcal{F}}^{(0)}(\vec{k}_1, 0; t_{12}, 0)\right]\right)^{-1} \mathcal{L}_{t_{12}}\left[\mathrm{i}\tilde{G}_{f\mathcal{F}}^{(0)}(\vec{k}_1, 0; t_{12}, 0)\right]\right](t_{12}). \quad \text{(C.9)}$$

Generally, however, the time-dependence of $\tilde{G}_{f\mathcal{F}}^{(0)}$ will not be that simple and we have to determine $\tilde{\Delta}_R$ numerically. This can be done by discretizing the time arguments in (C.6) and solving the resulting matrix equation for each $\vec{k}_1$-value of interest. Note that due to the retarded causal structure of $\tilde{G}_{f\mathcal{F}}^{(0)}$ and $\tilde{\Delta}_R$ they become lower triangular matrices after discretisation. Hence, this matrix equation can be solved with minimal computational effort via forward substitution.

Once the causal propagators are known we can insert them into the relation (3.78) for the complete macroscopic propagator, which immediately fixes the off-diagonal components. The computation of the remaining statistical propagator then reduces to performing the following

time integrals,

$$\Delta_{ff}(1,2) = \int d\bar{1} \int d\bar{2} \, \Delta_{\mathrm{R}}(1,\bar{1}) \, G^{(0)}_{ff}(-\bar{1},\bar{2}) \, \Delta_{\mathrm{A}}(-\bar{2},2) \tag{C.10}$$

$$= (2\pi)^3 \, \delta_{\mathrm{D}}(\vec{k}_1 + \vec{k}_2) \Bigg[\quad \tilde{G}^{(0)}_{ff}(\vec{k}_1, \vec{l}_1, \vec{l}_2; t_1, t_2)$$

$$+ \int_{t_{\mathrm{i}}}^{t_1} dt_{\bar{1}} \, \tilde{\Delta}_{\mathrm{R}}(\vec{k}_1, \vec{l}_1; t_1, t_{\bar{1}}) \, \tilde{G}^{(0)}_{ff}(\vec{k}_1, 0, \vec{l}_2; t_{\bar{1}}, t_2)$$

$$+ \int_{t_{\mathrm{i}}}^{t_2} dt_{\bar{2}} \, \tilde{G}^{(0)}_{ff}(\vec{k}_1, \vec{l}_1, 0; t_1, t_{\bar{2}}) \, \tilde{\Delta}_{\mathrm{A}}(\vec{k}_1, \vec{l}_2; t_{\bar{2}}, t_2) \tag{C.11}$$

$$+ \int_{t_{\mathrm{i}}}^{t_1} dt_{\bar{1}} \int_{t_{\mathrm{i}}}^{t_2} dt_{\bar{2}} \, \tilde{\Delta}_{\mathrm{R}}(\vec{k}_1, \vec{l}_1; t_1, t_{\bar{1}}) \, \tilde{G}^{(0)}_{ff}(\vec{k}_1, 0, 0; t_{\bar{1}}, t_{\bar{2}}) \, \tilde{\Delta}_{\mathrm{A}}(\vec{k}_1, \vec{l}_2; t_{\bar{2}}, t_2) \Bigg]$$

where we defined $\tilde{\Delta}_{\mathrm{A}}$ analogously to (C.4) and $\tilde{G}^{(0)}_{ff}$ as

$$\tilde{G}^{(0)}_{ff}(\vec{k}_1, \vec{l}_1, \vec{l}_2; t_1, t_2) := \frac{G^{(0)}_{ff}(1,2)}{(2\pi)^3 \, \delta_{\mathrm{D}}(\vec{k}_1 + \vec{k}_2)} \Bigg|_{\vec{k}_2 = -\vec{k}_1} . \tag{C.12}$$

Depending on whether there exist analytic expressions for $\tilde{\Delta}_{\mathrm{R}}$, $\tilde{\Delta}_{\mathrm{A}}$ and $\tilde{G}^{(0)}_{ff}$, these integrals can either be performed analytically or have to be evaluated numerically.

C.2. Test system in static space-time

In the case of static space-time test system introduced in subsection 3.2.3, we infer from (3.90) that

$$\mathrm{i}\tilde{G}^{(0)}_{f\mathcal{F}}(\vec{k}_1, \vec{l}_1; t_1, t_2) = -k_1^2 \, \bar{\rho} \, v(k_1) \left(\frac{t_{12}}{m} + \frac{\vec{k}_1 \cdot \vec{l}_1}{k_1^2} \right) \theta(t_{12}) . \tag{C.13}$$

Evaluating this at $\vec{l}_1 = 0$ and Laplace transforming it yields

$$\mathcal{L}_{t_{12}} \left[\mathrm{i}\tilde{G}^{(0)}_{f\mathcal{F}}(\vec{k}_1, 0; t_{12}, 0) \right](z) = -k_1^2 \, \frac{\bar{\rho} \, v(k_1)}{m} \, \frac{1}{z^2} , \tag{C.14}$$

which we can insert into (C.9) to find

$$\tilde{\Delta}_{\mathrm{R}}(\vec{k}_1, 0; t_{12}, 0) = \mathcal{L}_z^{-1} \left[-\frac{k_1^2 \, \frac{\bar{\rho} \, v(k_1)}{m}}{z^2 + k_1^2 \, \frac{\bar{\rho} \, v(k_1)}{m}} \right](t_{12}) = -k_1 \sqrt{\frac{\bar{\rho} \, v(k_1)}{m}} \, \sin\left(k_1 t_{12} \sqrt{\frac{\bar{\rho} \, v(k_1)}{m}} \right) . \tag{C.15}$$

Inserting this result as well as (C.13) into the right-hand side of (C.5) and performing the time integral leads to the expression (3.92) for the causal propagators. Using that expression together with the expression (3.91) for $G^{(0)}_{ff}$ in (C.11), we find the expression (3.95) for the statistical propagator after performing the remaining time integrals.

C.3. Cosmic structure formation in the large-scale limit

In the case of cosmic structure formation in the large-scale limit, as discussed in subsection 4.2.1, we find

$$i\tilde{G}_{f\mathcal{F}}^{(0,\mathrm{ls})}(\vec{k}_1,\vec{l}_1;\eta_1,\eta_2) = \frac{3}{2}\left[2 - \left(2 - \frac{\vec{k}_1\cdot\vec{l}_1}{k_1^2}\right)e^{-\frac{1}{2}\eta_{12}}\right]\theta(\eta_{12})\,e^{-\frac{\sigma_p^2}{2}\bar{T}_1^2 l_1^2}. \tag{C.16}$$

Evaluating this at $\vec{l}_1 = 0$ and Laplace transforming it yields

$$\mathcal{L}_{\eta_{12}}\left[i\tilde{G}_{f\mathcal{F}}^{(0,\mathrm{ls})}(\vec{k}_1,0;\eta_{12},0)\right](z) = \frac{3}{z} - \frac{3}{z + \frac{1}{2}}, \tag{C.17}$$

which we can insert into (C.9) to find

$$\tilde{\Delta}_{\mathrm{R}}^{(\mathrm{ls})}(\vec{k}_1,0;\eta_{12},0) = \mathcal{L}_z^{-1}\left[\frac{\frac{3}{2}}{z^2 + z - 3}\right](\eta_{12}) = \frac{3}{5}\left(e^{\eta_{12}} - e^{-\frac{3}{2}\eta_{12}}\right). \tag{C.18}$$

Inserting this result as well as (C.16) into the right-hand side of (C.5) and performing the time integral leads to the expression (4.19) for the causal propagators. Using that expression together with the large-scale limit (4.21) of $G_{ff}^{(0)}$ in (C.11), we find the expression (4.22) for the statistical propagator after performing the remaining time integrals.

D. Proofs of the Feynman rules

D.1. Causality rule

Consider a diagram which has only incoming arrows on its outer legs or contains a subdiagram which does so. From the continuity of the time-flow and the fact that there exist no propagators or vertices with incoming arrows only, $\Delta_{\beta\beta} = 0$ and $\mathcal{V}_{f\cdots f} = 0$, it then follows that there has to be at least one vertex in this diagram from which every possible path along the time-flow ends up in a closed loop, as illustrated in Figure D.1.

In general, there might be multiple possible loops, as the involved vertices might have multiple outgoing legs. In this case we consider the loop that is obtained by choosing for each vertex the path through the outgoing leg evaluated at the latest time argument. Then, the causal structures of the propagators (3.83) and vertices (3.97) imply that the diagram can only be non-vanishing if the time arguments along the loop satisfy $t_1^{\text{in}} \leq t_1^{\text{out}} \leq t_2^{\text{in}} \leq t_2^{\text{out}} \leq \cdots \leq t_1^{\text{in}}$.

A closer inspection allows to tighten this restriction even further, though. For this, we first insert the proportionality relation (3.53) of the free collective-field cumulants into the expressions (3.75) and (3.80) for the vertices and the retarded/advanced propagator, to infer

$$\mathcal{V}_{\beta\cdots\beta f\cdots f}(1,\ldots,n_\beta,1',\ldots,n_f') \propto \delta_{\text{D}}(\vec{l}_{r'}) \quad \forall\, r' \in \{1',\ldots,n_f'\}, \tag{D.1}$$

$$\Delta_{f\beta}(1,2) = \Delta_{\beta f}(2,1) = -\mathrm{i}\Delta_{\text{R}}(1,2) = -\mathrm{i}\,\underbrace{\mathcal{I}(1,2)}_{\propto\delta_{\text{D}}(\vec{l}_1+\vec{l}_2)} -\mathrm{i}\underbrace{\sum_{n=1}^{\infty}\left(\mathrm{i}G_{f\mathcal{F}}^{(0)}\right)^n(1,2)}_{\propto\delta_{\text{D}}(\vec{l}_2)}. \tag{D.2}$$

Combining both of these relations then yields

$$= \int \mathrm{d}\bar{1}\; \Delta_{\beta f}(1',\bar{1})\,\mathcal{V}_{ff\cdots f\beta\cdots\beta}(-\bar{1},2',\ldots,n_f',1,\ldots,n_\beta) \propto \delta_{\text{D}}(\vec{l}_{1'})\,. \tag{D.3}$$
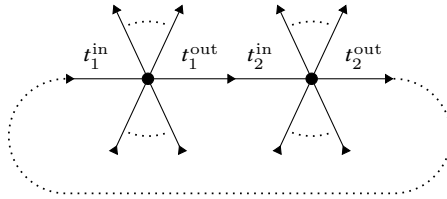

Figure D.1.: Diagram with a closed loop in its time flow.

Using this result in Figure D.1 tells us that the $\vec{l}$-argument at every outgoing β-leg of a vertex through which the loop passes is set to zero, which means that we actually have to apply the stricter case of the vertices' causal restriction (3.97). As a consequence, the considered type of diagram could in fact only be non-vanishing if the time arguments along the loop satisfied $t_1^{\mathrm{in}} \leq t_1^{\mathrm{out}} \leq t_2^{\mathrm{in}} \leq t_2^{\mathrm{out}} \leq \cdots \leq t_1^{\mathrm{in}}$. This, however, is always a contradiction and thus the diagram vanishes identically, concluding the proof of the Causality rule.

D.2. Homogeneity rule

Let the system under consideration be statistically homogeneous, and consider a diagram that contains a so-called tadpole subdiagram, i.e. a subdiagram which is connected to the rest of the diagram solely via a single propagator. We first use that due to the conservation of spatial Fourier modes, (3.102) and (3.103), such a tadpole subdiagram satisfies

$$1 \longleftarrow\!\!\!\!\!\oslash \propto \delta_{\mathrm{D}}(\vec{k}_1)\,, \tag{D.4}$$

where the hatched circle represents a subdiagram with no further outer legs than the one attached to the propagator on the left. Note that we do not have to consider tadpole diagrams using the other two possible propagators since they would vanish identically according to the Causality rule.

Then, we insert the proportionality relation (3.53) of the free collective-field cumulants into the definition (3.75) of the vertices, to obtain

$$\mathcal{V}_{\beta\cdots\beta f\cdots f}(1,\ldots,n_\beta,1',\ldots,n_f') \propto \vec{k}_{r'}\, v(k_{r'},t_{r'}) \quad \forall\, r' \in \{1',\ldots,n_f'\}\,. \tag{D.5}$$

If we now attach the tadpole diagram to the f-leg of some vertex, (D.4) and (D.5) together imply that the resulting diagram vanishes identically if $\vec{k}\, v(k,t) = 0$ at $\vec{k} = 0$. Fourier transforming this condition to real space,

$$0 \overset{!}{=} \vec{k}\, v(k,t)\Big|_{\vec{k}=0} = -\mathrm{i} \int \mathrm{d}^3q\, \vec{\nabla}_q v(q,t)\,, \tag{D.6}$$

reveals that it is always satisfied, as the integrand on the right hand side switches sign under a sign flip of $\vec{q}$. Physically, this corresponds to the fact that the volume integral of a particle's central force field over the whole space vanishes. This concludes the proof of the Homogeneity rule.

Note that for the gravitational potential (4.10) the condition (D.6) apparently does not hold in Fourier space, even though it is always satisfied in real space. The reason for this is that the Fourier transform of an $1/q$ potential is actually only properly defined as the limit of a large-scale regularisation,

$$v(k) \propto \lim_{k_\mathrm{c}\to 0} \int \mathrm{d}^3q\, \frac{\mathrm{e}^{-k_\mathrm{c}q}}{q}\, \mathrm{e}^{-\mathrm{i}\vec{k}\cdot\vec{q}} \propto \lim_{k_\mathrm{c}\to 0} \frac{1}{k^2 + k_\mathrm{c}^2}\,. \tag{D.7}$$

Using this proper definition, the condition (D.6) is indeed satisfied for the Fourier transformed gravitational potential. This is related to the so-called "Jeans swindle" [25]. In practice, however, one rarely encounters situations where using (D.7) makes a difference. In particular, this is true for all calculations in chapter 2, which is why we directly set k_c to zero in (4.10). Nevertheless, one should always keep (D.7) in mind.

E. Equations of motion of a particle in expanding space-time

The Lagrangian of a single classical point particle of mass m in an expanding space-time, expressed in comoving coordinates $\vec{q} = \vec{r}/a$ and cosmic time t, is given by

$$L(\vec{q}, \dot{\vec{q}}, t) = \frac{m}{2} a^2 \dot{\vec{q}}^2 - m V_G(\vec{q}, t),$$ (E.1)

with the cosmological gravitational potential V_G satisfying the Poisson equation

$$\nabla_q^2 V_G = \frac{4\pi G}{a} \left(\rho_{\mathrm{m}} - \bar{\rho}_{\mathrm{m}}\right),$$ (E.2)

as derived in [15, 51]. Here, ρ_{m} denotes the comoving mass density of the space-time's total matter content, and $\bar{\rho}_{\mathrm{m}}$ is its mean value, which is constant in space and time.

Following the steps detailed in [51], we transform the Lagrangian to the new time coordinate $\eta(t) := \ln\left(D_+(t)/D_+(t_{\mathrm{i}})\right)$ by demanding the action to be invariant under this transformation,

$$S = \int_{t_1}^{t_2} \mathrm{d}t\, L(\vec{q}, \dot{\vec{q}}, t) = \int_{\eta_1}^{\eta_2} \mathrm{d}\eta\, \frac{\mathrm{d}t}{\mathrm{d}\eta}\, L\left(\vec{q}, \frac{\mathrm{d}\vec{q}}{\mathrm{d}\eta}\frac{\mathrm{d}\eta}{\mathrm{d}t}, \eta(t)\right) \overset{!}{=} \int_{\eta_1}^{\eta_2} \mathrm{d}\eta\, L_\eta\left(\vec{q}, \frac{\mathrm{d}\vec{q}}{\mathrm{d}\eta}, \eta\right).$$ (E.3)

Using $\mathrm{d}\eta/\mathrm{d}t = H f_+$, where $H := \dot{a}/a$ is the Hubble function and $f_+ := \mathrm{d}\ln D_+/\mathrm{d}\ln a$ the growth function, we can read off the transformed Lagrangian,

$$L_\eta\left(\vec{q}, \frac{\mathrm{d}\vec{q}}{\mathrm{d}\eta}, \eta\right) = \frac{ma^2 H f_+}{2} \left(\frac{\mathrm{d}\vec{q}}{\mathrm{d}\eta}\right)^2 - \frac{m}{H f_+} V_G(\vec{q}, t(\eta)).$$ (E.4)

By means of a Legendre transformation we then obtain the respective Hamiltonian and deduce the resulting Hamiltonian equations of motion,

$$\frac{\mathrm{d}\vec{q}}{\mathrm{d}\eta} = \frac{\vec{p}_{\mathrm{can}}}{ma^2 H f_+},$$ (E.5)

$$\frac{\mathrm{d}\vec{p}_{\mathrm{can}}}{\mathrm{d}\eta} = -\frac{m}{H f_+} \vec{\nabla}_q V_G,$$ (E.6)

with the canonically conjugate momentum $\vec{p}_{\mathrm{can}}$.

For our purposes, though, it is more convenient to work with the rescaled momentum variable

$$\vec{p} := \frac{\vec{p}_{\mathrm{can}}}{ma^2 H f_+}$$ (E.7)

instead, since this choice will lead to equations of motion that take a very simple form during the matter- and Λ-dominated epochs of a ΛCDM cosmology. To obtain these, we express $\vec{p}_{\text{can}}$ in (E.5) and (E.6) in terms of $\vec{p}$, yielding

$$\frac{\mathrm{d}\vec{q}}{\mathrm{d}\eta} = \vec{p}\,, \tag{E.8}$$

$$\frac{\mathrm{d}\vec{p}}{\mathrm{d}\eta} = -\frac{\vec{p}}{a^2 H f_+} \frac{\mathrm{d}}{\mathrm{d}\eta}(a^2 H f_+) - \vec{\nabla}_q \tilde{V}_G\,, \tag{E.9}$$

where we defined the effective gravitational potential

$$\tilde{V}_G := \frac{V_G}{a^2 H^2 f_+^2}\,, \tag{E.10}$$

satisfying the modified Poisson equation (4.4). Using $H f_+ = \dot{D}_+/D_+$ as well as the fact that D_+ solves the linearised density contrast evolution equation (2.27). we finally find the equations of motion (4.2) and (4.3).

Note that our assumption of the functional Jacobian determinant in (3.4) being constant still holds for the equations of motion (4.2) and (4.3), even though $(\vec{q}, \vec{p}_{\text{can}}) \to (\vec{q}, \vec{p})$ is no canonical transformation. This can be checked explicitly by inserting those equations of motion into (3.14). In fact, it can be shown in general that any invertible time-dependent linear transformation of $(\vec{q}, \vec{p}_{\text{can}})$ preserves this property.

F. Next-to-lowest-order self-energies and propagators of dark matter

For the 4th diagram in (4.32), which we choose as our exemplary 1-loop diagram, the kernel functions $K_{\beta\beta,2}^{(1,\mathrm{P})}$ and $K_{\beta\beta,2}^{(1,\mathrm{C})}$ introduced in (4.56) and (4.57), respectively, read

$$
\begin{aligned}
K_{\beta\beta,2}^{(1,\mathrm{P})}(\vec{k}_1,\vec{k}',\eta_1,\eta_2)\Big|_{\text{diagram }4} &= \left(3 - 2e^{-\frac{\eta_2}{2}}\right) \frac{\left(\vec{k}_1\cdot(\vec{k}_1+\vec{k}')\right)\left(\vec{k}'\cdot(\vec{k}_1+\vec{k}')\right)}{k'^2\left|\vec{k}_1+\vec{k}'\right|^2} \\
&\times \Bigg[-\frac{1}{25}e^{-2\eta_1}\left(-50e^{2\eta_1}(3\eta_1+16) - 181e^{\frac{\eta_1}{2}} - 450e^{\frac{3\eta_1}{2}}\right.\\
&\quad \left. + 450e^{\eta_1} - 27e^{\frac{5\eta_1}{2}}(10\eta_1-49) + 9e^{3\eta_1}(15\eta_1-41) + 27\right) \\
&\quad -(\vec{k}_1\cdot\vec{k}')\frac{6}{5}\left(10\eta_1 - \frac{19}{3}e^{-\frac{3\eta_1}{2}} - 10e^{-\frac{\eta_1}{2}} - 21e^{\frac{\eta_1}{2}} + e^{-2\eta_1} + 15e^{-\eta_1} + 3e^{\eta_1} + \frac{55}{3}\right) \\
&\quad + \frac{\vec{k}_1\cdot\vec{k}'}{k'^2}\left(6\eta_1 - 8e^{-\frac{3\eta_1}{2}} - 36e^{-\frac{\eta_1}{2}} + \frac{27e^{-2\eta_1}}{25} + 24e^{-\eta_1} + \frac{12}{25}e^{\frac{\eta_1}{2}}(15\eta_1-71) + 53\right) \\
&\quad + \frac{(\vec{k}_1\cdot\vec{k}')^2}{k'^2}\left(-12\eta_1 - 8e^{-\frac{3\eta_1}{2}} - 48e^{-\frac{\eta_1}{2}} + \frac{24e^{\frac{\eta_1}{2}}}{5} + \frac{6e^{-2\eta_1}}{5} + 24e^{-\eta_1} + 26\right)\Bigg] \\
&\quad + (\eta_1 \leftrightarrow \eta_2),
\end{aligned}
\tag{F.1}
$$

$$
\begin{aligned}
K_{\beta\beta,2}^{(1,\mathrm{C})}(\vec{k}_1,\vec{k}',\eta_1,\eta_2)\Big|_{\text{diagram }4} &= \left(e^{\frac{\eta_1}{2}}-1\right)^2\left(e^{\frac{\eta_2}{2}}-1\right)^2 \frac{(\vec{k}_1\cdot\vec{k}')\left(\vec{k}_1\cdot(\vec{k}_1+\vec{k}')\right)}{k'^2\left|\vec{k}_1+\vec{k}'\right|^2} \\
&\times \left[3 + 4\frac{\vec{k}_1\cdot\vec{k}'}{k'^2}e^{-\eta_1}\left(e^{\frac{\eta_1}{2}}-1\right)\right]\left[3 - 4\frac{\vec{k}_1\cdot(\vec{k}_1+\vec{k}')}{\left|\vec{k}_1+\vec{k}'\right|^2}e^{-\eta_2}\left(e^{\frac{\eta_2}{2}}-1\right)\right].
\end{aligned}
\tag{F.2}
$$

Here, $(\eta_1 \leftrightarrow \eta_2)$ is to be understood as a short-hand notation for summing over both permutations of the time variables η_1 and η_2.

To obtain compact expressions for the complete next-to-lowest-order self-energies $\Sigma_{\beta\beta,2}$ and $\Sigma_{\beta f,1}$ as well as propagators $G_{ff,2}$ and $G_{\mathrm{R},1}$ introduced in subsection 4.3.2, it is convenient to introduce the dimensionless integration variables $r := k'/k_1$ and $\mu := (\vec{k}_1\cdot\vec{k}')/(k_1 k')$. We then

find

$$
\Sigma_{\beta f,1}(1,2)\Big|_{\vec{l}_1=\vec{l}_2=0} = (2\pi)^3\,\delta_{\mathrm{D}}\big(\vec{k}_1+\vec{k}_2\big)\,\frac{k_1^3\,\mathrm{e}^{2\eta_2}}{(2\pi)^2}\int\limits_0^\infty \mathrm{d}r\,\frac{P_\delta^{(\mathrm{i})}(k_1 r)}{r^3}
$$

$$
\times\left[\frac{\mathrm{e}^{\frac{3}{2}\eta_{12}}-1}{32}\left(4r\left(6r^6+5r^4-7r^2+6\right)-6\left(2r^8+r^6-6r^4+r^2+2\right)\frac{\ln(r+1)}{\ln(|r-1|)}\right)\right.
$$

$$
+\frac{\mathrm{e}^{2\eta_{12}}-\mathrm{e}^{-\frac{1}{2}\eta_{12}}}{4000}\left(-12r\left(150r^6-5r^4(30\eta_{12}-49)+r^2(230\eta_{12}-359)-60\eta_{12}+198\right)\right.
$$

$$
\left.\left.+\,18\left(r^2-1\right)^2\left(50r^4+r^2(-50\eta_{12}+165)-20\eta_{12}+66\right)\frac{\ln(r+1)}{\ln(|r-1|)}\right)\right], \tag{F.3}
$$

$$
\Sigma_{\beta\beta,2}^{(\mathrm{P})}(1,2)\Big|_{\vec{l}_1=\vec{l}_2=0} = (2\pi)^3\,\delta_{\mathrm{D}}\big(\vec{k}_1+\vec{k}_2\big)\,\frac{k_1^3\,\mathrm{e}^{-\frac{1}{2}(\eta_1+\eta_2)}}{(2\pi)^2}\int\limits_0^\infty \mathrm{d}r\,\frac{P_\delta^{(\mathrm{i})}(k_1)\,P_\delta^{(\mathrm{i})}(k_1 r)}{r^3}
$$

$$
\times\left[\frac{1}{1500}\left(2r\left(450r^6+75r^4(3\eta_1+3\eta_2+5)\right.\right.\right.
$$

$$
\left.+r^2(195\eta_1+195\eta_2+1267)-18(5\eta_1+5\eta_2+23)\right)
$$

$$
\left.-\,9\left(r^2-1\right)^2\left(50r^4+25r^2(\eta_1+\eta_2+5)-2(5\eta_1+5\eta_2+23)\right)\frac{\ln(r+1)}{\ln(|r-1|)}\right)
$$

$$
+\frac{\mathrm{e}^{\frac{1}{2}\eta_1}}{1500}\left(-2r\left(1425r^6+25r^4(27\eta_1+25)+39r^2(15\eta_1+92)-6(45\eta_1+166)\right)\right.
$$

$$
\left.+\,3\left(r^2-1\right)^2\left(475r^4+25r^2(9\eta_1+40)-90\eta_1-332\right)\frac{\ln(r+1)}{\ln(|r-1|)}\right)
$$

$$
+\frac{\mathrm{e}^{\frac{1}{2}(\eta_1+\eta_2)}}{16}\left(2r\left(12r^6+r^4+27r^2-6\right)-3\left(r^2-1\right)^2\left(4r^4+7r^2-2\right)\frac{\ln(r+1)}{\ln(|r-1|)}\right)
$$

$$
+\frac{\mathrm{e}^{2\eta_1}}{12}\left(1-\frac{3}{2}\mathrm{e}^{\frac{1}{2}\eta_2}\right)\left(2r\left(6r^6+5r^4-7r^2+6\right)-3\left(2r^8+r^6-6r^4+r^2+2\right)\frac{\ln(r+1)}{\ln(|r-1|)}\right)
$$

$$
-\frac{\mathrm{e}^{\frac{5}{2}\eta_1}}{3000}\left(1-\frac{3}{2}\mathrm{e}^{\frac{1}{2}\eta_2}\right)\left(-2r\left(900r^6-75r^4(18\eta_1-25)+r^2(2070\eta_1-2591)-540\eta_1+1422\right)\right.
$$

$$
\left.\left.+\,9\left(r^2-1\right)^2\left(100r^4-75r^2(2\eta_1-5)-60\eta_1+158\right)\frac{\ln(r+1)}{\ln(|r-1|)}\right)\right]
$$

$$
+\,(\eta_1\leftrightarrow\eta_2)\,, \tag{F.4}
$$

$$\Sigma_{\beta\beta,2}^{(\mathrm{C})}(1,2)\Big|_{\vec{l}_1=\vec{l}_2=0} = (2\pi)^3\,\delta_\mathrm{D}(\vec{k}_1+\vec{k}_2)\,\frac{k_1^3\,\mathrm{e}^{-\frac{1}{2}(\eta_1+\eta_2)}}{(2\pi)^2}\int_0^\infty\!\mathrm{d}r\int_{-1}^1\!\mathrm{d}\mu\,\frac{P_\delta^{(\mathrm{i})}\!\left(k_1\sqrt{1+r^2+2r\mu}\right)P_\delta^{(\mathrm{i})}(k_1 r)}{\left(1+r^2+2r\mu\right)^2}$$

$$\times\Bigg[-\frac{4}{25}(r+\mu)^2$$

$$+\frac{\mathrm{e}^{\frac{1}{2}\eta_1}}{5}\left(r^2\left(2\mu^2+1\right)+2r\mu\left(\mu^2+2\right)+3\mu^2\right)$$

$$-\frac{\mathrm{e}^{\frac{1}{2}(\eta_1+\eta_2)}}{16}\left(2r\mu^2+r+3\mu\right)^2$$

$$-\frac{\mathrm{e}^{\frac{5}{2}\eta_1}}{25}\left(r^2\left(10\mu^2-3\right)+2r\mu\left(5\mu^2+2\right)+7\mu^2\right)$$

$$+\frac{\mathrm{e}^{\frac{1}{2}(5\eta_1+\eta_2)}}{40}\left(r^2\left(20\mu^4+4\mu^2-3\right)+r\left(44\mu^3-2\mu\right)+21\mu^2\right)$$

$$-\frac{\mathrm{e}^{\frac{5}{2}(\eta_1+\eta_2)}}{400}\left(r\left(10\mu^2-3\right)+7\mu\right)^2\Bigg]$$

$$+\,(\eta_1\leftrightarrow\eta_2)\,,$$

$$\text{(F.5)}$$

$$G_{ff,2}^{(\mathrm{P})}(1,2)\Big|_{\vec{l}_1=\vec{l}_2=0} = (2\pi)^3\,\delta_\mathrm{D}(\vec{k}_1+\vec{k}_2)\,\frac{k_1^3\,\mathrm{e}^{-\frac{3}{2}(\eta_1+\eta_2)}}{(2\pi)^2}\int_0^\infty\!\mathrm{d}r\,\frac{P_\delta^{(\mathrm{i})}(k_1)\,P_\delta^{(\mathrm{i})}(k_1 r)}{r^3}$$

$$\times\Bigg[\frac{\mathrm{e}^{\frac{5}{2}\eta_1}}{315}\left(6r^7-22r^5-22r^3+6r-3\left(r^2-1\right)^4\frac{\ln(r+1)}{\ln(|r-1|)}\right)$$

$$+\frac{\mathrm{e}^{\frac{5}{2}\eta_1+\eta_2}}{105}\left(2r\left(3r^4+8r^2-3\right)-3\left(r^2-1\right)^3\frac{\ln(r+1)}{\ln(|r-1|)}\right)$$

$$+\frac{\mathrm{e}^{\frac{5}{2}(\eta_1+\eta_2)}}{40}\left(2r\left(-3r^6+6r^4-9r^2+2\right)+\left(3r^2+2\right)\left(r^2-1\right)^3\frac{\ln(r+1)}{\ln(|r-1|)}\right)$$

$$+\frac{\mathrm{e}^{\frac{1}{2}(7\eta_1+5\eta_2)}}{420}\left(90r^7-204r^5+286r^3-36r-9\left(r^2-1\right)^3\left(5r^2+2\right)\frac{\ln(r+1)}{\ln(|r-1|)}\right)$$

$$+\frac{\mathrm{e}^{\frac{1}{2}(9\eta_1+5\eta_2)}}{504}\left(2r\left(-21r^6+50r^4-79r^2+6\right)+3\left(7r^2+2\right)\left(r^2-1\right)^3\frac{\ln(r+1)}{\ln(|r-1|)}\right)\Bigg]$$

$$+\,(\eta_1\leftrightarrow\eta_2)\,,$$

$$\text{(F.6)}$$

$$
G_{ff,2}^{(C)}(1,2)\Big|_{\vec{l}_1=\vec{l}_2=0} = (2\pi)^3\,\delta_{\rm D}(\vec{k}_1+\vec{k}_2)\,\frac{k_1^3\,{\rm e}^{-\frac{1}{2}(\eta_1+\eta_2)}}{(2\pi)^2}\int\limits_0^\infty {\rm d}r\int\limits_{-1}^{1}{\rm d}\mu\,\frac{P_\delta^{(i)}\left(k_1\sqrt{1+r^2+2r\mu}\right)P_\delta^{(i)}(k_1r)}{\left(1+r^2+2r\mu\right)^2}
$$

$$
\times\Bigg[\frac{16}{1225}r^2\left(\mu^2-1\right)^2
$$

$$
+\frac{{\rm e}^{\frac{5}{2}\eta_1}}{175}4r\left(\mu^2-1\right)\left(r\left(6\mu^2-1\right)+5\mu\right)
$$

$$
-\frac{{\rm e}^{\frac{7}{2}\eta_1}}{245}4r\left(\mu^2-1\right)\left(r\left(10\mu^2-3\right)+7\mu\right)
$$

$$
+\frac{{\rm e}^{\frac{5}{2}(\eta_1+\eta_2)}}{100}\left(r^2\left(1-6\mu^2\right)^2+10r\mu\left(6\mu^2-1\right)+25\right)
$$

$$
+\frac{{\rm e}^{\frac{1}{2}(7\eta_1+5\eta_2)}}{70}\left(r^2\left(-60\mu^4+28\mu^2-3\right)+r\left(22\mu-92\mu^3\right)-35\right)
$$

$$
+\frac{{\rm e}^{\frac{7}{2}(\eta_1+\eta_2)}}{196}\left(r\left(10\mu^2-3\right)+7\mu\right)^2\Bigg]
$$

$$
+\left(\eta_1\leftrightarrow\eta_2\right),
$$

$$(\text{F.7})$$

$$
G_{{\rm R},1}(1,2)\Big|_{\vec{l}_1=\vec{l}_2=0} = (2\pi)^3\,\delta_{\rm D}(\vec{k}_1+\vec{k}_2)\,\frac{k_1^3\,{\rm e}^{2\eta_2}}{(2\pi)^2}\int\limits_0^\infty {\rm d}r\,\frac{P_\delta^{(i)}(k_1r)}{r^3}
$$

$$
\times\Bigg[\frac{e^{\eta_{12}}-e^{\frac{1}{2}\eta_{12}}}{80}\left(-4r\left(9r^6+r^2+6\right)-6\left(3r^4+5r^2+2\right)\left(r^2-1\right)^2\frac{\ln(r+1)}{\ln(|r-1|)}\right)
$$

$$
+\frac{e^{2\eta_{12}}-e^{-\frac{1}{2}\eta_{12}}}{280}\left(4r\left(15r^4-23r^2+6\right)-6\left(5r^2+2\right)\left(r^2-1\right)^2\frac{\ln(r+1)}{\ln(|r-1|)}\right)
$$

$$
+\frac{e^{3\eta_{12}}-e^{-\frac{3}{2}\eta_{12}}}{1680}\left(4r\left(21r^6-50r^4+79r^2-6\right)-6\left(7r^2+2\right)\left(r^2-1\right)^3\frac{\ln(r+1)}{\ln(|r-1|)}\right)\Bigg],
$$

$$(\text{F.8})$$

where

$$
\Sigma_{\beta\beta,2}(1,2) = \Sigma_{\beta\beta,2}^{(P)}(1,2)+\Sigma_{\beta\beta,2}^{(C)}(1,2),
\tag{F.9}
$$

$$
G_{ff,2}(1,2) = G_{ff,2}^{(P)}(1,2)+G_{ff,2}^{(C)}(1,2).
\tag{F.10}
$$

G. Statistical propagator of coupled dark matter and adiabatic baryons

In (5.146) we found an analytic expression for the statistical propagator of a gravitationally coupled system of dark matter and adiabatic baryons in static-space-time, given by

$$\Delta_{ff}^{\alpha\gamma}(1,2) = (2\pi)^3\,\delta_{\rm D}\big(\vec{k}_1+\vec{k}_2\big)\,\bar{\rho}^\alpha\,\bar{\rho}^\gamma\,P_\delta^{\rm (i)}(k_1)\,D'^\alpha(1)\,D'^\gamma(2) \tag{G.1}$$

with

$$D'^\alpha(1) = D_0'^\alpha\big(\vec{s}_1\big) + \sum_{\ell=\pm}\left[D_{{\rm c},\ell}'^\alpha\big(\vec{s}_1\big)\,\cos\big(k_1 t_1\,c_\ell'(k_1)\big) + D_{{\rm s},\ell}'^\alpha\big(\vec{s}_1\big)\,\sin\big(k_1 t_1\,c_\ell'(k_1)\big)\right]. \tag{G.2}$$

The different functions appearing in this expression read

$$D_0'^{\rm d}(\vec{s}) = -\frac{\bar{v}_{P_\mathcal{H}}^{\rm b}(k)}{1+\bar{v}_{P_\mathcal{H}}^{\rm b}(k)}\,\frac{\bar{v}_G^{\rm b}(k)}{\bar{v}_G^{\rm d}(k)}\,, \tag{G.3}$$

$$D_0'^{\rm b}(\vec{s}) = \frac{\bar{v}_{P_\mathcal{H}}^{\rm b}(k)}{1+\bar{v}_{P_\mathcal{H}}^{\rm b}(k)}\,\big(1+{\rm i}y\mathcal{H}_{\rm i}\big)\,{\rm e}^{-{\rm i}y\mathcal{H}_{\rm i}}\,, \tag{G.4}$$

$$\begin{aligned}
D_{{\rm c},\pm}'^{\rm d}(\vec{s}) = \frac{1}{2}\Bigg[&1 \pm \frac{\bar{v}(k)-2\bar{v}_P^{\rm b}(k)}{\sqrt{\bar{v}^2(k)-4\bar{v}_G^{\rm d}(k)\,\bar{v}_P^{\rm b}(k)}} \\
&+ \frac{\bar{v}_{P_\mathcal{H}}^{\rm b}(k)}{1+\bar{v}_{P_\mathcal{H}}^{\rm b}(k)}\,\frac{\bar{v}_G^{\rm b}(k)}{\bar{v}_G^{\rm d}(k)}\left(1\mp\frac{\bar{v}(k)}{\sqrt{\bar{v}^2(k)-4\bar{v}_G^{\rm d}(k)\,\bar{v}_P^{\rm b}(k)}}\right)\Bigg]\,,
\end{aligned} \tag{G.5}$$

$$\begin{aligned}
D_{{\rm c},\pm}'^{\rm b}(\vec{s}) = \frac{1}{2}\Bigg[&1 \pm \frac{\bar{v}(k)}{\sqrt{\bar{v}^2(k)-4\bar{v}_G^{\rm d}(k)\,\bar{v}_P^{\rm b}(k)}} \\
&+ \frac{\bar{v}_{P_\mathcal{H}}^{\rm b}(k)}{1+\bar{v}_{P_\mathcal{H}}^{\rm b}(k)}\left(1\mp\frac{\bar{v}(k)-2\bar{v}_P^{\rm b}(k)}{\sqrt{\bar{v}^2(k)-4\bar{v}_G^{\rm d}(k)\,\bar{v}_P^{\rm b}(k)}}\right)\Bigg]\big(1-{\rm i}y\mathcal{H}_{\rm i}\,\bar{v}_{P_\mathcal{H}}^{\rm b}(k)\big)\,{\rm e}^{-{\rm i}y\mathcal{H}_{\rm i}}\,,
\end{aligned} \tag{G.6}$$

$$D_{{\rm s},\pm}'^{\rm d}(\vec{s}) = \frac{\vec{k}\cdot\vec{l}}{k}\,m^{\rm d}c_\pm(k)\,D_{{\rm c},\pm}^{\rm d}(\vec{s})\,, \tag{G.7}$$

$$D_{{\rm s},\pm}'^{\rm b}(\vec{s}) = \frac{\vec{k}\cdot\vec{l}}{k}\,m^{\rm b}c_\pm(k)\,\frac{D_{{\rm c},\pm}^{\rm b}(\vec{s})}{1-{\rm i}y\mathcal{H}_{\rm i}\,\bar{v}_{P_\mathcal{H}}^{\rm b}(k)}\,, \tag{G.8}$$

$$c'_\pm(k) = \frac{1}{\sqrt{2}} \sqrt{\bar{v}'(k) \pm \sqrt{\bar{v}'^2(k) - 4\bar{v}'^{\mathrm{d}}_G(k)\, \bar{v}'^{\mathrm{b}}_P(k)}}, \tag{G.9}$$

where we further defined the mass-, density- and enthalpy-weighted potentials

$$\bar{v}'^{\alpha}_G(k) := \frac{\bar{\rho}^\alpha}{m^\alpha}\, v^{\alpha\alpha}_G(k) \quad = -\frac{4\pi\, G\, \bar{\rho}^\alpha_{\mathrm{m}}}{k^2}, \tag{G.10}$$

$$\bar{v}'^{\mathrm{b}}_{P_P}(k) := \mathcal{H}_{\mathrm{i}}\, \frac{\bar{\rho}^{\mathrm{b}}}{m^{\mathrm{b}}}\, v^{\mathrm{b}}_P(k) = \frac{c_S^2}{\gamma}\, w(k), \tag{G.11}$$

$$\bar{v}'^{\mathrm{b}}_{P_H}(k) := \bar{\rho}^{\mathrm{b}}_{\mathrm{m}}\, v^{\mathrm{b}}_{P_H}(k) \quad = (\gamma - 1)\, w(k), \tag{G.12}$$

$$\bar{v}'^{\mathrm{b}}_P(k) := \bar{v}'^{\mathrm{b}}_{P_P}(k) \left(1 + \bar{v}'^{\mathrm{b}}_{P_H}(k)\right), \tag{G.13}$$

$$\bar{v}'(k) := \bar{v}'^{\mathrm{d}}_G(k) + \bar{v}'^{\mathrm{b}}_G(k) + \bar{v}'^{\mathrm{b}}_P(k), \tag{G.14}$$

in analogy to the expressions (5.62) to (5.64) in the isothermal case.

Publications

This is the list of peer-reviewed publications the author of this thesis was involved in.

Results from the following publications were used in this thesis

- M. Bartelmann, F. Fabis, D. Berg, E. Kozlikin, R. Lilow, and C. Viermann. "A microscopic, non-equilibrium, statistical field theory for cosmic structure formation". In: New Journal of Physics, 18.4 (2016), p. 043020.

- M. Bartelmann, F. Fabis, E. Kozlikin, R. Lilow, J. Dombrowski, and J. Mildenberger. "Kinetic field theory: effects of momentum correlations on the cosmic density-fluctuation power spectrum". In: New Journal of Physics, 19.8 (2017), p. 083001.

- F. Fabis, E. Kozlikin, R. Lilow, and M. Bartelmann. "Kinetic field theory: exact free evolution of Gaussian phase-space correlations". In: Journal of Statistical Mechanics: Theory and Experiment 2018.4 (2018), p. 043214.

Results from the following publications do not appear in this thesis

- C. Viermann, F. Fabis, E. Kozlikin, R. Lilow, and M. Bartelmann. "Nonequilibrium statistical field theory for classical particles: Basic kinetic theory". In: Physical Review E 91.6 (2015), p. 062120.

Bibliography

[1]   Matthias Bartelmann et al. "A microscopic, non-equilibrium, statistical field theory for cosmic structure formation". In: *New Journal of Physics* 18.4 (2016), p. 043020.

[2]   Matthias Bartelmann et al. "Kinetic field theory: effects of momentum correlations on the cosmic density-fluctuation power spectrum". In: *New Journal of Physics* 19.8 (2017), p. 083001.

[3]   Robert Lilow. "Developing a Macroscopic Reformulation of Statistical Field Theory for Classical Particles to Investigate Cosmic Structure Formation". Master's thesis. Heidelberg University, Department of Physics and Astronomy, 2015.

[4]   Scott Dodelson. *Modern cosmology*. San Diego, Calif: Academic Press, 2003. 440 pp.

[5]   F. Bernardeau et al. "Large-scale structure of the Universe and cosmological perturbation theory". In: *Physics Reports* 367.1 (1, 2002), pp. 1–248.

[6]   A. Einstein. "Die Grundlage der allgemeinen Relativitätstheorie". In: *Annalen der Physik* 354.7 (), pp. 769–822.

[7]   P. a. R. Ade et al. "Planck 2015 results - XIII. Cosmological parameters". In: *Astronomy & Astrophysics* 594 (1, 2016), A13.

[8]   E. R. Harrison. "Fluctuations at the Threshold of Classical Cosmology". In: *Physical Review D* 1.10 (15, 1970), pp. 2726–2730.

[9]   Y. B. Zel'dovich. "A Hypothesis, Unifying the Structure and the Entropy of the Universe". In: *Monthly Notices of the Royal Astronomical Society* 160.1 (1, 1972), 1P–3P.

[10]   David H. Lyth and Antonio Riotto. "Particle physics models of inflation and the cosmological density perturbation". In: *Physics Reports* 314.1 (1, 1999), pp. 1–146.

[11]   P. a. R. Ade et al. "Planck 2015 results - XVII. Constraints on primordial non-Gaussianity". In: *Astronomy & Astrophysics* 594 (1, 2016), A17.

[12]   J. M. Bardeen et al. "The statistics of peaks of Gaussian random fields". In: *The Astrophysical Journal* 304 (1, 1986), pp. 15–61.

[13]   Sean M. Carroll, William H. Press, and Edwin L. Turner. "The Cosmological Constant". In: *Annual Review of Astronomy and Astrophysics* 30.1 (1, 1992), pp. 499–542.

[14]   Ya. B. Zel'dovich. "Gravitational instability: An approximate theory for large density perturbations." In: *Astronomy and Astrophysics* 5 (1, 1970), pp. 84–89.

[15]   P. J. E. Peebles. *The large-scale structure of the universe*. Princeton series in physics. Princeton, N.J: Princeton University Press, 1980. 422 pp.

[16]   T. Buchert. "Lagrangian theory of gravitational instability of Friedman-Lemaitre cosmologies and the 'Zel'dovich approximation'". In: *Monthly Notices of the Royal Astronomical Society* 254 (1992), pp. 729–737.

[17]   T. Buchert and J. Ehlers. "Lagrangian theory of gravitational instability of Friedman-Lemaitre cosmologies – second-order approach: an improved model for non-linear clustering". In: *Monthly Notices of the Royal Astronomical Society* 264 (1993), pp. 375–387.

[18]   T. Buchert. "Lagrangian Theory of Gravitational Instability of Friedman-Lemaitre Cosmologies - a Generic Third-Order Model for Nonlinear Clustering". In: *Monthly Notices of the Royal Astronomical Society* 267 (1994), p. 811.

[19]   F. R. Bouchet et al. "Perturbative Lagrangian approach to gravitational instability." In: *Astronomy & Astrophysics* 296 (1995), p. 575.

[20]   C.-P. Ma and E. Bertschinger. "Cosmological Perturbation Theory in the Synchronous and Conformal Newtonian Gauges". In: *The Astrophysical Journal* 455 (1995), p. 7.

[21]   J. Ehlers and T. Buchert. "Newtonian Cosmology in Lagrangian Formulation: Foundations and Perturbation Theory". In: *General Relativity and Gravitation* 29 (1997), pp. 733–764.

[22]   U. Seljak. "Analytic model for galaxy and dark matter clustering". In: *Monthly Notices of the Royal Astronomical Society* 318 (2000), pp. 203–213.

[23]   P. Valageas. "Dynamics of gravitational clustering. I. Building perturbative expansions". In: *Astronomy & Astrophysics* 379 (2001), pp. 8–20.

[24]   A. Cooray and R. Sheth. "Halo models of large scale structure". In: *Physics Reports* 372 (2002), pp. 1–129.

[25]   P. Valageas. "A new approach to gravitational clustering: A path-integral formalism and large-N expansions". In: *Astronomy & Astrophysics* 421.1 (1, 2004), pp. 23–40.

[26]   P. Valageas and D. Munshi. "Evolution of the cosmological density distribution function: new analytical model". In: *Monthly Notices of the Royal Astronomical Society* 354 (2004), pp. 1146–1158.

[27]   C.-P. Ma and E. Bertschinger. "A Cosmological Kinetic Theory for the Evolution of Cold Dark Matter Halos with Substructure: Quasi-Linear Theory". In: *The Astrophysical Journal* 612 (2004), pp. 28–49.

[28]   F. Bernardeau and P. Valageas. "Propagators in Lagrangian space". In: *Physical Review D* 78.8, 083503 (2008), p. 083503.

[29]   M. Pietroni. "Flowing with time: a new approach to non-linear cosmological perturbations". In: *Journal of Cosmology and Astroparticle Physics* 10, 036 (2008), p. 36.

[30]   S. Anselmi, S. Matarrese, and M. Pietroni. "Next-to-leading resummations in cosmological perturbation theory". In: *Journal of Cosmology and Astroparticle Physics* 6, 015 (2011), p. 15.

[31]   M. Pietroni et al. "Coarse-grained cosmological perturbation theory". In: *Journal of Cosmology and Astroparticle Physics* 2012.1 (2012), p. 019.

[32]   J. J. M. Carrasco, M. P. Hertzberg, and L. Senatore. "The effective field theory of cosmological large scale structures". In: *Journal of High Energy Physics* 9, 82 (2012), p. 82.

[33]   S. Anselmi and M. Pietroni. "Nonlinear power spectrum from resummed perturbation theory: a leap beyond the BAO scale". In: *Journal of Cosmology and Astroparticle Physics* 12, 013 (2012), p. 13.

[34]   P. Valageas, T. Nishimichi, and A. Taruya. "Matter power spectrum from a Lagrangian-space regularization of perturbation theory". In: *Physical Review D* 87.8, 083522 (2013), p. 083522.

[35]   R. A. Porto, L. Senatore, and M. Zaldarriaga. "The Lagrangian-space Effective Field Theory of large scale structures". In: *Journal of Cosmology and Astroparticle Physics* 5, 022 (2014), p. 22.

[36]   J. J. M. Carrasco et al. "The Effective Field Theory of Large Scale Structures at two loops". In: *Journal of Cosmology and Astroparticle Physics* 7, 057 (2014), p. 57.

[37]   P. J. E. Peebles and J. T. Yu. "Primeval Adiabatic Perturbation in an Expanding Universe". In: *The Astrophysical Journal* 162 (1, 1970), p. 815.

[38]   Daniel J. Eisenstein and Wayne Hu. "Baryonic Features in the Matter Transfer Function". In: *The Astrophysical Journal* 496.2 (1998), p. 605.

[39]   J. H. Jeans. "I. The stability of a spherical nebula". In: *Phil. Trans. R. Soc. Lond. A* 199.312 (1, 1902), pp. 1–53.

[40]   M. J. Rees and J. P. Ostriker. "Cooling, dynamics and fragmentation of massive gas clouds: clues to the masses and radii of galaxies and clusters". In: *Monthly Notices of the Royal Astronomical Society* 179.4 (1, 1977), pp. 541–559.

[41]   S. D. M. White and M. J. Rees. "Core condensation in heavy halos: a two-stage theory for galaxy formation and clustering". In: *Monthly Notices of the Royal Astronomical Society* 183.3 (1, 1978), pp. 341–358.

[42]   Mark Vogelsberger et al. "A model for cosmological simulations of galaxy formation physics". In: *Monthly Notices of the Royal Astronomical Society* 436.4 (21, 2013), pp. 3031–3067.

[43]   P. C. Martin, E. D. Siggia, and H. A. Rose. "Statistical Dynamics of Classical Systems". In: *Physical Review A* 8.1 (1, 1973), pp. 423–437.

[44]   E. Gozzi. "Hidden BRS invariance in classical mechanics". In: *Physics Letters B* 201.4 (18, 1988), pp. 525–528.

[45]   E. Gozzi, M. Reuter, and W. D. Thacker. "Hidden BRS invariance in classical mechanics. II". In: *Physical Review D* 40.10 (15, 1989), pp. 3363–3377.

[46]   Gene F. Mazenko. "Fundamental theory of statistical particle dynamics". In: *Physical Review E* 81.6 (1, 2010), p. 061102.

[47]   Shankar P. Das and Gene F. Mazenko. "Field Theoretic Formulation of Kinetic Theory: Basic Development". In: *Journal of Statistical Physics* 149.4 (1, 2012), pp. 643–675.

[48]   Felix Fabis et al. "Kinetic field theory: exact free evolution of Gaussian phase-space correlations". In: *Journal of Statistical Mechanics: Theory and Experiment* 2018.4 (2018), p. 043214.

[49]   Joseph Liouville. "Sur la Théorie des Équations transcendantes". In: *Journal de Mathématiques Pures et Appliquées* 3 (1838), pp. 342–349.

[50]   Joseph E. Mayer and Elliott Montroll. "Molecular Distribution". In: *The Journal of Chemical Physics* 9.1 (1, 1941), pp. 2–16.

[51]   Matthias Bartelmann. "Trajectories of point particles in cosmology and the Zel'dovich approximation". In: *Physical Review D* 91.8 (20, 2015), p. 083524.

[52]   Sabino Matarrese and Massimo Pietroni. "Resumming cosmic perturbations". In: *Journal of Cosmology and Astroparticle Physics* 2007.6 (2007), p. 026.

[53]   Changbom Park. "Cosmic momentum field and mass fluctuation power spectrum". In: *Monthly Notices of the Royal Astronomical Society* 319.2 (1, 2000), pp. 573–582.

[54]   J. A. Peacock and S. J. Dodds. "Non-linear evolution of cosmological power spectra". In: *Monthly Notices of the Royal Astronomical Society* 280.3 (1, 1996), pp. L19–L26.

[55]   Scoccimarro Román. "A New Angle on Gravitational Clustering". In: *Annals of the New York Academy of Sciences* 927.1 (25, 2006), pp. 13–23.

[56]   P. Valageas. "Impact of shell crossing and scope of perturbative approaches, in real and redshift space". In: *Astronomy & Astrophysics* 526 (1, 2011), A67.

[57]   Diego Blas, Mathias Garny, and Thomas Konstandin. "Cosmological perturbation theory at three-loop order". In: *Journal of Cosmology and Astroparticle Physics* 2014.1 (2014), p. 010.

[58]   Martín Crocce and Román Scoccimarro. "Renormalized cosmological perturbation theory". In: *Physical Review D* 73.6 (17, 2006), p. 063519.

[59]   P. Valageas. "Large-N expansions applied to gravitational clustering". In: *Astronomy & Astrophysics* 465.3 (1, 2007), pp. 725–747.

[60]   P. Valageas. "Expansion schemes for gravitational clustering: computing two-point and three-point functions". In: *Astronomy & Astrophysics* 484.1 (1, 2008), pp. 79–101.

[61]   Diego Blas, Mathias Garny, and Thomas Konstandin. "On the non-linear scale of cosmological perturbation theory". In: *Journal of Cosmology and Astroparticle Physics* 2013.9 (2013), p. 024.

[62]   Adi Nusser. "Analytic solutions for coupled linear perturbations". In: *Monthly Notices of the Royal Astronomical Society* 317.4 (1, 2000), pp. 902–906.

[63]   Sabino Matarrese and Roya Mohayaee. "The growth of structure in the intergalactic medium". In: *Monthly Notices of the Royal Astronomical Society* 329.1 (1, 2002), pp. 37–60.

[64]   Masatoshi Shoji and Eiichiro Komatsu. "Third-Order Perturbation Theory with Nonlinear Pressure". In: *The Astrophysical Journal* 700.1 (2009), p. 705.

[65]   Celia Viermann. "Basic Kinetic Theory and Fluid dynamics in Non-Equilibrium Statistical Field Theory for Classical Particles". Master's thesis. Heidelberg University, Department of Physics and Astronomy, 2015.

[66]   M. L. Bartelmann. *Theoretical astrophysics: an introduction.* Physics textbook. OCLC: ocn815366960. Weinheim: Wiley-VCH, 2013. 320 pp.

[67]   J. J. Monaghan. "An introduction to SPH". In: *Computer Physics Communications* 48.1 (1, 1988), pp. 89–96.

[68]   Daniel Geiß. "Developing a Model for Baryonic and Mixed Matter in the Frame of SFTCP to Investigate Cosmic Structure Formation". Master's thesis. Heidelberg University, Department of Physics and Astronomy, 2017.

[69]   Jan Thorben Schneider. "Probing Fluid Dynamics In Statistical Field Theory For Classical Mesoscopic Particles". Bachelor's thesis. Heidelberg University, Department of Physics and Astronomy, 2016.

[70]   Arne Bahr. "Combining Dark And Baryonic Matter In Non-Equilibrium Statistical Field Theory". Bachelor's thesis. Heidelberg University, Department of Physics and Astronomy, 2016.

[71]   Franz Schwabl. *Statistical Mechanics.* OCLC: 318297888. New York: Springer-Verlag Berlin Heidelberg, 2006.

[72]   Joseph Silk. "Cosmic Black-Body Radiation and Galaxy Formation". In: *The Astrophysical Journal* 151 (1, 1968), p. 459.

[73]   Saleem Zaroubi. "The Epoch of Reionization". In: *The First Galaxies.* Astrophysics and Space Science Library. Springer, Berlin, Heidelberg, 2013, pp. 45–101.

[74]   Y. P. Jing et al. "The Influence of Baryons on the Clustering of Matter and Weak-Lensing Surveys". In: *The Astrophysical Journal Letters* 640.2 (2006), p. L119.

[75]   W. P. Lin et al. "The Influence of Baryons on the Mass Distribution of Dark Matter Halos". In: *The Astrophysical Journal* 651.2 (2006), p. 636.

[76]   Douglas H. Rudd, Andrew R. Zentner, and Andrey V. Kravtsov. "Effects of Baryons and Dissipation on the Matter Power Spectrum". In: *The Astrophysical Journal* 672.1 (2008), p. 19.

Acknowledgements